UNIVERSITÄT SIEGEN

Dongsheng Li

Sensor Placement Methods and Evaluation Criteria in Structural Health Monitoring

Schriftenreihe der Arbeitsgruppe
für Technische Mechanik
im Institut für Mechanik und Regelungs-
technik - Mechatronik

Herausgeber: Claus-Peter Fritzen

Band 5

Impressum
Prof. Dr.-Ing. Claus-Peter Fritzen
Arbeitsgruppe für Technische Mechanik
Institut für Mechanik und Regelungstechnik - Mechatronik
Universität Siegen
57068 Siegen
ISSN 2191-5601
URN urn:nbn:de:hbz:467-5932
Zugl.: Siegen, Univ., Diss., 2011

SENSOR PLACEMENT METHODS AND EVALUATION CRITERIA IN STRUCTURAL HEALTH MONITORING

Dissertation

zur Erlangung des akademischen Grades

Doktor-Ingenieur

vorgelegt von

M.Sc. Dongsheng LI

eingereicht dem Fachbereich

Maschinenbau

der Universität Siegen

Referent:	Prof. Dr.-Ing. C.-P. Fritzen
Korreferenten:	Prof. Dr. C. Papadimitriou, Univ. of Thessaly, Greece

Tag der mündlichen Prüfung:

8. Dezember 2011

ACKNOWLEDGEMENTS

The major part of the research work in this dissertation was carried out in the period from September 2005 to October 2007 when I was a doctoral student at the Institut für Mechanik und Regelungstechnik (IMR) – Mechatronik der Universität Siegen. During that time and later on, I benefited from many discussions with my kind supervisor, Prof. Dr.-Ing. C.-P. Fritzen, and other colleagues at the Institute.

First of all, I would like to express my sincere appreciation for my supervisor, Prof. Dr.-Ing. C.-P. Fritzen for his vision and valuable suggestions through his pleasant guidance. In many cases, he challenged me to clarify some ideas and formulations and encouraged me to delibrate my approach in the full spectrum.

My colleagues, Dipl.-Ing. Rolf T. Schulte and Mr. Gerhard Dietrich gave me helpful advices and assisted me in preparing as well as setting up the experiment apparatus of a truss structure. Dipl.-Ing. Maksim Klinkov and Dipl.-Ing. Peter Kraemer have discussed many times interesting dynamic problems in engineering with me, which are invaluable in deepening my understanding of the subject at hand and have inspired me in many aspects. Furthermore, Dipl.-Ing. Peter Kraemer has guided me to use several application programs and assisted me in familiarizing the IMR and the university. My colleagues, Msc. Kejia Xing, Mr. Wolfgang Richter, Mrs. Gisela Thomas have helped me a lot in renting an apartment and other things during my two-years' wonderful stay at Siegen. As a whole, the staffs at IMR have created a friendly working atmosphere. Their friendship is invaluable.

Professor Papadimitriou has reviewed and evaluated the dissertation. To him I would like to express my sincere gratitude and appreciation. I am also indebted to Professor Thomas G., Carne from Sandia Laboratory, who has provided me the model of the ladder structure. Moreover, our communications and discussions have sharpened our understanding of the original idea of the MinMAC algorithm. I acknowledge thanks for Professor Zhang L.M. from Nanjing University of Aeronautics and Astronautics for his suggestion to my dissertation.

Furthermore, Professor Carne has consistently encouraged me and finally guided me to win the 2008 Dominick J. Demichele Scholarship Award by Society of Expermental Mechanics, which supported me to attend the XXVII International Modal Analysis Conference (IMAC).

I would like to express my sincere thanks and respect for the vision of Professor LI, Hong-Nan and his support of my research work on the dissertation through the whole process. The German Academic Exchange Service (DAAD) and China Scholarship Council (CSC) have granted me a full scholarship for my research and a two-year stay in Germany, which is gratefully acknowledged.

My parents, my wife, my daughter and my friends have constantly encouraged me. Without these supports the dissertation could not be possible. In retrospect, my cute daughter was still on my knees when I began this research and now she is ready preparing for the primary school. Time flies. Alas!

Dalian, China, Feb. 2011 LI, Dongsheng

CONTENTS

NOMENCLATURE

Abbrevations and Acronyms

DOFs	Degrees of freedom
FEM	Finite Element Model
SHM	Structural Health Monitoring
MKE	Modal Kinetic Energy
ECP	Eigenvector Component Product
MSSP	Mode Shape Summation Plot
DPR	Drive Point Residue
EI	Effective Independence Method
FIM	Fisher Information Matrix
QRD	QR Decomposition Mehtod
MAC	Modal Assurance Criteria
SVD	Singular Value Decomposition
MinMAC	MinMAC algorithm
MaxSV	Maximize the smallest singular value of the FIM
MaxTRACE	Maximize the trace of the FIM
GRSP	Guyan Reduction Sensor Placement
SNBSPM	System Norm Based Sensor Placement Method
OLS	Ordinary Least Squares method
RLS	Representative Least Squares method
MSE	Mean Squared Error
FRF	Frequency Response Function

Vectors and Matrices

$\mathbf{M}$	mass matrix of a structure
$\mathbf{K}$	stiffness matrix of a structure
$\mathbf{C}$	Rayleigh damping matrix of a structure
Φ	rectangular mode shape matrix ($\Phi \in \mathbf{R}^{n\times m}$, and $m \le n$)
$\mathbf{y}$	response measurement vector corresponding to sensor positions

$\mathbf{q}$	modal coordinate vector, ($q \in \mathbf{R}^{m\times 1}$)
$\boldsymbol{\varepsilon}$	Gaussian white noise with zero mean and a variance of Ψ_0^2
$\boldsymbol{E_D}$	Effective Independence indices
$\mathbf{P}$	Projection matrix
σ_1	largest singular value of a matrix
σ_m	smallest singular value of a matrix
$\mathbf{X}$	an n x p design matrix
$\boldsymbol{\beta}$	a p x 1 vector of unknown coefficients
$\hat{\boldsymbol{\beta}}_S$	an OLS estimator with a subset of s components,
$\hat{\boldsymbol{\beta}}_{OLS}$	an OLS estimator with all n components

Scalars

n	number of candidate sensor positions
m	number of target mode shapes to be identified or correlated
s	desired number of sensors to be placed

Operators

E[ ]	Expectation operator
tr( )	trace of a matrix
det( )	determinant of a matrix
rank()	rank of a matrix
diag	A column vector formed by the diagonal terms of a matrix
*pinv***()**	Moore-Penrose psudoinverse of a matrix
$[\ ]^T$	transpose of a matrix
$[\ ]^{-1}$	inverse of a matrix
$[\ ]^+$	Moore-Penrose psudoinverse of a matrix

$[\ ]_i$	the i^{th} component of a vector
$\otimes$	term-by-term matrix multiplication
$\sum$	summation symbol
$\prod$	consecutive multiplication
$\lvert\ \rvert$	absolute value
$\lVert\ \rVert$	norm of a vector or a matrix
$\delta()$	a small perturbed part of a vector or matrix
$\hat{\mathbf{y}}$	estimate of a variable
$\tilde{\mathbf{y}}$	a perturbed vector or matrix by adding or substracting a small part

ABSTRACT

Sensor placement is an important issue in structural health monitoring. The dissertation presents an overview of current research efforts and development in the field of sensor placement methods in structural health monitoring.

The first part of the dissertation discusses existing influential sensor placement methods along with our comments. Based on these discussions, the connection between Modal Kinetic Energy method and the Effective Independence method are revealed. In light of the connection, a fast computation method of the Effective Independence method based on QR decomposition is proposed and coded in Matlab as well. In addition, the QR method and the MinMAC algorithm are treated in a similar manner with disclosure of their relationship with other existing methods. The second contribution of the dissertation is the extension of the MinMAC algorithm through forward- and backward combinational approaches to enhance its ability to find global optimum sensor combination.

Furthermore, five current evaluation criteria of sensor placement methods are discussed and a novel criterion with consideration of practical issues in structural health monitoring is proposed. The proposed criterion strives to achieve the best accuracy for modal identification to serve for further damage identification and structural health monitoring. A representative least squares method is thus developed to deal with the global optimum search of the new objective.

The sensor placement method corresponding to the new criterion takes actual loading conditions of a structure in addition to its eigen dynamic characteristics into consideration, and thus is termed as loading dependent sensor placement method, which is the main contribution of the dissertation. It includes actual responses in the design of measuring sensor topology and opens a new horizon in the field of sensor placement method. With the aid of this new criterion, several existing criteria are found to be approximately equivalent and are nearly step-by-step approximation of the new Representative Least Squares criterion. Finally, a truss structure is experimented with various loading conditions and the above proposed ideas and methods are verified.

1 Introduction

1.1 Problem and motivation

Structural health monitoring has attracted much attention in both research and development in academics and industries in recent years [*Balageas et al.* 2006; *Bohle* 2005; *Li et al.* 2004] . This reflects the facts of continuous deterioration conditions of important civil infrastructures, especially long-span bridges. Among them, many were built in the fifties with a 40-to-50-year designed life span. The failures and even collapses of these deficient structures stimulate increasing concerns about structural integrity, durability and reliability, i.e., the health status of an existing older structure, throughout the world.

Currently, there are no assuring measures for the structural safety. A structure is tested for deteriorations or damages with local nondestructive evaluation techniques only after signs that are resulted from fault accumulations are severe and obvious enough. When the necessity of such tests is finally noticed, damages have already exacerbated the system's reliability in many cases and some structures are even on the verge of collapse. Though routine visual inspection is mandatory for important structures in some countries, for instance, bridges in the United States scheduled to be inspected every two years, its effectiveness in finding all the possible defects is questionable. A recent survey by US Federal Highway Administration [*Moore and Wiss* 2001] revealed that at most 68% of the condition ratings were correct and in-depth inspections could not find interior deficiencies. For instance, the Minneapolis bridge (Interstate 35W bridge) broke into sections and collapsed on Aug.1, 2007 even though it had already passed every routine inspection conducted annually since 1993 [*Wald and Chang* 2007]. The limitation of visual inspection is thus obvious and structural health monitoring emerges as a promising approach.

The term „**Structural Health Monitoring“** *refers to the use of in-situ, continuous or regular (routine) measurement with permanently installed sensors and analyses of key structural and environmental parameters under operating conditions, for the purpose of warning impending abnormal states or accidents at an early stage to avoid casualties as well as giving maintenance and rehabilitation advices*[*Balageas et al.* 2006; *Li et al.* 2004]. This tentatively proposed definition of structural health monitoring complements that given by Housner [*Housner et al.* 1997]. This definition em-

phasizes the essence of the advance alert ability of structural health monitoring. Structural health monitoring is based on a basic premise, i.e., structural deterioration or damage will alter the inherent structural characteristics, mainly stiffness distribution, and will therefore change the dynamic features of the structure, namely, natural frequencies, modal damping and mode shapes. Through measuring the changes of the dynamic features, damage could be identified in four levels, damaged or not, damage location, severity and remaining service life.

Structural health monitoring is expected to provide vital information for the safe operation of key civil structures and enables operational cost reduction by performing prognostic and preventative maintenance, and also shows great potential for disaster mitigation. In general, a typical structural health monitoring (SHM) system includes three major components: a sensor system, a data processing system (including data acquisition, transmission and storage), and a health evaluation system (including diagnostic algorithms and information management). The sensors utilized in SHM are required to monitor not only the structural status, for instance stress, displacement, acceleration etc., but also influential environmental parameters, such as wind speed, temperature, humidity, soil condition of its foundation and external loadings, if possible. A large number of sensors will be involved in a health monitoring system, for instance, there are in total 786 sensors permanently installed in the TsingMa Bridge [*Ko et al.* 2003]. The raw data are acquired at a rate of 63.46MB per hour for the TsingMa and Kap Shui Mun Bridges and 55.87MB per hour for the TingKau Bridge. The challenging task of data acquisition, transmission and storage in such a large quantity demands to deploy sensors in a structure as less as possible. This is one motivation of current dissertation.

Nevertheless, many of the sensors, for instance, the wind speed sensor and the strain gauges, can be installed at somewhere according to their special characteristics [*Farrar and Lieven* 2007]. Therefore, the methods of sensor placement in the research are concerning mainly about how to deploy accelerometers for global structural health monitoring. Although, there are 33,65 and 72 accelerometers instrumented in the TsingMa Bridge, TingKau Bridge in Hongkong, and the Jiangyin Bridge in Jiangsu China, respectively, even 116 accelerometers in another Anhui Tongling Bridge [*Liu et al.* 2002], the number of accelerometers employed are, in fact, far less than the enormous candidate positions of the structure [*Doebling et al.* 1996;

SCHULTE 2006]. In particular, many structures have to be tested under operational conditions, in which the sensors are not easily amenable to be removed or relocated since many connection and communication cables were already buried in the (concrete) structure. Furthermore, sensor positions determine the quality of modal parameter identification, and are crucial in the subsequent model updating and damage quantification. Therefore, how to optimally deploy sensors so that the data acquired from those locations will result in the best identification of structural characteristics is a challenging task [*STASZEWSKI et al.* 2004], which is the central topic to be treated in the dissertation.

1.2 Problem formulation

We describe first the basic formulations of sensor placement problem in structural health monitoring to facilitate our mathematical treatments, and then discuss three aspects associated with the placement problem before outlining the work. The review of different sensor placement methods and their interconnections are postponed to Chapter 2 after the problem model and mathematical symbols are established.

1.2.1 Model for sensor placement in structural health monitoring

The sensor placement problem can be investigated from uncoupled modal coordinates of governing structural equations as follows[*CLOUGH and PENZIEN* 1993; *INMAN* 2006; *LI et al.* 2007]],

$$\begin{cases} \ddot{\mathbf{q}}_i + \mathbf{M}_i^{-1}\mathbf{C}_i\dot{\mathbf{q}}_i + \mathbf{M}_i^{-1}\mathbf{K}_i\mathbf{q}_i = \mathbf{M}_i^{-1}\Phi^T\mathbf{B}_o\mathbf{u}, \\ \mathbf{y} = \Phi\mathbf{q} + \varepsilon \end{cases} \tag{1.1}$$

where, $\mathbf{q}_i$ is the i^{th} modal coordinate and is also the i^{th} element of the modal coordinate vector $\mathbf{q}$ in the 2nd equation, $\mathbf{M}_i$, $\mathbf{K}_i$ and $\mathbf{C}_i$ are the corresponding i^{th} modal mass, stiffness and damping matrix, respectively, Φ is the mode shape matrix with its i^{th} column as the i^{th} mass-normalized mode shape, $\mathbf{B}_0$ is simply a location matrix formed by ones (corresponding to actuators) and zeros (no actuators), specifying the positions of the force vector $\mathbf{u}$. The superscripts $^{-1}$ and ^{T} represent inversion and transpose of a matrix, respectively. $\mathbf{y}$ is a measurement column vector indicating

which positions of the structure are possibly to be measured, and ε is a stationary Gaussian white noise with zero mean and a variance of Ψ_0^2, describing measurement uncertainties.

It should be noted that Eq.(1.1) is a transformed general equation of motion in structural dynamics, $\mathbf{M}\ddot{\mathbf{x}} + \mathbf{C}\dot{\mathbf{x}} + \mathbf{K}\mathbf{x} = \mathbf{B}_o\mathbf{u}$, with $\mathbf{x}$ substituted by $\Phi\mathbf{q}$ ($\mathbf{x} = \Phi\mathbf{q}$) and then left multiplied by Φ^T to decouple the equation. The damping matrix, $\mathbf{C}$, can be of a general Rayleigh damping matrix, $\mathbf{C} = \alpha\mathbf{M} + \beta\mathbf{K}$ [*CLOUGH and PENZIEN* 1993]. Generalization can, of course, be made for structures with general damping distribution. The knowledge of structural dynamics will be assumed throughout the dissertation.

In fact, $\ddot{\mathbf{y}} = \Phi\ddot{\mathbf{q}} + \varepsilon_1$ if acceleration is measured in practice. Both measurement equations (of displacement and acceleration) are, however, identical in mathematical formulation. The displacement measurement equation as shown in Eq.(1.1) is thus preferred because of notation convenience. Hereinafter, the sensor placement problem described in Eq.(1.1) is termed Model (1) and will be concentrated. The conclusion thus derived is, of course, applied to acceleration measurement.

1.2.2 Basic sensor placement problems

Sensor placement problem described in Model (1) is, essentially, divided into three aspects [*UDWADIA* 1994]: (1) what is the least number of accelerometers required to be installed in a structure for structural health monitoring? If there are additional sensors, should we install them as redundant sensors or place them in other positions; (2) where should these accelerometers be installed, including those additional ones if available? And (3) how could we evaluate the effectiveness of different sensor placement methods. These three aspects are, indeed, intervening with each other, and the core problem is the second one, which largely depends, however, on the third aspects [*PICKREL* 1999; *UDWADIA* 1994]. On the other hand, only after the last two aspects are clearly understood, it is then possible to know exactly the required number of accelerometers to be installed.

The first problem can be said to be already partially solved. It is known that the minimum number of sensors to be instrumented could not be less than the number of

mode shapes to be identified, which is determined by the observability of the system. In other words, the identified mode shapes could not discriminate from each other when the length of each mode shape is shorter than the dimension of the subspace spanned by the mode shapes. The identified mode shapes, in such cases, cannot form the basis of the mode shape subspace, i.e., the identified mode shapes are dependent on each other and one or more of them can be determined by a combination of others. Moreover, a practical number of sensors, which is limitedly preset before experiments due to the availability of instruments and facilities, is usually larger than the minimum number because of the requirement to visualize the to-be-identified mode shapes[*PICKREL* 1999], and the demand for model correlation and updating[*CARNE and DOHRMANN* 1995].

The second problem, which depends largely, however, on the third aspect, is the essential and amazing one, and is the focus of this work. Without loss of generality, it is assumed here that the total degrees of freedoms (DOFs) of the structure described in Model (1) is *n*, the number of mode shapes used for sensor placement is *m*, and the available number of sensors is *s* ($s \le n$). It is noted that all the *n* DOFs are explicitly accessible in Model (1). If there are certain inaccessible DOFs for a structure, Eq.(1) can also be finally obtained by static or dynamic model reduction methods, or even an iterated version of the improved reduction scheme if more accuracy is necessary, to remove those inaccessible DOFs [*FRISWELL and MOTTERSHEAD* 1995]. Then the sensor placement problem becomes, basically, where to deploy the *s* available sensors out of the total *n* DOFs of a structure for dynamic testing or structural health monitoring, i.e., which rows of the measurement vector $\mathbf{y}$ in Eq.(1) are to be selected. It is equivalent to select which *s* out of total *n* rows from the rectangular mode shape matrix $\mathbf{\Phi}$ ($\mathbf{\Phi} \in \mathbf{R}^{n\times m}$) to form a sub-matrix $\mathbf{A}$ ($\mathbf{A} \in \mathbf{R}^{s\times m}$) to meet certain selection criteria in mathematics.

Therefore, the issue of sensor placement can be basically regarded as an integer optimization problem. However, this selecting (optimization) problem is a discrete NP hard combinatory integer problem, which has no deterministic analytical solution up to now [*KORTE and VYGEN* 2000]. Moreover, since global optimal search for combinations of different sensor positions is prohibitive, it is not practical because of its computational burden, especially for structures with more than thousands of DOFs and not considered further in this work. Both account for the endeavors of various sub-

optimal forward addition or backward deletion algorithms, or a hybrid combination of them, as well as recent search methods based on artificial intelligence, for instance, genetic algorithm or simulate annealing, to deal with the prohibitive search range. Evidently, selection of certain search algorithms depends on chosen evaluation criteria. We will leave the evaluation criteria of sensor placement to Chapter 1 for a detailed discussion.

1.3 Objective and structure of the work

The objective of current work is to deepen the understanding of existing influential sensor placement methods and their interrelationship and to develop an effective method to deploy accelerometers suitable for structure health monitoring. Furthermore, we aim to find a sufficient evaluation criterion to judge which topology configuration of accelerometers outperforms than others.

A detailed chapter-by-chapter overview is given in the following (see Figure 1.1).

Chapter 1 introduces the motivation and the necessity of investigating sensor placement methods for structural health monitoring, along with highlighting the own contributions and clarifying the organization of the work. Moreover, a basic mathematical model for sensor placement method is established, which lays the foundation for further discussions in the dissertation.

Chapter 2 reviews existing influential sensor placement methods, namely, Modal Kinetic Energy method, the Effective Independence method, QR row decomposition method and the MinMAC method, *etc.*. Furthermore, their connections and interrelationship are treated from a mathematical point of view. Specifically, the connection between Modal Kinetic Energy and the Effective Independence method is revealed and a fast computational algorithm for the Effective Independence method is developed.

Chapter 3 extends the traditional MinMAC algorithm into a forward- and backward combinational approach, which is proposed to overcome the disadvantages of tradi-

tional MinMAC algorithm and enhances its ability to search for global optimum sensor combinations.

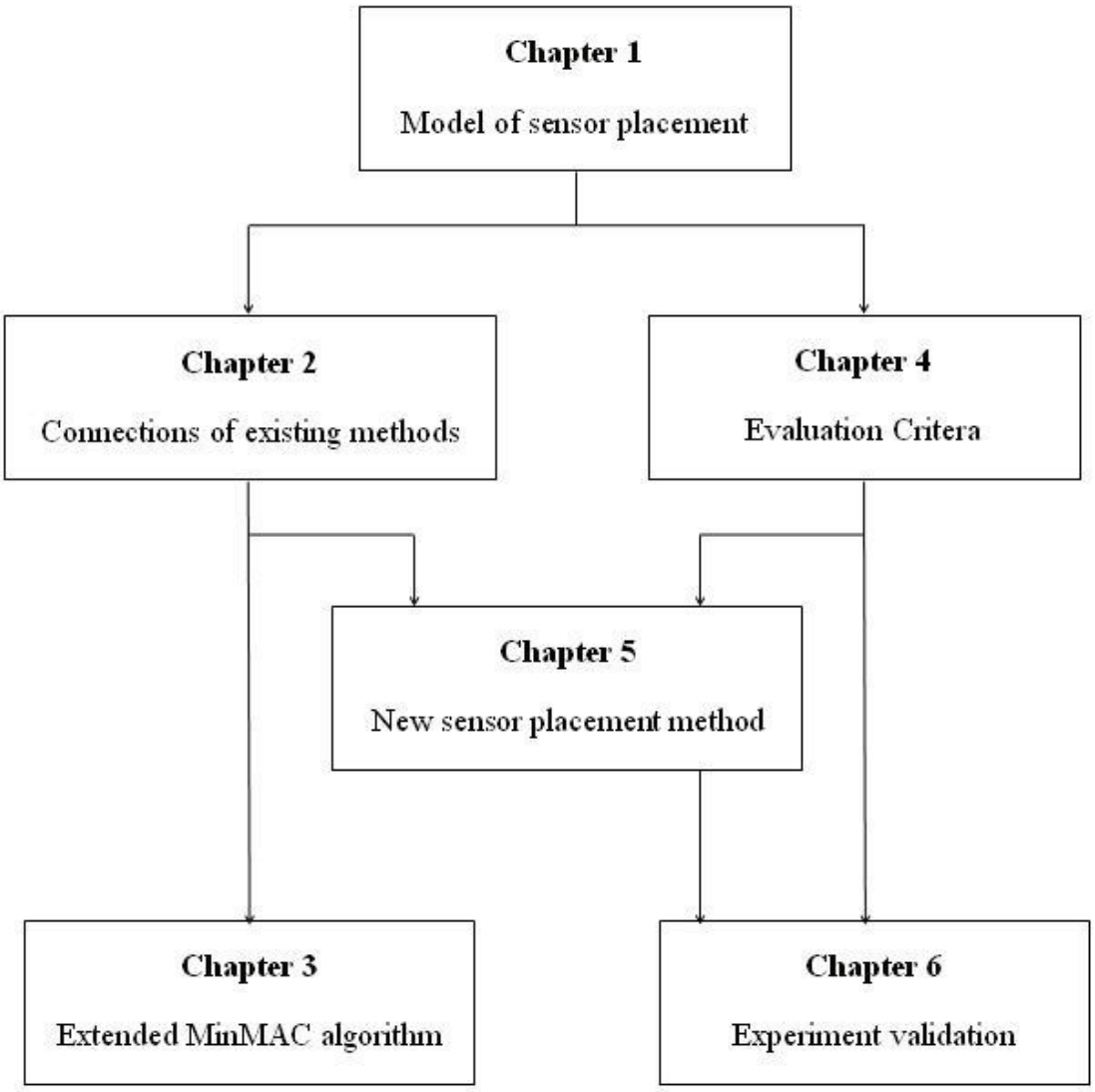

Figure 1.1: Organization of the work. The left part of the chart is concerned with the sensor placement methods and the right part deals with the evaluation criteria. All theoretical developments come together in the experiment validation of Chapter 6.

Chapter 4 presents a detailed discussion of five existing influential evaluation criteria for sensor placement methods. Based on the insights gathered from these discussions, a novel criterion is proposed from the perspective of “almost global unbiasedness”.

Chapter 5 develops a Representative Least Squares method to meet the new criterion proposed in Chapter 4 along with a loading dependent sensor placement method, specially tailored for structural health monitoring. The theory of representative least squares method is examined, and compared with classical ordinary least squares method. Three computational approaches to find the solution for the representative least squares method are initiated. It is found that two existing influencing criteria can be regarded as a step-by-step approximation of the new criterion which is an exact solution.

Chapter 6 utilizes a truss structure to validate the proposed loading dependent sensor placement method in Chapter 5 and its corresponding criterion. Different excitations are applied to the truss and its modal characteristics are identified with different sensor combinations to compare their accuracy.

Chapter 7 summarizes the conclusions of this work. Additionally, some unsolved problems and suggestions for future research related to sensor placement methods are envisaged.

2 Analysis of Influential Sensor Placement Methods

The problem of sensor placement has attracted increasing attention from various perspectives, as can be seen from the abundance of literature [*KUBRUSLY and MALEBRANCHE* 1985; *LI et al.* 2008; *PAPADOPOULOS and GARCIA* 1998], and the references therein. In this Chapter, we will review several of the most influential methods both from historical points of view and from their impacts on practice and the development of sensor placement theory. Of course, bias and omissions could not be avoided for such a daunting task because of personal preference and limitations. For instance, the damage sensitivity based methods are ignored since they are beyond the scope of the current topic.

In the issue of sensor placement, the mode shapes of interest play a central role. Many sensor placement methods can be finally traced back to be certain row combinations of the mode shapes in consideration. The differences between the methods lie only in their various weights to the mode shapes as illustrated in the next section. For simplicity of explanation, the original mode shapes, arranged column-wise as a matrix, are assumed to be real and already orthonormalized with respect to an identity mass matrix in the following, if not explicitly stated otherwise.

2.1 Review of existing sensor placement methods

The heuristic visual inspection method is the simplest among the sensor placement methodologies proposed for dynamic testing and perhaps the first method in practical modal tests before the sensor placement problem is seriously questioned. By this method, the responses of a structure are first visually inspected, the mode shapes of interest are examined and the locations with high amplitude of modal responses are then selected according to the experience of practitioner engineers. This method is mostly derived from, and dependent on the intuition of practical engineers [*COOTE et al.* 2005]. Though practical for some simple structures tested in laboratory, the visual inspection method encounters great difficulties in large complicated structures in structural health monitoring since it is not obvious to judge where a structure has large vibration amplitudes just by visual inspection.

2.1.1 Modal kinetic energy method

The first rigorous sensor placement strategy is perhaps the modal kinetic energy (MKE) method, which is an extension of the traditional heuristic visual inspection. The MKE method examines the mode shapes of significance and selects locations with high amplitudes of responses as follows

$$MKE_{pq} = \mathbf{\Phi}_{pq} \sum_{k} \mathbf{M}_{pk} \mathbf{\Phi}_{kq} \tag{2.1}$$

where MKE_{pq} is the kinetic energy associated with the p^{th} dof in the q^{th} target mode, $\mathbf{\Phi}_{pq}$ is the p^{th} coefficient in the corresponding mode shape, $\mathbf{M}_{pk}$ is the term in the p^{th} row and k^{th} column of the finite element model (FEM) mass matrix, and $\mathbf{\Phi}_{kq}$ is the k^{th} coefficient in the q^{th} FEM target mode shapes [*PAPADOPOULOS and GARCIA* 1998]. The selected mode shapes are demanded to represent most of the energy contained in the responses.

The MKE method gives a measure of the dynamic contribution of each FEM physical dof to each of the target mode shapes, and provides a rough idea where the maximum responses could be measured. When the mass matrix is an identity equivalent matrix, the modal kinetic energy indices are, in fact, the squared Frobenius row norms of the mode shape matrix if we regard each row as a vector.

The reason to adopt MKE resides in that it tells which DOFs may capture most of the relevant dynamic features of the structure. The MKE helps to select those sensor positions with possible large amplitudes, and to increase the signal to noise ratio, which is critical in harsh and noisy circumstances. Many other methods are compared with the MKE to demonstrate their validity and efficiency, and even the Effective Independence method adopts MKE as its first stage to select candidate sensors from all candidate DOFs of a structure [*KAMMER* 1991].

2.1.2 Eigenvector component product and mode shape summation plot method

Similar to the MKE to compute the squared Frobenius norms of each row of the mode shape matrix weighted by structural mass distribution, the Eigenvector Com-

ponent Product (ECP) method computes the absolute products of each row vector [*HEYLEN et al.* 1998], whereas the mode shape summation plot method (MSSP) computes their absolute sum. It is noted that the term 'Eigenvector' is used here instead of mode shape due to the conventions. Anyway, they convey the same meaning in this context.

In ECP, the sensor positions with large ECP index values are selected as candidate sensor positions [*LARSON et al.* 1994] as following,

$$ECP_i = \prod_{k=1}^{m} \left| \mathbf{\Phi}_{ik} \right| \tag{2.2}$$

where, ECP_i is the ECP index for the i^{th} sensor position, m denotes the number of mode shapes of significance and $\prod$ consecutive element multiplications.

This technique selects sensor positions with larger ECP indices ECP_i and has the advantage to prevent deploying sensors at or near nodes of selected modes. However, the ECP tends to cluster sensors in a small area, and is not able to capture global mode shapes with clustered sensors.

By the MSSP [*DE CLERCK and AVITABLE* 1998], the components of a mode shape corresponding to a sensor position (a row in the mode shape matrix) are drawn in a graph and the absolute summation are calculated for each row (candidate sensor positions). The positions with large MSSP indices are selected as sensor positions as follows,

$$MSSP_i = \sum_{k=1}^{m} \left| \mathbf{\Phi}_{ik} \right| \tag{2.3}$$

where, $MSSP_i$ is the MSSP index for the i^{th} sensor position.

The MSSP method has the advantage to graphically show the contributions of candidate sensor positions to the total responses of a structure, and is easy to compute. The MSSP can be regarded as the L_1 norm since the rows of the mode shape matrix are absolutely summed together [*HORN and JOHNSON* 1985]. In this respective, the MKE method in Section 2.1.1 can be considered as the L_2 norm of the mode shape matrix.

Both the ECP and MSSP methods are intuitive and aim to avoid nodal sensor positions or sensor positions containing insignificant modal kinetic energy. However, experiences show that they could only provide possible good candidate sensor pools, and could not offer much insight about the best sensor combinations. Consequently, the ECP and MSSP methods can be employed as a preliminary tool to exclude certain sensor positions, similar to the function of the MKE in the Effective Independence method to be discussed in Section 2.1.4

2.1.3 Drive point residue method

The Drive Point Residue (DPR) method is computed as follows [*CHUNG and MOORE* 1993],

$$DPR = \Phi \otimes \Phi \, \Lambda^{-1} \tag{2.4}$$

where Λ^{-1} is the inverse of the diagonal eigenvalue matrix and $\otimes$ represents a term-by-term matrix multiplication.

The DPR, which is equivalent to modal participating factors, is a measure of how much a particular mode is excited at a particular DOF [*LARSON et al.* 1994]. For a linear structure, Betti's law and Maxwell's law states that the response at point *p* due to excitation at point *q* is equal to the response at point *q* due to the same excitation at point *p*. Therefore, candidate sensor positions with large DPR values are anticipated with large response as well. It is worth to note that the formulation in Eq.(2.4) is used for modes that are scaled as for displacement over force measurements. When accelerometers are used, the modes should be scaled for acceleration over force measurements by multiplying the squares of eigen-frequencies, separately.

In order to insure that an excitation location will give uniform participation of as many target modes as possible, it is desired to find a high average residue for a given DOF. An averaged DPR was ever used by LMS International [*KIENTZY et al.* 1989].

It should be noted that there are other variants of derivative methods formed by averaged or weighted MKE, ECP, MSSP and DPR methods. The readers are invited to consult reference [*PAPADOPOULOS and GARCIA* 1998] for details.

2.1.4 Effective independence method

The Effective Independence (EI) Method is one of the most influential and commonly used methods, as shown in its highly cited record [*KAMMER* 1991]. The EI method quantifies the independence between two or more reduced mode shapes, and has many attractive properties. In particular, it provides a natural criterion to differentiate truncated mode shapes for sensor placement, and has been applied to a wide range of large structural dynamic testing, as also recommend by Ewins [*EWINS* 2000], Heylen *et.al*. [*HEYLEN et al.* 1998] and Friswell *et.al*. [*FRISWELL and MOTTERSHEAD* 1995] for modal testing and modal updating, and already embedded in commercial software MSC/NASTRAN [*PECK and TORRES* 2004].

The objective of the EI is to select measurement positions that make the mode shapes of interest as linearly independent as possible while containing sufficient information about the target modal responses in the measurements. The method originates from estimation theory by sensitivity analysis of the parameters (modal coordinates) to be estimated, and then it arrives at the maximization of the Fisher information matrix, for instance, the determinant or the trace. It is reflected in the coefficient variance-covariance matrix. Thus, the covariance matrix of the estimate error of the modal coordinates would be minimized.

From the measurement output expression in Eq.(1.1), the EI takes the covariance matrix of the estimate error for an efficient unbiased estimator as follows,

$$E\left[(\mathbf{q}-\hat{\mathbf{q}})(\mathbf{q}-\hat{\mathbf{q}})^T\right]=\left[\left(\frac{\partial \mathbf{y}}{\partial \mathbf{q}}\right)^T\left[\boldsymbol{\Psi}_0^2\right]^{-1}\left(\frac{\partial \mathbf{y}}{\partial \mathbf{q}}\right)\right]^{-1}=\left[\frac{1}{\boldsymbol{\Psi}_0^2}\boldsymbol{\Phi}^T\boldsymbol{\Phi}\right]^{-1}=\mathbf{A}^{-1} \tag{2.5}$$

in which $\mathbf{A}$ is the Fisher information matrix (FIM), $\Psi_0{}^2$ represents the common variance of the stationary Gaussian measurement white noise $\boldsymbol{\varepsilon}$ in Eq.(1.1), *E* denotes the expected value, and $\hat{\mathbf{q}}$ is the vector of an efficient unbiased estimator of $\mathbf{q}$. It is noteworthy that in the formulation of Eq.(2.5) the measurements have the noise level. For a general case of measurements with different noise levels, the variance $\Psi_0{}^2$ maybe not a constant matrix, but a diagonal one.

Maximizing $\mathbf{A}$ will result in the best state estimate of $\mathbf{q}$. In practice, the analysis begins by solving the following eigenvalue equation,

$$\left[\boldsymbol{\Phi}^T\boldsymbol{\Phi} - \lambda\mathbf{I}\right]\psi = 0 \tag{2.6}$$

where ψ are the orthogonal eigenvectors. The effective independence coefficients of the candidate sensors are then computed by the following formation,

$$E_D = \left[\boldsymbol{\Phi}\psi\right] \otimes \left[\boldsymbol{\Phi}\psi\right]\lambda^{-1} \cdot \mathbf{1} \tag{2.7}$$

in which $\mathbf{1}$ is an *n* x 1 column vector with all elements of 1. E_D is the EI indices, which evaluate the contribution of a candidate sensor location to the linear independence of the modal partitions $\boldsymbol{\Phi}$.

The selecting procedure is to sort the elements of the E_D coefficients, and to remove the smallest one at a time. The E_D coefficients are then updated according to the reduced modal shape matrix, and the process is repeated iteratively until the number of remained sensors equals to a preset value. The remaining DOFs serve as the measurement locations.

Alternatively, the EI index can be computed as the diagonal of the following matrix,

$$E_D = \mathrm{diag}(\boldsymbol{\Phi}\left[\boldsymbol{\Phi}^T\boldsymbol{\Phi}\right]^{-1}\boldsymbol{\Phi}^T) \tag{2.8}$$

The bracketed term in the right-hand side of the expression, $\mathbf{P} = \boldsymbol{\Phi}\left[\boldsymbol{\Phi}^T\boldsymbol{\Phi}\right]^{-1}\boldsymbol{\Phi}^T$, is a projection matrix formed by the mode shape matrix $\boldsymbol{\Phi}$ with the idempotent properties: $\mathbf{P}^2 = \mathbf{P}$, and $\mathbf{P}^T = \mathbf{P}$. From these properties, it is easy to show that the E_D indices are in the range between 0 and 1, i.e., $0 \le E_D \le 1$ as shown in Appendix 2A. The E_D indices or the diagonal terms of the projection matrix $\mathbf{P}$ are called as leverage of each predicted value, $\hat{\mathbf{y}}$, on its actual measurement, $\mathbf{y}$, in Eq.(1.1) in statistics [*CHATTERJEE* 1988; *COOK and WEISBERG* 1982]. It can clearly be interpreted as the amount of leverage each row $\mathbf{y}_i$ has in determining its corresponding regression value regardless of the actual value of $\mathbf{y}_i$, and is solely determined by the row location $\boldsymbol{\Phi}_i$ in the mode shape space spanned by the columns of matrix $\boldsymbol{\Phi}$. A large (small)

value of an E_D index indicates that Φ_i lies far from (near to) the bulk of other points in the mode shape matrix Φ.

There are many variants of the EI method. The so-called energy optimization technique is derived from MKE and EI by optimizing the kinetic energy matrix measured by candidate sensor locations [*HEO et al.* 1997]. In one study [*COOTE et al.* 2005], it was shown that the energy optimization technique appears more favorable because the EI results in clustering of sensors and did not reduce the off-diagonal MAC (Modal Assurance Criteria) terms particularly well. Other variants are adding weights for different mode shapes, for instance, residue weighted, or mass weighted. Among them, one technique is called EFI-DPR in which the modes in EI are weighted by the corresponding driving-point residues [*MEO and ZUMPANO* 2005]. In this manner, the EFI-DPR tries to avoid selecting sensor locations with low energy contents with a consequent possible loss of information, which is one limitation of the EI method.

2.1.5 QR decomposition method

The QR Decomposition (QRD) method proposed by Link *et. al.* aims to locate a subset of structural DOFs of an analytical model as measurement points such that the linear independence of the mode shapes to be measured is maximized [*SCHEDLINSKI and LINK* 1996]. The underlying idea is that the most linear independent rows of the modal matrix indicate the DOFs that should be chosen as measurement locations since they form the smallest possible modal matrix, which provides a MAC matrix with minimized off-diagonal terms to enhance the ability to distinguish between similar mode shapes. In computation, the QRD method extracts those rows to form the effective subset by QR decomposition of a transposed mode shape matrix.

In comparison, the similarity between EI and QRD is quite straightforward. The EI seeks for the most independent rows from the perspective of column independence whereas the QRD search directly for the most independent rows as many as the number of mode shapes of interest.

From matrix calculus, we know that the row rank is equal to the column rank of a matrix. When the first *m* linearly independent rows, whose number equals the column number of the matrix in our case, are found by QR decomposition, it arrives at a col-

umn independent sub-matrix as well. Link claimed that *m* sensors are enough, and that additional sensors don't improve the measurement information and may increase the off-diagonal terms of the MAC matrix since the additional *s-m* sensors are found in the vicinity of the first *m* sensors. The second statement is, of course, true. The reason is that the row linear independence of the selected modal sub-matrix will not improve even when more rows (another *s-m* rows) are added. The additional rows are definitely linear dependent on the first *m* rows and thus increase the off-diagonal terms of the MAC matrix.

2.1.6 MinMAC algorithm

The MinMAC algorithm proposed by Carne and Dohrmann aims to ensure modal correspondence between the mode shapes computed by an FEM and those measured or identified ones in dynamic testing [*CARNE and DOHRMANN* 1995]. To achieve this, both sets of mode shapes have to be differentiated as much as possible. It is equivalent to maximize the angles formed by unit mode shape vectors, or to minimize the dot product between them, which is the same as the Modal Assurance Criteria (MAC). Small maximum off-diagonal term indicates less correlation between corresponding mode shape vectors, and renders the mode shapes discriminable from each other. This is the reason to minimize the off-diagonal elements of the MAC matrix. Moreover, Carne and Dohrmann use intuition to determine an initial measurement set of DOFs that adequately covers the structure and areas of special interest to ensure modal visualization besides correspondence.

The MinMAC algorithm achieves this objective as follows. First, an intuition sensor set (much less than the required number of sensors) is selected based on experience and requirements of structural topology for visualization of mode shapes. Second, it adds other available candidate sensors one by one, and selects one that minimizes the maximum off-diagonal element of the MAC matrix at each step. Third, the MinMAC repeats the second step by adding one sensor at a time until a required number of sensors are selected.

2.1.7 SVD-based methods

Similar to the EI method, an SVD-based method directly decompose the mass weighted information matrix [*PARK and KIM* 1996]. It complements the EI by providing a guide for an allowable number of degrees to be deleted at each iteration stage, which renders the selection computation much faster. To some degree, it equals to maximize the smallest singular value of the fisher information matrix [*REYNIER and ABOU-KANDIL* 1999], and called MaxSV in sequels. In their approach, the estimate of modal coordinates is found in a least-squares sense and a distance associated with a covariance matrix of the estimated error is minimized. The MaxSV is then related to minimize the noise effect by the minimization of the distance measure.

Another approach uses a signal subspace correlation (SSC) technique to deploy sensors [*CHERNG* 2003]. This technique is based on the analytical formulation of singular value decomposition (SVD) for a candidate-blocked Hankel matrix formed by subspace correlation technique. The SSC accounts for factors that contribute to the estimated results, such as mode shapes, damping ratios, sampling rate and matrix size (or number of data used). With the aid of SSC, it will be shown that using information of mode shapes and that of singular values are equivalent under certain conditions.

As well known in matrix analysis theory, different matrix norms are equivalent in the sense that one norm can be always bounded in a range by another norm with appropriate constant scaling factors [*HORN and JOHNSON* 1985]. The trace, the determinant and the maximum singular value are just different norms of a FIM matrix [*GOLUB and VAN LOAN* 1996]. (Generally speaking, trace and determinant are not conventional matrix norms. However, since FIM (Fisher Information Matrix) is a special matrix as defined by $FIM = tr(A^T A) = \sum_{i=1}^{n}\sum_{j=1}^{n}\left|a_{ij}\right|^2 = \left\|A\right\|_F^2$, its trace can be viewed as a special matrix norm as the square the Frobenius norm). That is to say, different sensor placement methods based on maximization of the trace (MaxTRACE), determinant (EI) or maximum singular value (MaxSV) of the information matrix will yield similar, if not the same, results for most cases [*BASSEVILLE et al.* 1987; *EMERY and NENAROKOMOV* 1998]. There is strong evidence that the three criteria are approximately equivalent

although there is unfortunately no definite proof of such equivalence up to now [*BICCHI and CANEPA* 1994; *PAN* 2000].

2.1.8 Guyan reduction method

The Guyan reduction sensor placement (GRSP) method selects the master DOFs as the locations of sensors during the process of Guyan reduction [*PENNY et al.* 1994]. It is based on the belief that low ratios of leading diagonal stiffness to mass terms indicate good DOFs to retain in terms of describing the kinetic energy, and that the inertia forces at slave coordinates are negligible compared with the elastic forces.

A major disadvantage of the GRSP method is that it strongly depends on the meshing size of the FEM, and is interested only in the lower modes, which is not always the case. To overcome the inaccuracy of Guyan reduction in the approximation of higher modes, sophisticated reduction techniques, for instance, the improved reduced system method and the system equivalent reduction expansion process [*O'CALLAHAN et al.* 1989; *PAPADOPOULOS and GARCIA* 1996], can also be employed. Another similar method along this line is the static flexibility approach [*FLANIGAN and BOTOS* 1992]. This method optimizes the static transformation matrix with the assumption that the best master DOFs are those for which the FEM mode shapes can be represented as a linear combination of static flexibility shapes with minimum errors. By this method, the mode shapes and static flexibility shapes can be alternatively viewed as two different bases for an n-dimensional space. When certain candidate sensors are eliminated, the space is shortened and the least squares fitting of the static flexibility shapes to the mode shapes can be regarded as a measure for master DOFs, which is the idea for the static flexibility approach.

2.1.9 System norm based sensor placement method

The method proposed in [*SHIH et al.* 1998] combining the controllability and observability measures is similar to the method of Gawronski [*GAWRONSKI* 2004]. The system norm based sensor placement method developed by Gawronski aims to find optimal sensor locations through balanced representation of the controllability and observability grammians. It ranks the relative importance of sensor positions according to

their non-negative contribution to the $\mathbf{H}_2$ or $\mathbf{H}_\infty$ norms of the structure. This method is revealed to be a weighted MSSP method, and the weighting coefficients are modal participation factors [*LI et al.* 2006].

2.1.10 Space domain sampling method

The space domain sampling method is proposed by Stubbs [*STUBBS and PARK* 1996], and can be regarded as an extension of Shannon's time-domain sampling theorem in space domain. It assumes that all considered modes are multiples of a basic fundamental frequency and that the sensor positions are determined only by the highest mode. The space domain sampling method is basically an equidistant sensor distribution technique and picks sensor positions at equidistant points for the half wavelength of the highest mode of interest. It does not take the characteristics of lower modes into consideration and the sensor positions determined only by the highest mode may not capture most of the kinetic energy. Therefore, the nodes of lower modes are easily included in the measurement set, which render one or several lower modes unobservable, or difficult to separate them from noise because of their low degree of observability. Furthermore, it is well-known that equidistant points could not yield the best sensor positions [*BOS.* 2007].

Another line of thinking similar to the space sampling method is to use the roots of Chebyshev polynomials as sensor positions [*PAPE* 1994]. The underlying principle is that a continuous function can be approximated by Chebyshev polynomials more exactly than other orthonormal polynomials without Gibbs phenomenon, namely the desirable effect of minimizing the maximum error in interpolation. By placing sensors at the roots of Chebyshev polynomials, the mode shapes are expected to be approximated by measurements at these positions better than other positions. However, these roots tend to cluster near the ends of the measurement interval rather than at the center, where the modal kinetic energy is usually higher than those positions near constraints. Another interpolation method investigated for sensor placement is to use spline shape functions [*LIMONGELLI* 2003].

Both spatial Shannon's sampling method and the interpolation methods using Chebyshev polynomials or spline functions regard the sensor placement as sampling problem in space domain, and aim to observe or to approximate the structural re-

sponses using the designated sampling points through constructing structural state with minimum errors.

2.1.11 Information based methods

The information based sensor placement methods are categorized by mutual information and information entropy approaches.

The mutual information between two measurements is defined as the 2-base logarithm of their joint probability density divided by both individual probability densities, and establishes a criterion of their mutual dependence [*TRENDAFILOVA et al.* 2001]. The idea of mutual information stems from Shannon's notion of information among measurements. The mutual information is, in fact, a general correlation function between two measurements. If two measurements are made at locations with a small distance, they are nearly similar and mutually dependent, the degree of which can be measured using averaged mutual information. With the increase of the measurement distance, two measurements are becoming asymptotically independent and the mutual information is approaching zero. The distance corresponding to the first minimum of the averaged mutual information is selected as the optimal one. It is considered that this distance will make the measurements at different points independent in the sense of information. The sensor placement method based on average mutual information concept will give also an equidistant configuration of sensor topology as the method of spatial Shannon's sampling theorem discussed in Section 2.1.10. In addition, the sensor placement method based on average mutual information concept takes only structural response information as inputs and does not take the individual feature of a structure, for instance, their analytical mode shapes, into account.

Besides the mutual information concept, information entropy is investigated by Papadimitriou et. al. [*PAPADIMITRIOU* 2004] as a methodology to deploy sensors. It aims to design the sensor configuration such that the resulting sensor positions are most informative about the structural model parameters selected for estimation. The most informative measured data are the ones that give the least uncertainty in the parameter estimates or, equivalently, the ones that minimize the information entropy, which quantifies the amount of useful information contained in the measured data. By this method, the optimal sensor configuration is selected as the one that minimizes the

information entropy measure since it gives a direct measure of the uncertainty in the model parameter estimates through the Bayesian perspective.

Another approach similar to the information entropy concept is to minimize the expected value of the Bayesian loss function [*HEREDIA-ZAVONI and ESTEVA* 1998; *ROBERT-NICOUD et al.* 2005]. It was shown in both methods that the information entropy depends on the determinant of the FIM, but not the trace as the EI method does.

2.2 Comments on existing sensor placement methods and their connections

The methods presented in Section 2.1 are, in fact, interrelated and connected in many respects. The latent relationship between these methods will be exposed in this section, which composes one major part of the contribution of the dissertation.

2.2.1 Connection between EI and MKE

Although the theory of both MKE and EI methods are quite straightforward and well developed, and both are widely discussed and applied, the same degree of understanding cannot be said to exist. Researchers may notice that EI can arrive at similar results as that of MKE in many circumstances, especially for the first several iterations of the EI and MKE in the cases of structures with homogeneous mass distributions, and may have a vague feeling that MKE and EI have something in common. Their relationship is, however, not explicitly and mathematically reported, at least to the knowledge of the author from the literature. From the viewpoint of the author, the difference and consistency of MKE and EI will increase the understanding of both methods and the role of each candidate sensor position played in EI. Furthermore, their relationship is essential to the basis of theoretical considerations and to the development of other effective sensor placement methods. In this section, such latent connection between the two methods is revealed.

2.2.1.1. Connection between EI and MKE for cases with identity equivalent mass matrix

For simplicity to expose the relationship between MKE and EI, an identity equivalent mass matrix (i.e., $\mathbf{M} = \alpha\mathbf{I}$) is assumed at the outset, and then the effects of non-identity equivalent mass matrix on sensor placement will be discussed. Under the assumption of an identity equivalent mass matrix and normalized mode shapes with respect to the mass matrix, the MKE index can be rewritten as the following formula,

$$MKE = \mathrm{diag}(\mathbf{\Phi}\mathbf{\Phi}^T) \tag{2.9}$$

where, operator diag denotes a column vector formed by the diagonal terms of a matrix.

Since the mode shapes are normalized with respect to the mass matrix, the middle term in the right hand side of Eq.(2.8) is just an identity matrix. Consequently, the EI index in Eq.(2.8) boils down to be the diagonal of the following matrix,

$$E_D = \mathrm{diag}(\mathbf{\Phi}\mathbf{\Phi}^T) \tag{2.10}$$

From the above Eq.(2.9) and Eq.(2.10), it can be certainly observed that the result of EI in the first computation should be the same as that of the MKE, which is already shown clearly in the examples of references using EI methods[*KAMMER and TINKER* 2004; *MEO and ZUMPANO* 2005]. The two formations of EI and MKE are identical under this circumstance. It is, therefore, unnecessary to apply MKE first when implementing EI as originally proposed by Kramer [*KAMMER and YAO* 1994]. In the following iterations, the EI indices are weighted by an inversion term of the reduced Fisher information matrix, but the MKE is not. And this is why EI is different from MKE afterwards.

When the EI in the second iteration is considered, we found that the measured sensor output formulated in Eq.(1.1) should be rewritten because a previously assumed output component is not measured anymore. Without loss of generality, the k^{th} index of EI in Eq.(2.8) in the first iteration is assumed to be the smallest and to be excluded. Then, the reduced output vector in Eq.(1.1) should be reformulated as follows,

$$\mathbf{y}_1 = \mathbf{\Phi}_1\mathbf{q}_1 + \boldsymbol{\varepsilon}_1 \tag{2.11}$$

where, $\mathbf{y}_1$ denotes the remaining measurements with the k^{th} measurement deleted in $\mathbf{y}$ of the Eq.(1.1), and ε_1 is the corresponding stationary Gaussian measurement white noise, and likewise, $\mathbf{\Phi}_1$ is the same mode shape matrix as $\mathbf{\Phi}$ in Eq.(1.1) only with the k^{th} row deleted, $\mathbf{q}_1$ is a new modal coordinate vector with the same dimensions as that of $\mathbf{q}$ in Eq.(1.1). The model described in Eq.(2.11) becomes a reduced system with only *n*-1 DOFs since the previous k^{th} DOF in the original model is rejected. Basically, we can view sensor placement broadly as an issue of system reduction, and the low-dimensional reduced system defined in Eq.(2.11) is to represent the original full-scale system in Eq.(1.1) as exactly as possible. The information discarded by excluding *n-k* sensor positions should be insignificant compared to the *k* sensors retained as a whole.

In the new reduced system with order of *n*-1, the mode shape matrix should be renormalized as the original one. Following the same procedures similar from Eq.(2.5) to Eq.(2.7) with ortho-normalized mode shapes ($\mathbf{\Phi}_1{}^T\mathbf{\Phi}_1 = \mathbf{I}$), a formulation with the same rationale can be easily obtained,

$$E_{D1} = \mathrm{diag}(\mathbf{\Phi}_1\left[\mathbf{\Phi}_1{}^T\mathbf{\Phi}_1\right]^{-1}\mathbf{\Phi}_1{}^T) = \mathrm{diag}(\mathbf{\Phi}_1\mathbf{\Phi}_1{}^T) \tag{2.12}$$

The EI index in Eq.(2.12) is degenerated once again in form into the MKE index of Eq.(2.9) in its 2nd iteration. Therefore, the key difference between the EI and MKE is that in the following iterations of EI, the reduced mode shape matrix is not renormalized, but the MKE is initially using an already normalized mode shape matrix. A reorthonormalized EI in its iterations is merely MKE.

To strengthen our arguments further, we consider a special case, in which only one mode shape is considered to compute for sensor placement by MKE and EI, respectively. In this case, the MKE indices are simply the squares of the mode shape components corresponding to the sensor positions in Eq.(2.9), *i.e.* $MKE_i = \mathbf{\Phi}_i{}^2$, and the EI indices ($E_{Di} = \mathbf{\Phi}_i{}^2 / (\sum_{i=1}^{n} \mathbf{\Phi}_i{}^2)$) are the squares of the mode shape components only divided by a constant (the squared Euclidean norm of the mode shape according to Eq.(2.8)). The only difference between both indices is a constant coefficient. Their ranked sequence is the same, no matter how many sensors are to be used.

We can now consider EI from another viewpoint. The mode shapes used in EI, regardless of ortho-normalized or not, can be decomposed using orthogonal-triangular decomposition (QR) as follows [*GOLUB and VAN LOAN* 1996],

$$\mathbf{\Phi} = \mathbf{QR} \tag{2.13}$$

where $\mathbf{Q}$ is an *n* x *k* unitary matrix with the same dimensions as $\mathbf{\Phi}$, and $\mathbf{R}$ is a *k* x *k* upper triangular matrix. Thus, the EI index can be also computed using the above decomposed $\mathbf{Q}$ and $\mathbf{R}$ matrix by substituting Eq.(2.13) into Eq.(2.8),

$$E_D = \mathrm{diag}(\mathbf{QR}\left[\mathbf{R}^T\mathbf{Q}^T\mathbf{QR}\right]^{-1}\mathbf{R}^T\mathbf{Q}^T) = \mathrm{diag}(\mathbf{QQ}^T) \tag{2.14}$$

The expression of EI in Eq.(2.14) is the same in form as that of MKE in Eq.(2.9). During each iteration of EI, it computes "the MKE index" using the reduced ortho-normalized mode shapes $\mathbf{Q}$ instead of $\mathbf{\Phi}$, retains DOFs with large MKEs, and deletes those with small MKEs.

The rationale behind the QR decomposition in Eq.(2.14) is the same as the above reasoning for the idea of viewing sensor placement as system reduction. QR decomposition is, in fact, an extension of the Gram-Schmidt orthogonalization applying to the dependent columns of reduced mode shapes $\mathbf{\Phi}_1$, which is not strictly orthogonal anymore after a certain row of the previous orthogonal mode shapes is deleted in the proceeding iteration. Consequently, the QR decomposition in Eq.(2.13) extracts an orthogonal subspace spanned by the columns of $\mathbf{Q}$. The $\mathbf{Q}$ in Eq.(2.13) is an *n* x *k* ortho-normal matrix. This means that the columns of the reduced mode shape matrix $\mathbf{\Phi}_1$ resulted from iterations of EI will be remapped onto the subspace spanned by the ortho-normalized columns of $\mathbf{Q}$. And it is exactly these columns of $\mathbf{Q}$ that will combine to form the reduced measurement vector $\mathbf{y}$. In dynamic testing, it is also these columns of $\mathbf{Q}$ that are identified as mode shapes of the reduced system being measured.

As a result, the difference and consistency between MKE and EI is clear. EI requires iteration computations, but MKE not. In the following iterations of EI, it redistributes the modal kinetic energy into the retained DOFs and recomputes their MKE index for the reduced system using re-orthonormalized mode shapes. EI can thus be regarded as an iterated version of MKE with re-orthonormalized mode shapes.

2.2.1.2. Connection between EI and MKE for cases with non-identity equivalent mass matrix

For cases of a general mass matrix, namely non-identity equivalent mass matrix (i.e., $\mathbf{M} \neq \alpha \mathbf{I}$), the above reasoning in Section 2.2.1.1 can be generalized. The MKE index is computed by,

$$MKE = \mathrm{diag}(\mathbf{M}\boldsymbol{\Phi}\boldsymbol{\Phi}^T) = \mathrm{diag}(\mathbf{M}^{1/2}\boldsymbol{\Phi}\boldsymbol{\Phi}^T\mathbf{M}^{1/2}) \tag{2.15}$$

where, $\mathbf{M}^{1/2}$ is the square root of the semi-definite mass matrix $\mathbf{M}$. In MKE, each candidate DOF is weighted by the corresponding component in the mass matrix. For those DOFs associated with large components in the mass matrix, they are given more weights in the ranking of their importance for sensor placement. Hence, MKE reflects the characteristics of mass distribution for a given structure as well. In this respect, MKE share certain common interests with the GRSP to focus on candidate sensor positions with comparative large mass concentrations.

On the other hand, the EI index is not explicitly related to the mass distribution of a structure. Once the mass matrix is determined and the mode shapes are obtained, the sensor placement scheme with EI does not take uneven mass distribution of a structure into consideration in its iterations anymore, although the mode shapes are initially orthonormalized with respect to the mass matrix, $\Phi^T\mathbf{M}\Phi = \mathbf{I}$.

An interesting observation can be obtained by comparing Eq.(2.15) with Eq.(2.10) for the case of non-identity equivalent mass matrix. MKE assigns more weights for the DOFs with large mass concentration by left multiplying the EI indices at the first iteration with the mass matrix. When the mass is only slight unevenly distributed throughout the whole structure, which is common in engineering practice, the relative sequence of the MKE indices will agree with that of the EI very well. In this sense, MKE can be regarded as a weighted EI without iterations for structures with general mass distributions.

2.2.1.3. Fast computation of EI through QR downdating

Conventionally, the EI method is computed through two different approaches, one

through the eigenvalue decomposition as shown from Eq. (2.5) to Eq.(2.7), and the other through computing the diagonal terms of the mode shape projection matrix in Eq.(2.8). The former is annotated hereinafter as Method A, in which the core processes are featured by the explicit formation and eigenvalue decomposition of an FIM, and the later is termed afterwards as Method B.

Method A is convenient to compute with standard eigenvalue decomposition algorithms but requires the explicit formation and eigenvalue decomposition of an FIM, during which roundoff errors are accumulated through inner products. Furthermore, the sensitivity of relative errors for the eigenvalue decomposition of the FIM depends adversely on the square of the condition of the mode shape matrix $\mathbf{\Phi}$ in the method A. On the other hand, method B through projection matrix approach is, at first glance, rather simple. However, it suffers from the same roundoff errors' accumulation during the explicit formation of the FIM as the Method A. In addition, the computational burden of the projection matrix is intense and the roundoff errors are twofold worsened, especially when the rows are far more than the columns of the mode shape matrix $\mathbf{\Phi}$, *i.e.*, the number of candidate sensor positions *n* is much larger than the number of interested mode shapes *m* with the consideration of iterations in the EI in mind.

Fortunately, the relationship between the EI and MKE in Section 2.2.1.1 provides an efficient and stable means for the computation of the EI index through decomposed orthonormal matrix $\mathbf{Q}$ in Eq.(2.14). Since the matrix $\mathbf{Q}$ is orthonormal, it can be rewritten as *n* row vectors, $\mathbf{Q} = [q_1^T, q_2^T, \cdots, q_n^T]^T$, with each row vector, q_k^T, of 1x*m* dimension. Eq.(2.14) then boils down to the computation of the row norms of $q_k^T, 1 \le k \le n$, as follows

$$E_D = \mathrm{diag}(\mathbf{Q}\mathbf{Q}^T) = [q_1^T \cdot q_1, q_2^T \cdot q_2, \cdots, q_n^T \cdot q_n]^T = [\|q_1\|_2^2, \|q_2\|_2^2, \cdots, \|q_n\|_2^2]^T \tag{2.16}$$

The above reformulation of Eq.(2.14) into Eq.(2.16) with the QR decomposition enables a nice way to compute the EI indices in the following two steps,

(1) Decompose a (reduced) mode shape matrix $\mathbf{\Phi}$ with the QR decomposition to obtain an *n* x *m* orthonormal matrix $\mathbf{Q}$.

(2) Compute the norms of the row vectors that form $\mathbf{Q}$ and get the EI indices.

The remaining procedures, such as to select the sensor positions with the smallest EI index to remove and to iterate until the number of sensors equals to a required value, are routinely the same. It is worth to note that the upper triangular matrix $\mathbf{R}$ is useless in the first step and does not need to be stored after the QR decomposition, which can save computer memory capacity and increase computation efficiency to a certain degree. This approach is expected to produce more accurate results than Method A and B since the QR decomposition is a well known stable and precise algorithm in matrix computations [*LI et al.* 2009a].

To analyze and compare computational efficiency of the new approach with Method A and B, the two-step approach to compute the EI indices through the QR decomposition in the last paragraph is named Method C. In addition to its accuracy, the Method C is supposed to compute much faster than the Method A and B. To this end, we examine the computational efficiency in terms of floating point operations (flops) required by the three methods. In the Method A, the FIM, $A_0 = \mathbf{\Phi}^T \mathbf{\Phi}$ *, has to be formed first through matrix multiplication, which needs m^2n flops [*GOLUB and VAN LOAN* 1996]. The eigenvalue decomposition of the FIM involves $8m^3$ flops, and the implementation of subsequent three times matrix multiplications and additions requires flops in order of $2mn$. Therefore, the total computation flops needed by the Method A is

$$T_A = 2m^2 n + 8m^3 + 2mn \tag{2.17}$$

Similarly, the Method B can be treated in the same way. Computation of the projection matrix spanned by the mode shape $\mathbf{\Phi}$ requires 3 times matrix multiplications and one time matrix inversion. The inversion of the FIM involves $2m^3$ flops besides the m^2n flops to its formation as in Method A. The remaining two times matrix multiplication requires $mn^2 + m^2n$ flops. Consequently, the computation flops demanded by the Method B is

$$T_B = 2m^2 n + 2m^3 + mn^2 \tag{2.18}$$

It is straightforward to evaluate the computational efficiency for the Method C likewise, in which only two steps are required and it is unnecessary to form an explicit FIM as

* The constant $\Psi_0^{\ 2}$ is dropped here for convenience.

the Method A and the Method B anymore. The computation of an *n* by *m* mode shape matrix with the skinny QR decomposition involves $2m^2(n-m/3)$ flops in the first step. Addition of the squared *n* by *m* orthonormal matrix $\mathbf{Q}$ in the second step requires only 2*mn* flops, which is negligible compared with the QR decomposition. On the whole, the computation flops involved in the Method C is

$$T_C = 2m^2 n - \tfrac{2}{3}m^3 + 2mn \tag{2.19}$$

It is obvious to conclude by comparing Eq.(2.19) with Eq.(2.18) and Eq.(2.17) that the computation flops for the proposed Method C is less than that demanded by Method A and the Method B as long as the candidate DOFs of a structure is more than 2. The condition of more than 2 candidate DOFs is naturally satisfied since otherwise there is no need to investigate where to deploy sensors. As a result, Method C is always superior in computation efficiency than the Method A and B. To demonstrate how efficient the Method C outperforms Method A and Method B, we compare the computational burden of the sensor placement problem for a model structure to offer some insights. The model structure in question has in total 120 candidate DOFs and 30 interested mode shapes, and the available number of sensors are the least 30, which equals to the mode shape number. The required flops for Method A, Method B and Method C in one loop of the EI are 439200, 702000 and 222600, respectively. The Method C counts less than half of the flops as does the Method A and almost one fourth of the flops executed by the Method B. Furthermore, such differences in the amount of work involved in the three methods discussed above reside in just one iteration. When the total 90 iterations of the EI for the model structure are considered, the saved computation flops by the Method C is significant.

The reasons why Method C surpass Method A and Method B are that Method C does not need to explicitly form the FIM as what the Method A and Method B demand and saves the flops required to multiply matrices, but operates directly on the mode shape matrix Φ. Moreover, the formation of the FIM through inner products in double precision exacerbates the accumulation of roundoff errors and is exposed to errors due to the amplified numerical rank deficiency. For a typical large structure, candidate sensor positions counts in order of thousands to tens of thousands. The amount of work for sensor placement is thus not insignificant, and computation un-

certainties are of great concern. Hence, Method C is particularly preferable because of its accuracy and efficiency for such intensive computations.

As shown in Section 2.1.4, the EI requires as many as *n*-*s* iterations, during which the core processes, for instance, the eigenvalue decomposition in the Method A, the inversion of the FIM in the Method B and the QR decomposition of Method C, have to be computed repetitively. Although Method C secures a better overall computational efficiency over Method B and Method C, the fundamental QR decomposition process in Method C still appears too expensive if repeatedly executed for each reduced mode shape matrix after a row in the previous mode shape matrix is removed during all iterations of the EI, in particular, when huge numbers of candidate sensor positions for large civil structures are considered. In the following, a downdating algorithm is embedded to eliminate repeated execution of the QR decomposition on reduced mode shape matrices, and improve the computational efficiency of Method C to a greater extent.

In the first iteration of Method C, the QR decomposition can be rewritten as [*BJÖRCK* 1996; *YOO and PARK* 1996],

$$\mathbf{\Phi} = \begin{pmatrix} z^T \\ \mathbf{\Phi}_1 \end{pmatrix} = \mathbf{QR} = \begin{pmatrix} p^T \\ \mathbf{Q}_1 \end{pmatrix} \mathbf{R} \tag{2.20}$$

where $z^T \in \mathbf{R}^{1\times m}$ and $p^T \in \mathbf{R}^{1\times m}$ are the first row of $\mathbf{\Phi} \in \mathbf{R}^{n\times m}$ and $\mathbf{Q} \in \mathbf{R}^{n\times m}$, respectively. It is assumed in Eq.(2.20) that the row, $p^T \in \mathbf{R}^{1\times m}$, has the least E_D index or the row norm among all *n* rows in $\mathbf{Q}$ and is to be removed in the subsequent iteration according to the EI. If it is not the case, the row with the least E_D index, $p^T \in \mathbf{R}^{1\times m}$, can be exchanged to the top of $\mathbf{Q}$ without any difficulty. The QR downdating means to find a new QR decomposition with $\mathbf{Q}_1$ in dimension of *n*-1 by *m* after a row (a candidate sensor position) is removed from the previous mode shape matrix $\mathbf{\Phi}$ with dimension of *n* by *m* satisfying the condition,

$$\mathbf{\Phi}_1 = \mathbf{Q}_1 \mathbf{R}_1 \tag{2.21}$$

The QR downdating is, in fact, a rank one modification to the previous QR decomposition and has the advantage to perform as fewer operations and as little storage requirement as possible. On the contrary, recomputing the QR decomposition in every

iteration of the EI is too costly since it requires operations in order of m^2n as expressed in Eq.(2.19).

Recent progress in the field of matrix computation renders such skinny QR downdating possible as shown by Yoo and Park [*YOO and PARK* 1996]. Firstly, a series of plane rotations, $\mathbf{U}$, operates on the first row of $\mathbf{Q}$, $p^T \in \mathbf{R}^{1\times m}$, to transform it into a unit row vector that has only one nonzero component in its first position that equals one as

$$\mathbf{\Phi} = \begin{pmatrix} z^T \\ \mathbf{\Phi}_1 \end{pmatrix} = \begin{pmatrix} p^T & \alpha \\ \mathbf{Q}_1 & h \end{pmatrix} \mathbf{U}^T \mathbf{U} \begin{pmatrix} \mathbf{R} \\ 0 \end{pmatrix} = \begin{pmatrix} 1 & 0 \\ 0 & \mathbf{Q}_1 \end{pmatrix} \begin{pmatrix} v^T \\ \mathbf{R}_1 \end{pmatrix} = \begin{pmatrix} v^T \\ \mathbf{Q}_1\mathbf{R}_1 \end{pmatrix} \tag{2.22}$$

where α, a constant, and $h, v \in \mathbf{R}^{(n-1)\times 1}$ are the complementary parameter and vectors satisfying the conditions: $p^T p + \alpha^2 = 1$ and $\mathbf{Q}_1^T p + \alpha h = 0$. Consequently, when the first row of $\begin{pmatrix} p^T & \alpha \\ \mathbf{Q}_1 & h \end{pmatrix}$ is transformed to a unit row vector, $e_1^T = [1,0,0,\cdots,0] \in \mathbf{R}^{1\times(n+1)}$, the first column will also become $e_1 = [1,0,0,\cdots,0]^T \in \mathbf{R}^{m\times 1}$ since $\begin{pmatrix} p^T & \alpha \\ \mathbf{Q}_1 & h \end{pmatrix}$ is orthogonal, which is the key for the Gram-Schmidt downdating algorithm [*DANIEL et al.* 1976].

However, the orthogonal factor $\mathbf{Q}_1$ may lose orthogonality obtained from the Gram-Schmidt procedure when the condition of $\mathbf{\Phi}$ is large, especially when many iterations are considered. To overcome this difficulty, the Householder transformations are applied to recover orthogonality, which utilizes the fact that a full QR decomposition of a matrix $\mathbf{A} \equiv \begin{pmatrix} 0_{m\times m} \\ \mathbf{\Phi} \end{pmatrix} \in \mathbf{R}^{(m+n)\times m}$ by the Householder transformations can be completely determined by the skinny QR decomposition of $\mathbf{\Phi}$ obtained by the Gram-Schmidt process. Using this relation, the full Gram-Schmidt QR decomposition of a matrix $\mathbf{\Phi}$ augmented with a square matrix of zero elements on top, can be written as,

$$\mathbf{A} = \begin{pmatrix} 0_{m\times m} \\ \mathbf{\Phi} \end{pmatrix} = \begin{pmatrix} 0_{m\times m} & \mathbf{Q}^T \\ \mathbf{Q} & \mathbf{I} - \mathbf{Q}\mathbf{Q}^T \end{pmatrix} \begin{pmatrix} \mathbf{R} \\ 0_{n\times m} \end{pmatrix} \tag{2.23}$$

Since deleting the first row of $\mathbf{\Phi}$ is equivalent to deleting the (m+1)th row of $\mathbf{A}$, the downdated new upper triangular factor $\mathbf{R}_1$ for $\mathbf{\Phi}_1$ can be obtained by downdating the

full QR decomposition of $\mathbf{A}$. This is done by determining a series of Householder downdating transformations for deleting the first row of $\mathbf{\Phi}$ according to the first row of $[\mathbf{Q}, \mathbf{I} - \mathbf{Q}\mathbf{Q}^T]$ with the same Gram-Schmidt process as in Eq.(2.22), and we finally obtain the downdated QR decomposition factors, $\mathbf{Q}_1$ and $\mathbf{R}_1$, for $\mathbf{\Phi}_1$. This is called the Householder-Gram-Schmidt Downdating (HGSD) algorithm, referring [*YOO and PARK* 1996] for more details. The Gram-Schmidt downdating algorithm for the skinny QR decomposition of $\mathbf{\Phi}$ is mathematically equivalent to downdating the full Householder QR decomposition of $\mathbf{A}$, and the effect is as if the downdating transformation is computed based on the full QR decomposition with the orthogonal factor computed from the Householder transformations.

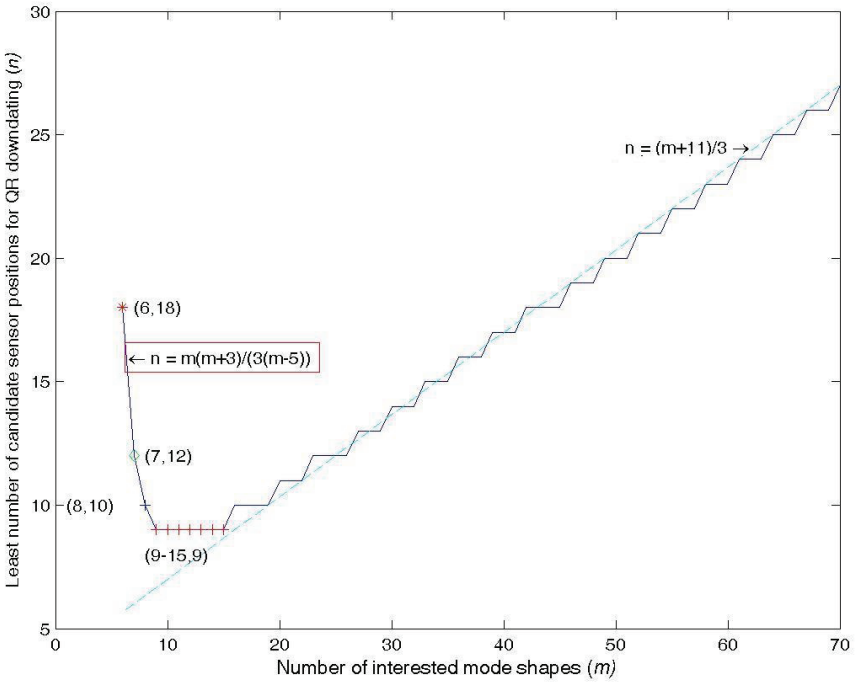

Fig.2-1, Condition of the relation between interested mode shapes (*m*) and the least number of candidate sensor positions (*n*) that QR downdating outperforms a new QR decomposition.

By replacing the first step of Method C, the QR decomposition, with the QR downdating Algorithm HGSD, we can further improve the computational efficiency of the EI. Later on such modified Method C is called Method D for the purpose of comparison and notation convenience. It is not difficult to evaluate the flops involved in the Meth-

od D. The computation includes the QR downdating Algorithm HGSD and the norms of the squared orthonormal matrix $\mathbf{Q}$. The former needs approximately $2m^2+10mn$ flops and the latter requires the same 2*mn* flops as Method C. Therefore, the computation flops involved in the Method D in total is

$$T_D = 2m^2 + 12mn \tag{2.24}$$

The model structure is employed again to illustrate the computational efficiency of Method D and its comparison with that of the other three methods discussed previously. The flops required by Method A, B, C and D to compute the sensor placement for the model structure are 439200, 702000, 222600 and 45000, respectively. The ratio of computation complexity of the Method A, Method B and Method C to Method D are 9.7600: 15.6000: 4.9467: 1. It is obvious that the Method D executes almost 9, 14 and 4 times faster than the Method A, Method B and Method C, respectively, and that the improvement of computational efficiency over the other three methods is considerable in this case.

Moreover, it can be shown that the Method D outperforms the other three for almost all cases. Recall that the overall computational complexity of the HGSD is approximately $2m^2+10mn$ and that a brand new QR decomposition starting from scratch demands $2m^2(n-m/3)$ flops. It is trivial to reveal that the exact condition for the QR downdating by the HGSD outperforming over a new QR decomposition is: $n > \frac{m^2+3m}{3(m-5)} = \frac{1}{3}(m+8) + \frac{40/3}{m-5}$. The blue solid curve in Fig.2-1 shows the nonlinear relationship between the number of interested mode shapes (*m*) and the least number of candidate sensor positions (*n*) that the QR downdating outperforms a new QR decomposition. The curve is clearly divided into three regions. In the fist region for *m* ranging from 6 to 9, *n* is sharply decreasing with the increase of *m*. To offer some insights for this tendency, three points are indicated with a red asterisk (*m*=6), a green diamond (*m*=7) and a blue plus (*m*=8), respectively. The least number of sensor positions for the three cases are 18, 12 and 10, separately. The second region is flat, in which the least number of sensors stays a constant, 9, regardless of the variation of *m* in the range of 9 to 15. The third region starts from 15 (*m*=15) and the curve follows approximately a linear relationship, $n = \frac{1}{3}(m+11)$, as indicated by the cyan

dotted line. As we already know that the necessary number of sensor positions at last equals to the number of interested mode shapes for adequate modal identification. Consequently, the conditions restrained by the second and third regions in Fig.2-1 are naturally satisfied when the number of interested mode shapes *m* is greater than 9.

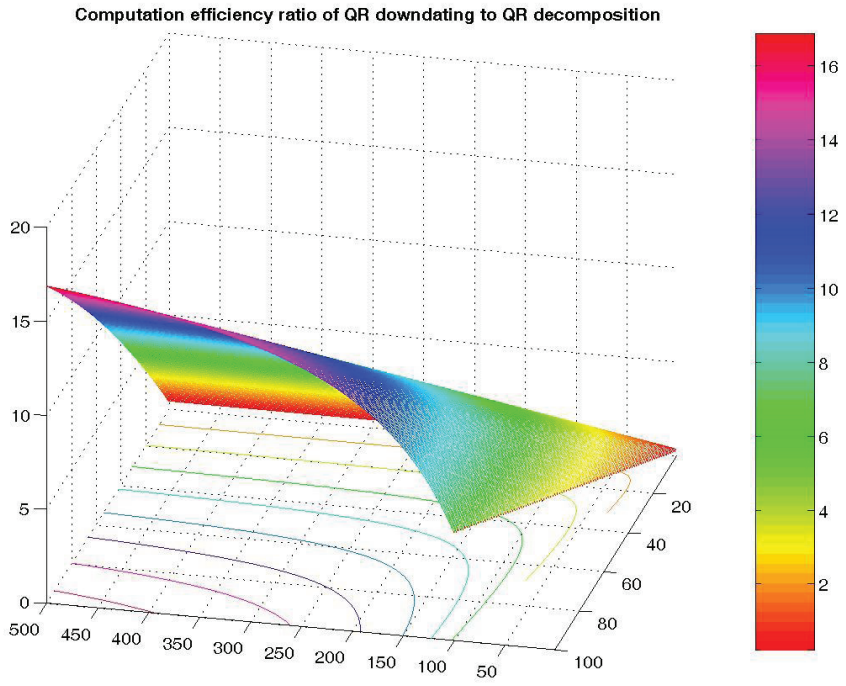

Fig. 2-2, Relative computation efficiency ratios of the QR downdating to a new QR decomposition.

Furthermore, Fig.2-2 shows the relative computing efficiency ratios of the QR downdating to a new QR decomposition. The inclined vertical axis in the horizontal plane is the number of mode shapes of interest *m* and the vertical axis in the horizontal plane indicates the number of candidate sensor positions *n*. The vertical axis shows the relative computation efficiency ratios of the QR downdating to a new QR decomposition. The figure is based on the computation flops required by the QR downdating in Eq.(2.24) and that by the QR decomposition in Eq.(2.19). The contours in the horizontal plane differentiate regions with various computation efficiency ratios. It is obvious that the QR downdating far outperforms repetitive QR decomposition by a ratio in an order of tens when there are more than 50 mode shapes and 300 candi-

date sensor positions. As mentioned earlier, candidate sensor positions counts in order of thousands to tens of thousands with more than tens of interested mode shapes for a large structure, and the improvement of the QR downdating over a completely new QR decomposition is substantial, in particular, when iterations of the EI are considered.

I have coded the Algorithm HGSD in the Matlab [*HIGHAM and HIGHAM* 2005; *MATLAB*] as shown in Appendix 2B. The appended function can be directly copied and pasted to run, and further tailored to embed in their own programs. (Anyway, we do not guarantee that the source codes are the most efficient, and it is the users' obligation to justify its applications).

2.2.2 Relationship between EI and QRD

The QRD method operates QR decomposition on a transposed mode shape matrix and finds the most independent rows as described in Section 2.1.5. Since the diagonal elements of the upper triangular matrix in QR decomposition is arranged in descending order of their absolute values, the first m linearly independent rows selected in this way by QRD are also those rows with large row norms. In this sense, the QRD method in the selection of its first row (first sensor location) during its first run has the same physical significance as that of EI. The other rows selected by QRD and EI differ since EI orthonormalizes the columns whereas QRD on the rows.

As a summary, the QRD method selects sensor positions according to their row norms and linear independency in the row space, whereas EI computes QR decomposition in the column space of the modal matrix. To be more precisely, the EI operates on the original full modal matrix to search iteratively for a sub-matrix with columns as independent as possible, whereas the QRD method finds a sub-matrix from the perspective of row independence for one time. Both the EI and QRD will give quite similar results when the required number of sensors, s, equals to the number of modes m, i.e. the final modal sub-matrix is square, as shown on the airplane model to select 29 response locations for 29 modes both by the EI and QRD [*PICKREL* 1999]. When more sensors are needed, they will give different sensor combinations. Moreover, the difference between EI and QRD results from the reorthogo-

nalization of the column space or the row space of the original full modal matrix during the EI or QRD computation, respectively.

2.2.3 Connection between EI and MinMAC

To discuss the relationship between the EI and MinMAC algorithm, we consider first a special case, in which only two mode shapes are of interest to compute for sensor placement by the EI and MinMAC, respectively. Both mode shapes are assumed to be already unit orthonormalized. Without loss of generality, they can be written as $\Phi = \begin{bmatrix} \mathbf{A}_1 \mathbf{A}_2 \\ a_1 \; a_2 \end{bmatrix}$, $\Phi \in \mathbf{R}^n$, where $[a_1, a_2]$ is the row with the smallest Frobenius norm, i.e. $a_1^2 + a_2^2$ is minimum among all the rows, and is to be deleted according to the EI in the first iteration. For the reduced mode shapes $\Phi = [\mathbf{A}_1 \quad \mathbf{A}_2]$ after one EI iteration, we can then compute its MAC matrix as follows, $MAC_1 = \begin{bmatrix} \mathbf{A}_1^T \mathbf{A}_1 & \mathbf{A}_1^T \mathbf{A}_2 \\ \mathbf{A}_2^T \mathbf{A}_1 & \mathbf{A}_2^T \mathbf{A}_2 \end{bmatrix}$. The off-diagonal term of the MAC matrix is $\mathbf{A}_1^T \mathbf{A}_2$. Since $\Phi^T \Phi = \begin{bmatrix} \mathbf{A}_1^T \mathbf{A}_1 + a_1^T a_1 & \mathbf{A}_1^T \mathbf{A}_2 + a_1^T a_2 \\ \mathbf{A}_2^T \mathbf{A}_1 + a_2^T a_1 & \mathbf{A}_2^T \mathbf{A}_2 + a_2^T a_2 \end{bmatrix} = \begin{bmatrix} 1 & 0 \\ 0 & 1 \end{bmatrix}$, we know that $\mathbf{A}_1^T \mathbf{A}_2 = -a_1 a_2$. By MinMAC algorithm, $a_1 a_2$ is to be minimized, which is equivalent of the EI to minimize the row Frobenius norm, $a_1^2 + a_2^2$. This equivalence of EI and MinMAC for the case with two mode shapes can not simply be generalized to the cases with more than two mode shapes since the minimization of the multiple of any two variables does not always lead to the minimization of the sum of their squares. However, it can be tackled to a certain degree. Without loss of generality, we compare the j^{th} and k^{th} row when m mode shapes are involved as follows,

$$\left(\sum_{p=1}^{m} \left| \Phi_{np} \right| \right)^2 = \sum_{p=1}^{m} \Phi_{np}{}^2 + 2 \sum_{\substack{p=1,q=1 \\ p \neq q}}^{m} \Phi_{np} \Phi_{nq}, \; \mathrm{n} = j, k \tag{2.25}$$

The term in brackets on the left hand side of Eq.(2.25) is the MSSP indices as discussed in Section 2.1.2, and can be regarded as the L_1 norm of the j^{th} or k^{th} row. The first term on the right in Eq.(2.25) is the j^{th} or k^{th} MKE indices explained in Section 2.1.1.

Under the formulation in Eq.(2.25), the EI tries to maximize the first term on the right hand side of Eq.(2.25), whereas the MinMAC aims to minimize the second term. Two situations are considered. When the L_1 norm of the j^{th} row equals to the L_1 norm of the k^{th} row, maximization of the first term (EI indices) will naturally lead to the minimization of the second term (MinMAC) for the whole scale. The EI and MinMAC are equivalent in a global sense under this situation. When the L_1 norms of the j^{th} and k^{th} rows do not equal, we can assume that $\left|\Phi_{jp}\right| \geq \left|\Phi_{kp}\right|, p = 1,2,...m$, and more specifically, $\left|\Phi_{j1}\right| \geq \left|\Phi_{j2}\right| \geq ... \geq \left|\Phi_{jm}\right|, \left|\Phi_{k1}\right| \geq \left|\Phi_{k2}\right| \geq ... \geq \left|\Phi_{km}\right|$. This is, of course, a rare case, but used here for demonstration purpose. The maximum off-diagonal terms of the MAC matrix will possibly be determined by $\left|\Phi_{j1}\Phi_{j2}\right|$ for the j^{th} row, and $\left|\Phi_{k1}\Phi_{k2}\right|$ for the k^{th} row, and it is clear that $\left|\Phi_{j1}\Phi_{j2}\right| \geq \left|\Phi_{k1}\Phi_{k2}\right|$. Then, MinMAC tends to keep the k^{th} row and discard the j^{th} row. On the other side, EI will definitely choose the j^{th} row to remove.

We can treat this relationship from a perspective of matrix theory to a lesser effort. The EI tries to maximize the trace of the projection matrix, $\Phi\Phi^T$, according to Eq.(2.10) with orthonormalized mode shapes during its iterations and it is a well-known equation in matrix theory that,

$$tr(\Phi\Phi^T) = tr(\Phi^T\Phi). \tag{2.26}$$

The bracket term on the right hand side of Eq.(2.26) is just the MAC matrix, whose off-diagonal terms are to be minimized by the MinMAC algorithm with each mode shape normalized to unit length. Therefore, the maximization of the diagonal terms of the projection matrix on the left hand of Eq.(2.6) by the EI leads naturally to the minimization of the off-diagonal terms of the MAC matrix by the MinMAC algorithm since $\left\|\Phi\Phi^T\right\|_2 = \left\|\Phi^T\Phi\right\|_2$. Therefore, the EI method is equivalent to the MinMAC algorithm in the global sense, as already observed for the case of two mode shapes.

On the other hand, there are minor differences between the EI and MinMAC. The latter tries to minimize its maximum off-diagonal terms by tracking every off-diagonal terms of the MAC matrix, whereas the former minimizes all the off-diagonal terms in the sense of the whole MAC matrix. Namely, the minimization of the off-diagonal terms by iterative EI in the norm sense could not always leads to the decreasing of the maximum off-diagonal terms defined to be minimized by MinMAC, as shown in

the GARTEUR SM-AG-19 Testbed model [*BALMES* 2005]. Secondly, the EI method includes an implicit step of reorthonormalization during its iterations. This implicit re-orthonormalization step results in small deviation from the directions of the reduced mode shapes, while the MinMAC sticks stubbornly to the directions of the reduced mode shapes. This adds for the differences between the EI and MinMAC. Fortunately, such deviation is usually quite small, otherwise the final reduced mode shapes will not point to the same directions as that of the original full mode shapes, and renders the mode shapes indistinguishable. As a result, the EI and MinMAC have similar global trend in their sensor selections with small ripples of difference.

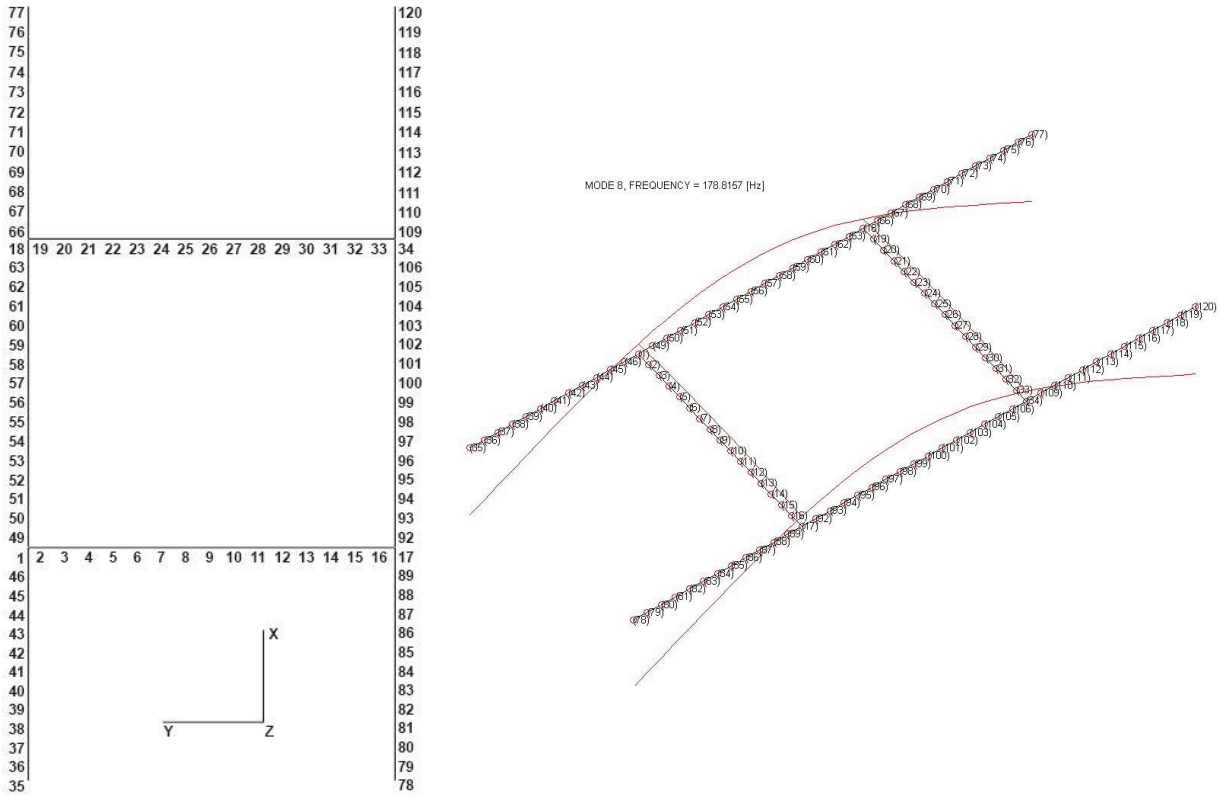

Fig. 2-3, A ladder structure and its 8th mode shape

2.2.4 Comments on the weighting of the mode shapes in EI

There are investigations in the literature to assign different weights on the mode shapes to emphasize their relative importance [*MEO and ZUMPANO* 2005], which will be dealt with in this subsection. The role of weighting in EI can be expressed as

$$\widetilde{\mathbf{\Phi}} = \mathbf{\Phi W} \tag{2.27}$$

where $\mathbf{W}$ is a diagonal weight matrix with each diagonal term the relative weight of corresponding mode shape and $\widetilde{\mathbf{\Phi}}$ represents the weighted mode shapes matrix.

Table 2-1, Frequencies of the first 12 bending modes in z direction

Mode No.	1	2	3	4	5	6	7	8	9	10	11	12
Frequencies: (Hz)	178.82	223.84	272.87	333.65	344.00	371.19	390.83	460.12	547.58	640.23	941.07	942.47

Following the same rationale in Section 2.2.1.1, the weighted mode shape matrix can be decomposed using orthogonal-triangular decomposition (QR) as follows

$$\widetilde{\Phi} = \mathbf{QRW} = \mathbf{Q}\widetilde{\mathbf{R}} \tag{2.28}$$

Table 2-2, MAC matrix for full sensor set

1	0	0.001	0.002	0.000	0.000	0.007	0.000	0.003	0.000	0.014	0.000
	1	**0.783**	0.000	0.000	0.003	0.000	0.000	0.004	0.000	0.000	0.007
		1.000	0.007	0.073	0.174	0.087	0.000	0.007	0.001	0.002	0.014
			1.000	0.012	0.004	0.057	0.002	0.001	0.018	0.020	0.045
				1.000	**0.473**	0.000	0.000	0.066	0.019	0.000	0.000
					1.000	0.417	0.001	0.050	0.020	0.008	0.000
						1.000	0.000	0.003	0.000	0.009	0.000
							1.000	0.354	0.000	0.000	0.000
			Sym.					1.000	**0.531**	0.005	0.032
									1.000	0.000	0.000
										1.000	0.000
											1.000

The EI indices becomes then

$$E_D = \mathrm{diag}(\mathbf{Q}\widetilde{\mathbf{R}}\left[\widetilde{\mathbf{R}}^T\mathbf{Q}^T\mathbf{Q}\widetilde{\mathbf{R}}\right]^{-1}\widetilde{\mathbf{R}}^T\mathbf{Q}^T) = \mathrm{diag}(\mathbf{Q}\mathbf{Q}^T) \tag{2.29}$$

Therefore, the EI indices do not change for the mode shapes with different weights. A direct consequence is that any attempt to weight the mode shapes through assigning different weighting factors turns out to be fruitless.

However, a preferred advantage associated with this property is that EI differentiate each mode shape only by their directions and the coupling of them. As a result, the EI is invariant under different mode shape normalization methods, for instance, normalization with respect to mass or unit length normalization. This is actually a significant property of EI and could not be found in other existing sensor placement methods.

2.3 Comparison of different sensor placement methods on a ladder structure

A simulation model of a ladder structure is shown in Fig.2-3. On the left is the FEM meshing, and the 8th mode (ranking in available 22 modes) is displayed on the right side. The model is provided by Carne, and unfortunately detailed material properties and dimensions are unavailable.

We have chosen 12 target modes, which represent first 12 bending modes of the rails and rungs. The frequencies of the 12 bending modes are shown in Table 2-1. Only translational modes in z direction are considered in this work to keep this example manageable in a small scale.

Table 2-2 shows the MAC matrix for the full sensor set, i.e. all 112 node positions in z direction. Examining this matrix, one can surprise that several off-diagonal terms are fairly large. In particular, the element (2,3) is 0.783, and element (9,10) is 0.531. This is due to the similarity of mode shapes between third and fourth as well as between tenth and eleventh. In is worth to note that only the mode shape components of translational DOFs in z direction are considered in this example, and they are thus not necessary to be orthogonal. The orthogonal property applies to full mode shapes.

We will use the ladder example to compute sensor positions with the methods discussed in Section 2.1.1. Two cases are considered. In Case 1, total 12 sensor positions will be selected, which corresponds to the minimum number of sensors. In Case 2, 20 sensor positions are to be chosen. The number of 20 is chosen arbitrarily for demonstration purpose. One may select 4 end points of the ladder as an intuition set, 35, 77, 78, 120, for the MinMAC algorithm. Table 2-2 shows the comparison results for two cases. It is clear that no two methods give the same results.

Table 2-2, Sensor positions obtained by different methods

	Case 1 (12 sensors)	Case 2 (20 sensors)
MKE	78,77,120,35,79,119, 76, 36, 80, 8, 118, 9	..., 7, 75, 10, 6, 37, 27, 28, 11 [a)]
ECP	78,79,120,77,119,80,35,118,76,36,102,53	..., 95, 103, 96, 54, 52, 101, 60, 37 [a)]
MSSP	78,120,77,79,35,119,76,36,80,118,75, 37	..., 8, 7, 102, 6, 103, 9, 101, 10 [a)]
DPR	27,26,25,28, 24,29,23,22,30,54,55, 53	..., 56, 57, 52, 21, 58, 51,20, 59 [a)]
EI	120,115,101,95,88,42,35,34,30,22,18, 11	120,115,101,100,95,94,88,43, 42,35,34,33, 30,26,22,20,18,12,11,6
QRD	78,120,77,35,8,27,56,100,94,22,109,31	…, 79, 119, 76, 36, 9, 26, 101, 55 [a)]
MinMAC	120,104,101,100,99,98,96,78,77,35,9, 6	120,104,103,102,101,100,99, 98,96,78,77,45, 44,43,35,30,29,9,6,2
MaxSV	4,9,25,26,31,35,76,77,78,79,119,120	17,18,31,35,36,37,49,63,75,76,77,78, 79,80,92,103,106,118,119,120 [b)]
Max-TRACE	8,9,35,36,76,77,78,79,80,118,119,120	7,8,9,10,11,25,26,27,28,29,35,36, 76,77,78,79,80,118,119,120 [b)]

Note: [a)] ..., means the sensors selected in Case 1 are also included in Case 2.

[b)] the set of sensor positions are obtained by guided search in 1e6 iterations and believed to be sub-optimal, but not guaranteed to be global optimal.

Table 2-2 shows the comparison results for two cases. It is clear that no two methods give the same results. To demonstrate the discrepencies of these methods, sensor positions selected by two representative methods, namely MKE and EI, are indicated with blue and red squares in Fig. 2-4, respectively. Sensor positions chosen by other sensor placement methods in Table 2-2 are not listed here for conciseness.

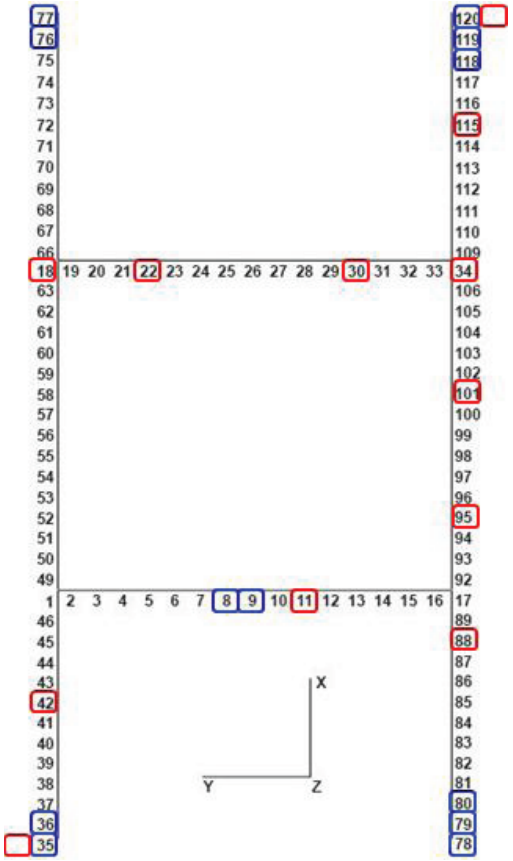

Fig. 2-4, Sensor positions chosen by MKE (blue squares) and EI (red squares) for the ladder structure

Appendix 2A.

To compute the EI indices from the projection matrix, the idempotency relation, $\mathbf{P}^2 = \mathbf{P}$, is required. Consider the diagonal terms of the projection matrix,

$$p_{ii} = (\mathbf{P})_{ii} = (\mathbf{P} \cdot \mathbf{P})_{ii} = \mathbf{P}(i,:) \cdot \mathbf{P}(:,i) = \sum_{\substack{i=1 \\ i \neq j}}^{n} p_{ij}^2 + p_{ii}^2,$$

Since the first term in the right hand side of the equation is nonnegative, therefore it can be concluded,

$$p_{ii} - p_{ii}^2 = p_{ii}(1 - p_{ii}) \geq 0.$$

In the end, $0 \leq p_{ii} \leq 1$.

Appendix 2B.

```
function [Q2,R2] = QR-HGSD(Q,R);
% QR-GSD(Q,R) computes the updated Q2 and R2 with a lower dimension
% after the first row in Q is removed. Q2*R2=Q(2:end,:)*R.
[row, col]  = size(Q);
unitvector  =  zeros(row,1);      % unit vector, e1
unitvector(1)  =  1;

en1  =     zeros(row+col,1);      % unit vector, e(col+1)
en1(col+1)  =  1;

unitmatrix  = eye(col,col);
R2  =  [ R;   zeros(1,col)];     % for step 4.

% 1, Computes the alpha and h, which are orthogonal to Q
   %(a) computes the first row:
   g  =  unitvector;
   for k  =  1:col;
       g  =  g-(g.'*Q(:,k))*Q(:,k);
   end

   %(b) determine the Householder vector x for H:x=g+sign(g1)||g||2*e1
   x  =  g+sign(g(1))*norm(g,'fro')*unitvector;

   %(c) compute the first column:
   v  =  unitvector-2*x*(x.'*unitvector)/(x.'*x);
   f  =  en1;

   for k  =  col:-1:1;
       v  =  v-Q(:,k)*(Q(:,k).'*v);
       u  =  [-unitmatrix(:,col-k+1);Q(:,col-k+1)];
       f  =  f-(f.'*u)*u;
   end

   %(d) computes the alpha and h
   alpha  =  v(1);
   h  =  v(2:row);
   f =  f(1:col);
```

```
% 3,Determines an orthogonal matrix U
firstcolum   =   [f;alpha];
Q2  =   [f',alpha;Q(2:end,:),h];

   for k   =   col:-1:1;
       twoterms   =   firstcolum(k:k+1);
       [c,s,r]      =   givens(twoterms(1),twoterms(2));
       firstcolum(k:k+1)=r;

       Q2(:,[k,k+1]) =   Q2(:,[k,k+1])*[c,-s;s,c];

      % 4, Modify the upper triangular factor
       R2([k,k+1],:) =   [c,s;-s,c]*R2([k,k+1],:);
   end


   % Form the final updated QR matrix
   Q2(1,:)=[]; Q2(:,1)=[];
   R2   =   R2(2:col+1,:);

   if Q2(1,1)*Q(2,1)<0
      Q2  = -Q2;
      R2  = -R2;
   end

% The end


   function [c,s,r] = givens(a,b)
% GIVENS computes c and s in a Givens rotation
% Given scalars a and b computes c and s in
% a Givens rotation such that
% 0 = -s*a + c*b, and r = c*a + s*b
if b == 0
   c = 1.0; s = 0.0; r = a;
        else if abs(b) > abs(a)
                tt = a*a+b*b;
                s = b/tt; c = a/tt;
      r(1) = c*a + s*b;   r(2) =  -s*a + c*b;
        else
                t = b/a; tt = sqrt(1+t*t);
                c = 1/tt; s = t*c;
      r(1) = c*a + s*b;   r(2) =  -s*a + c*b;
end
end
```

3 Extended MinMAC Algorithm

An extension of the MinMAC algorithm to aid sensor placement for modal tests is discussed in this chapter. The extension is, essentially, a forward-backward combinational MinMAC algorithm. The original MinMAC algorithm proposed by Carne can be regarded as a forward sequential MinMAC algorithm, which maximizes the discrimination between mode shapes of interest starting from a small intuition set [*CARNE and DOHRMANN* 1995]. The proposed forward-backward combinational MinMAC algorithm incorporates advantages of both forward addition and backward deletion approaches, and is more suitable for global optimality searching. Moreover, the extended MinMAC algorithm is applied to the I-40 Bridge for sensor placement. Furthermore, the similarities and differences between the MinMAC and the Effective Independence method are analyzed.

3.1 The MinMAC algorithm and its computation steps

As already discussed in Section 2.1.6, the MinMAC algorithm proposed by Carne and Dohrmann aims to ensure modal correspondence of two mode shapes. In this section, the background and objectives of the MinMAC algorithm are first reviewed. Consequently, it is extended to a back- and forward combinational MinMAC algorithm.

3.1.1 Objective of the MinMAC algorithm

The MinMAC algorithm proposed by Carne and Dohrmann is designed to ensure modal correspondence between the mode shapes computed by finite element model and those measured ones from online modal tests in structural health monitoring. To achieve this objective, both sets of mode shapes have to be differentiated as much as possible. It is equivalent to maximize the angles formed by the paired mode shape vectors or to minimize the dot product between them, which is the same as the Modal Assurance Criteria (MAC). This is the reason to minimize the off-diagonal elements of the MAC matrix.

Moreover, Carne and Dohrmann use intuition to determine an initial measurement set of DOFs. The intuition set is expected to adequately cover the structure and areas of special interest to ensure modal visualization besides correspondence.

3.1.2 Computation of the MinMAC algorithm

A small maximum off-diagonal term indicates less correlation between corresponding mode shape vectors and renders the mode shapes discriminable from each other. The MinMAC algorithm achieves this objective as follows. First, an intuition sensor set (much less than the required number of sensors) is selected based on test engineer's experience and requirements of structural topology for visualization of mode shapes. Secondly, other candidate sensors are included one by one sequentially and the one that minimizes the maximum off-diagonal element of the MAC matrix at each step is chosen. Thirdly, the MinMAC repeats the second step by adding one sensor at a time until a required number of sensors are selected.

3.2 Extension of the MinMAC algorithm

The original MinMAC algorithm can be regarded as a forward sequential addition algorithm, which adds one sensor at each iteration step. However, the non-decreasing aspect of the MinMAC algorithm, i.e., the maximum off-diagonal term doesn't decrease monotonically with the number of sensors, is often encountered in practice. To overcome the contra-decreasing problem of the original MinMAC algorithm, a forward-backward combinational extension is developed as follows,

First, an intuition sensor set, $\mathbf{U}_0$ (including, to say, a number of sensors, s_0) is chosen. Then, one sensor is added to this initial set until a preset number of sensors, which is somewhat larger than the number of sensors as required, for instance, ten percent more than required (1.1s), is reached. This is the same forward sequential MinMAC procedure as originally proposed by Carne. The extension differs from the original forward approach in the stopping criterion. The extended MinMAC algorithm is continued to obtain a sensor set, $\mathbf{U}_1$, consisting a certain number of sensors (to say, s_1, $\mathbf{s}_1 \le 1.1\mathbf{s}$) larger than the required one (s) where the original MinMAC stops.

Secondly, one sensor at each step is excluded from the sensor set ($\mathbf{U}_1$) until the required number of sensors (s) is reached. This is the backward sequential MinMAC approach, the essential extension to the forward one. Therefore, two function curves are established. One is the curve of the maximum off-diagonal term with respect to the number of sensors increasing from s_0 to s_1 obtained in the first stage, and the

other is the curve of the maximum off-diagonal term with respect to the number of sensors decreasing from s_1 to s found in the second stage. Both curves are compared and the one with a smaller value at the point s is selected. Which curve is to be selected, depends on the abilities of the forward and backward approaches to minimize the maximum off-diagonal terms of the MAC matrix. In this manner, the maximum off-diagonal term of the MAC matrix may, in many instances, be further minimized than the traditional MinMAC algorithm.

Naturally, the forward stopping number of sensors (s_1) in the first step can be varied according to the structure under consideration. The effects of various numbers (s_1) of sensors on the selection set (including s sensors) of the above two step processes can be compared and the one with the smallest maximum off-diagonal term of the MAC matrix can be chosen. This can be implemented as the third step, if necessary.

3.3 Application of the extended MinMAC algorithm to the I-40 bridge

The extended MinMAC algorithm proposed in Section 3.2 is applied to the I-40 Bridge, only the first two steps in Section 3.2 are computed. The third step repeats the second one and is not demonstrated here.

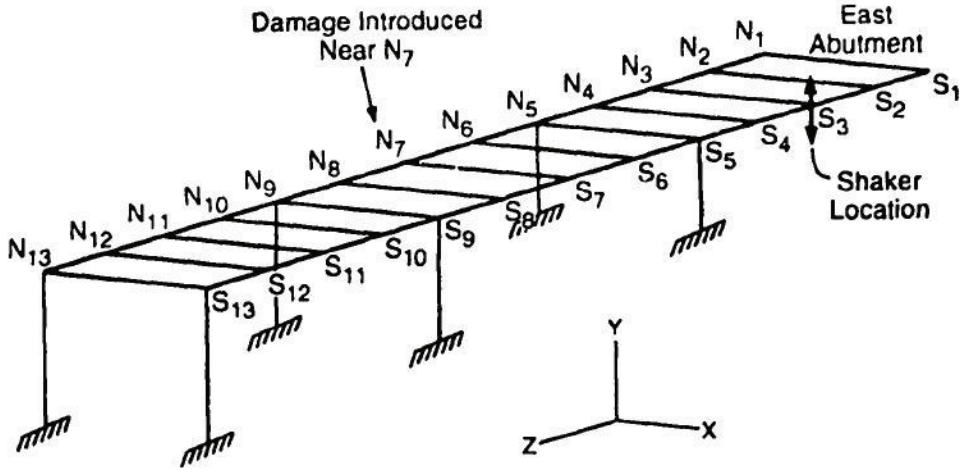

Fig.3-1 Location of shaker and accelerometers of the I-40 Bridge.

The I-40 Bridge was located over the Rio Grande in Albuquerque, New Mexico. It consists of twin spans made up of a concrete deck supported by two welded-steel plate girders and three steel stringers. The tested section has three spans. The end spans are of equal length, approximately 39.9m, and the center span is approximately 49.4m long. There are 13 accelerometers used along the length of the bridge on each side, for a total of 26 responses. The shaker consists of a 96.5 kN reaction mass supported by three air springs resting on top of drums filled with sand. The shaker was located on the eastern span directly above the south plate girder and midway between the abutment and first pier. Figure 3-3 shows the shaker and accelerometer locations. Full details of the modal testing of this bridge can be found in Farrar, et al.[*FARRAR et al.* 1994]. There were in total 26 DOFs (n=26), and six identified mode shapes (m=6) available. The mode shapes extracted from the case of "Test t11tr" are used for the computation of extended MinMAC.

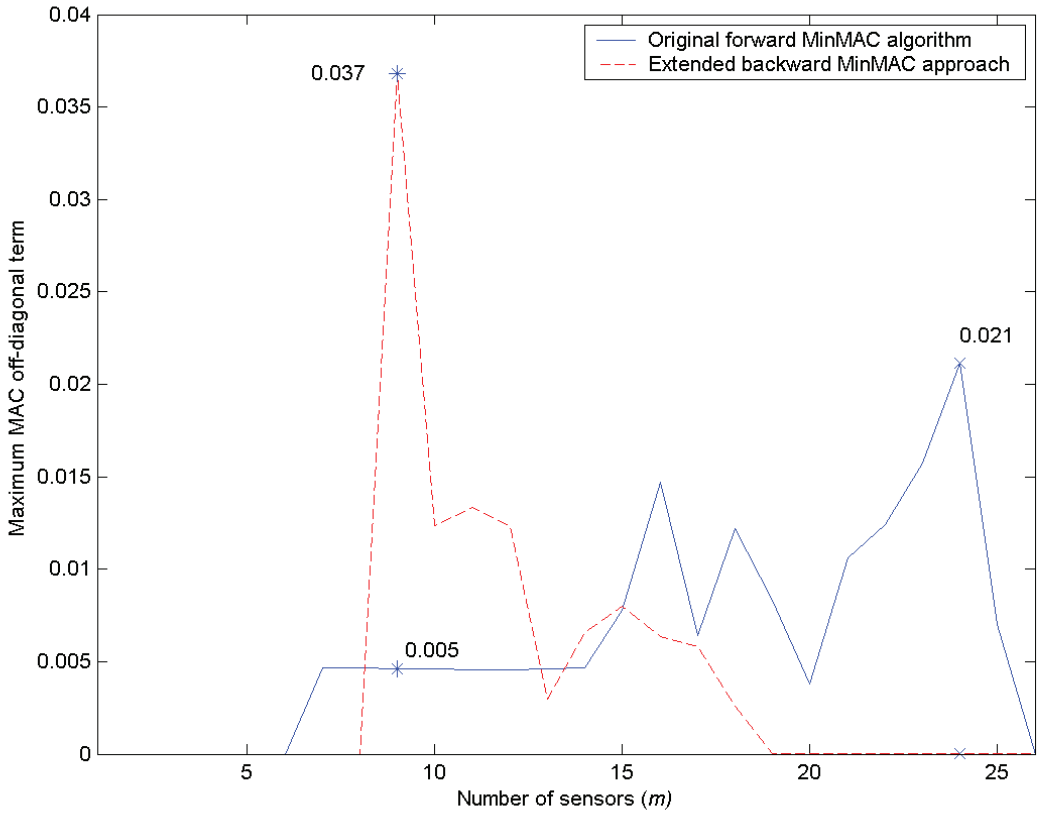

Fig.3-2 Maximum MAC off-diagonal terms with respect to the number of sensors.

The first step of the extended MinMAC algorithm with s_1 and s_0 as 26 and 6 is computed. When the MinMAC algorithm is considered, an intuition sensor set has to be

designated a priori. For the I-40 Bridge, the least sensor number is six since there are six mode shapes of interest. If six sensors are to be included in an intuition sensor set, the six sensor positions maybe, S3, S7, S11, N3, N7, N11, which are all mid-span positions and supposed to have relative large vibration amplitudes. In addition, the six positions may also be selected by computing the Modal Kinetic Energy (MKE) or Effective Independence (EI) indices as detailed in Section 2.1. When starting from this intuition set, one sensor at a time is sequentially added until another 20 sensor positions are selected. It is expected that the maximum MAC off-diagonal terms will decrease with more sensors included. This is really the case, a decreasing trend as shown in the first segment of the blue solid curve in Fig.3-2 until 8 sensors (s = 14) are added. An interesting phenomenon is observed, however, that the maximum MAC off-diagonal terms become unexpectedly larger although more sensors are included as can be seen obviously in Fig.3-2 for added numbers of sensors, 10, 12, and 18 (s = 16, 18, and 24), respectively.

To consider the sensor placement problem in a backward way for the MinMAC algorithm, *i.e.* we expand the original MinMAC algorithm to a backward manner, to remove a sensor a time. This is the second step of the extended MinMAC algorithm. All 26 dofs can be regarded as a natural intuition set from a backward deletion viewpoint. The maximum MAC off-diagonal terms with decreasing number of sensors are depicted by the red dashed line in Fig.3-2. It was supposed that the maximum MAC off-diagonal terms would increase when more sensors are excluded. This is the increasing trend shown in Fig.3-2 when we observe the red dashed curve backwards as a whole. However, there are clearly ripples for excluded number of sensors 16, 13 and 10 (s = 10, 13, and 16), respectively. The maximum MAC off-diagonal terms become smaller when more sensors are excluded from the previous measurement set although they are expected to become larger in these cases. A similar phenomenon was also observed in Pickrel [*PICKREL* 1999], where decreasing a sensor number leads to smaller MAC off-diagonal terms. In their case, 20 target modes of an airplane were selected, and it was shown that the largest off-diagonal MAC term is 0.8 for a set of 249 measured dofs, whereas 0.2 for 202 measured dofs. The reason for such increasing/decreasing contradiction is that a newly included or excluded sensor may conflict with other previously selected ones, or even with the original intuition set. Mathematically speaking, the row vector of the mode shape matrix specified at the newly included or excluded sensor position has strong linear relationship with other

row vectors. Namely, this row vector is nearly a linear combination of other row vectors. Such contra- increasing/decreasing trend in the original MinMAC algorithm justifies the necessity to extend the MinMAC algorithm in the first paragraph of Section 3.2.

To illustrate the advantage of the extended MinMAC algorithm over a number of approaches, two cases for the I-40 Bridge are considered. In Case 1, twenty-four accelerometers will be deployed (s = 24) whereas nine in Case 2 (s = 9). It is assumed that in both cases s_1 and s_0 are 26 and 6, respectively.

In Case 1, 24 accelerometers will be used (s = 24). For the forward addition approach, it means that eighteen additional sensors are to be selected besides the six sensors included in the intuition set, *i.e.* only two sensors will not be used. The not-to-be-used two sensors found by the MinMAC algorithm are S12 and N2. The maximum MAC off-diagonal value with the 24 sensors is 0.021 corresponding to the peak of the blue solid line at the abscissa of 24 as shown in Fig.3-2. According to the requirement of the extended MinMAC algorithm, the remaining two sensors are sequentially added until all 26 dofs are included, *i.e.* s_1 = 26. Then the second step of the extended MinMAC algorithm is implemented. Starting from the 26 sensors, one sensor is removed from the group in each iteration. Two sensor positions are to be excluded sequentially. As a result, the two excluded sensor positions are S1 and N1. The maximum MAC off-diagonal value with the remaining twenty four sensors is approximately 0. Apparently, the sensor positions obtained by the backward deletion approach are preferred ones than the forward addition approach and to be finally chosen by the extended MinMAC algorithm. This case powerfully demonstrates that the extended MinMAC algorithm is more suitable to find an optimal maximized MAC off-diagonal value than the original MinMAC algorithm through combining both forward and backward approaches.

In Case 2, nine sensors (s = 9) are required. Three additional sensors are to be selected besides the six sensors included in the intuition set, S3, S7, S11, N3, N7, and N11 (s_0 = 6) and they are S1, S13 and N13. The maximum MAC off-diagonal value with the 9 sensors is 0.005 corresponding to the abscissa of 9 in Fig.3-2. For the backward deletion approach of the extended MinMAC algorithm, seventeen sensor positions are to be excluded sequentially. As a result, nine sensors are selected and they are S2, S3, S7, S18, S11, N3, N7, N8, and N11. The maximum MAC off-

diagonal value with the 9 sensors is 0.037 by the backward approach, which corresponds to the peak of the red dashed curve at the abscissa of 9 as shown in Fig.3-2. It is obvious that the maximum MAC off-diagonal value obtained by the backward deletion approach is nearly 7 times larger than that calculated by the forward addition MinMAC algorithm. Therefore, the 9 sensor positions obtained by the forward addition approach is preferred and finally chosen.

In the above two cases, required numbers of sensors are 24 are 9, respectively. In one case, the forward addition approach is preferred whereas the backward deletion approach is preferred in the other case. Both cases demonstrate clearly that it is necessary to combine backward and forward approaches to search for an optimal maximum MAC off-diagonal value although the application example is rather limited.

There is one note about the influence of the choice of the intuition sensor set, $\mathbf{U}_0$, on the final selection of sensor positions. If a newly added sensor conflicts with one or several of the original intuition set, the intuition set maybe reformed if the exclusion of certain sensor from the original intuition set $\mathbf{U}_0$ is not considered to be much detrimental to the mode shape visualization. Afterwards, the two steps can be recomputed. Further research is advised on how to select a intuition sensor set, $\mathbf{U}_0$, more appropriately and on the influence of the intuition sensor set, $\mathbf{U}_0$, on final selection of sensor positions.

For the purpose of comparison with the EI, the results of the EI are given below. In case 1, the two sensor positions deselected by the EI are S1 and N1, which is the same as that of the extended MinMAC algorithm, but much different from the original MinMAC algorithm. The 9 sensor positions selected by the EI are S3, S7, S11, S12, S15, N3, N7, N11, and N12 for Case 2.

4 A New Evaluation Criterion for Sensor Placement Methods

As shown clearly in Section 2.3 , there are no two methods resulting in the same sensor placement topologies for the ladder structure and it is premature to conclude at this stage that one method outperforms others. At least, every method discussed has its advantages, and disadvantages as the same time. It should be noted that a good method for sensor placement in a particular application is not necessarily good for another project. The effectiveness of certain sensor placement method depends on the evaluation criteria. In this chapter, we use the ladder structure in Section 2.3 to compare different criteria for evaluating sensor placement methods.

4.1 Existing evaluation criteria for sensor placement methods

Conventionally, five evaluation criteria are widely used, namely modal assurance criterion, singular value decomposition, measured energy per mode, Fisher Information Matrix, and visualization of the mode shape. The presentation of the five criteria follows mainly from the excellent references [*CARNE and DOHRMANN* 1995; *PENNY et al.* 1994]. They will be discussed in details in the following subsections along with our comments.

4.1.1 Modal assurance criterion

The Modal Assurance Criterion (MAC) [*ALLEMANG and BROWN* 1982; *EWINS* 2000] is the simplest way to pair mode shapes derived from an analytical model with those obtained experimentally as follows,

$$MAC_{jk} = \frac{\boldsymbol{\Phi}_{jm}^{T}\boldsymbol{\Phi}_{ka}}{(\boldsymbol{\Phi}_{jm}^{T}\boldsymbol{\Phi}_{jm})(\boldsymbol{\Phi}_{km}^{T}\boldsymbol{\Phi}_{km})} \tag{4.1}$$

where $\boldsymbol{\Phi}_{jm}$ is the j^{th} mode from experiments and $\boldsymbol{\Phi}_{ka}$ is the k^{th} mode from an analytical FEM model. The value of the MAC is between 0 and 1. A value of 1 means that the compared two or *n*-dimensional mode shape vectors lie in the same direction and one is a multiple of the other. This means that the experimental mode shape agrees with the analytical one exactly.

The MAC criterion can also be used to discriminate two experimental mode shapes. Furthermore, it is easy to calculate. Another convenience is that the mass and stiffness matrices of a structure, which are not available in many cases, are not needed while computing the MAC.

The MAC without mass weighting is, in fact, to compare the direction of two vectors. When two vectors point into nearly or exactly the same direction, the MAC value (or the correlation coefficient) equals or approaches to one. The off-diagonal terms of the MAC matrix provide an indication to which degree the truncated mode shape vectors are linearly dependent. This is the underlying idea of the MinMAC algorithm designed specially to accommodate the MAC criterion for sensor placement as discussed in Section 2.1.6.

Table 4-1, Evaluation of sensor positions by different methods

		MAC	SVD ratio	Average Energy	tr(FIM)	Visualization
MKE	Case 1	0.97742	32058	0.28358	3.4029	5
	Case 2	0.92369	311.56	0.38454	4.6145	4
ECP	Case 1	0.96805	3320.9	0.27119	3.2543	4
	Case 2	0.93809	106.44	0.34185	4.1022	3
MSSP	Case 1	0.98899	4.6749e+005	0.28023	3.3627	5
	Case 2	0.8327	598.46	0.38188	4.5826	5
DPR	Case 1	0.94039	1.1222e+006	0.10656	1.2787	5
	Case 2	0.95985	40030	0.16471	1.9765	5
EI	Case 1	0.82764	25.892	0.13273	1.5928	4
	Case 2	0.65058	16.344	0.1958	2.3496	3
QRD	Case 1	0.86768	35.314	0.20376	2.4451	1
	Case 2	0.86798	40.091	0.33893	4.0672	1
MinMAC	Case 1	0.7499	5623.5	0.21131	2.5357	3
	Case 2	0.69534	62.898	0.26777	3.2133	2
MaxSV	Case 1	0.94943	101.61	0.24684	2.9621	2
	Case 2	0.9553	33.52	0.33713	4.0456	1
MaxTRACE	Case 1	0.97742	32058	0.28358	3.4029	3
	Case 2	0.92618	152.57	0.37251	4.4701	2

The MAC criterion is used to evaluate the performance of the sensor placement methods discussed in Section 2.3 and the results are presented in Table 4-1. Only the maximum off-diagonal term of an MAC matrix is listed in the second column of

the table. It is obvious that the maximum off-diagonal term in Case 1 is larger than that in Case 2 for most discussed methods, except the DPR, QRD and MaxSV. The MinMAC algorithm outperforms other under the MAC criteria for almost all cases. The only exception is that the EI has an even slighter maximum off-diagonal term of the MAC matrix than the MinMAC algorithm.

4.1.2 Criterion of singular value decomposition (SVD) ratio

The singular value decomposition of the mode shape matrix specified at certain degrees of freedom provides another means to measure the chosen sensor locations [*FRISWELL and MOTTERSHEAD* 1995]. The criterion evaluates the ratio of the largest to the smallest singular value of the mode shape matrix as following,

$$\mathrm{SVDratio} = \frac{\sigma_1}{\sigma_m} \tag{4.2}$$

where σ_1 and σ_m are the largest and smallest singular value of the mode shape matrix Φ, respectively. The smaller the ratio, the better the choice of sensor locations. The lower limit of the SVD ratio is one in the case that the mode shapes are orthonormal, which is an ideal situation.

The SVD ratio criterion can also be termed as condition criterion since the SVD ratio of a truncated mode shape matrix is nothing else, but its condition number. There are three reasons to adopt the SVD ratio criterion: namely mode orthogonality, the condition for mode expansion, and the observability of the modes. In measuring the mode orthogonality, the MAC and SVD ratio criteria are equivalent to a certain degree. When the mode shape vectors are orthogonal, the MAC matrix is an identity matrix and the SVD ratio equals one since all of the singular values of the modal matrix are equal to one. The requirement to validate measured results with an FE model justifies the use of the SVD ratio as a criterion. The measured or identified mode shape vector has to be expanded to match the FE mesh coordinates since they doesn't usually collocate and the small number of measured DOFs has to be expanded according to the FE mesh. The expansion employs the generalized inverse of the truncated mode shape matrix. If the condition number or SVD ratio of the modal matrix is large, the inaccuracy of such expansion will be large. Therefore, model validation

demands small SVD ratio of the truncated modal matrix. Furthermore, the observability of a structure under consideration is determined by the rank of the observability matrix if the equation of motion is cast into state space formation [*PREUMONT* 2002]. If the SVD ratio is too large, the numerical rank of the observability matrix will be less than the theoretical mathematical rank because of computer truncation errors, which renders the structure unobservable.

The evaluation of the performance of the sensor placement methods discussed in 2.3 using the SVD ratio criterion is shown in the third column of Table 4-1. The EI surpasses the other methods for both, Case 1 and Case 2, with smallest SVD ratios. The QRD ranks the second and the worst is the DPR method with considerable large SVD ratios. It can be said that the reduced mode shape matrix obtained by the DPR method is ill-posed. The degree of mode orthogonality is rather low and the modes can not be discriminated when sensors are deployed under the DPR scheme.

4.1.3 Criterion of measured energy per mode

The kinetic energy of a structure is usually not evenly distributed within the modes of the structure. Higher modes are normally difficult to excite, especially for a structure under normal operational condition, since more energy is needed. The measured modes are then expected to capture a larger part of the total kinetic energy of the structure and the energy contained in the measured DOFs for each mode should be a significant portion of that mode for sufficient identification. The criterion of measured energy per mode shares similar underlying ideas with that of the modal kinetic energy method with the MKE in Section 2.1.1. Furthermore, the criterion of measured energy per mode is also a measure of signal to noise ratio, which is a critical consideration, especially in civil engineering where harsh environment noise is pervasive.

In this work, the average percentage energy captured by the measured DOFs with the sensor placement methods discussed in 2.3 is listed in the fourth column of the Table 4-1, in which all the modes are normalized to unit length, and the mass matrix is assumed to be identity equivalent **(**i.e.**,** $\mathbf{M} = \alpha\mathbf{I}$**)**. The MKE and MSSP outperform the other methods for both Case 1 and Case 2. The worst is the DPR method and the EI, ranking second to the last, has only a slighter improvement than the DPR.

4.1.4 Criterion of the Fisher information matrix

The criterion originates from estimation theory by sensitivity analysis of the parameters to be estimated. The Fisher Information Matrix (FIM) results from minimizing the covariance matrix of the estimate error for an efficient unbiased estimator from the perspective of statistics as discussed in Section 2.1.4. The FIM relates also to the information contained in the measured responses from the viewpoint of information theory.

In practice, different measures of the FIM are used. Three variants of the FIM are, the determinant, the trace, as well as the minimum singular value of the FIM, which are maximized to increase the information or to decrease the uncertainties of the estimates. The trace, the determinant and the maximum singular value are just different norms of a matrix. These three norms measures are equivalent as discussed in Section 2.1. That is to say, different sensor placement methods based on maximization of the trace (MaxTRACE), determinant (EI) or maximum singular value (MaxSV) of the information matrix will yield similar, if not the same, results for most cases [*BASSEVILLE et al.* 1987]. There is strong evidence that the three criteria are approximately equivalent although three is unfortunately no definite prove of such equivalence up to now [*PAN* 2000]. However, Kammer has shown that the determinant is much preferable than the other two, as used in the EI.

The trace criterion of the FIM evaluating the sensor placement methods discussed in 2.3 is listed in the fifth column of Table 4-1. The DPR ranks the worst. It is surprising that the EI ranks the second to the last under this criteria. The QRD performs better than the EI, but not as good as the MKE and MSSP, not to mention the best one MaxTRACE.

4.1.5 Criterion of the visualization of the mode shape

Test engineers have to first visualize the mode shape vectors identified from modal experiments to get a first impression of the overall motion of the structure under consideration, as argued by Carne [*CARNE and DOHRMANN* 1995] . The identified mode shapes are then further compared with those computed from an FE model for modal validation, updating or damage identification. As suggested by Pickrel [*PICKREL* 1999], the number of sensors required to visualize the mode shapes is at least five times the

number of mode shapes in order to provide a crude visual depiction of the shapes and avoid spatial aliasing. This criterion has no concrete mathematical formulations as the aforementioned four criteria. It depends on the structure and usually the points in the frame corner or middle are picked up. The intuition of a test engineer plays an important role in judging which group of candidate sensor positions is more critical than others. Furthermore, certain sensor positions have to be included in order to capture the global mode of a structure.

The visualization criterion has the advantage to effectively avoid the clustering of selecting sensor positions near a special flexible part of a structure or a substructure. Obviously, whether certain sensor positions belongs to a good visualization group or not could inevitably be kept from subjective bias. Nevertheless, the visualization criterion permits intuitive means for sensor placement and offers further insights.

The visualization ability of the sensor positions determined by the sensor placement methods discussed in 2.3 is listed in the last column of Table 4-1. The sensor combinations are ranked from 1 (best) to 5 (worst) according to their distribution in the structure. Contrary to the criterion of the FIM in Section 4.1.4, the QRD outperforms the MKE, MSSP and ECP.

4.1.6 Comments on the comparison results of the five criteria on sensor placement methods

The comparison in Table 4-1 leaves us more questions than to draw a simple conclusion. The criterion of SVD ratio shows that EI is better than QRD and MinMAC. Good performance of SVD ratios leads also to better MAC performance, as analyzed in Section 4.1.2 and argued by Friswell [*FRISWELL and MOTTERSHEAD* 1995]. Frustrating is that the visualization criterion contradicts with that of the FIM as illustrated in Section 4.1.5. Moreover, the criteria of average mode energy per mode and trace of information matrix produce no better results than other methods. When we compare the visualization criterion, QRD, MaxSV and MinMAC are better. The broad theoretical agreement between these methods as discussed in Section 2.2 does not show up in their practical application as evidently as their discrepancies. Despite the inconsistencies, EI, QRD, MinMAC and MaxSV may be said to give acceptable results for sensor placement for the case under consideration.

Furthermore, two processes and their roles deserve reconsideration in investigation of sensor placement for dynamic testing. One is the implicit intermediate process of reorthgonalization of reduced mode shapes in EI, and the other is the impact of renormalization of each mode shape. The former changes the directions of original mode shapes, whereas the latter redistributes weights between mode shapes of interest.

4.2 Proposal of a new criterion for evaluating the effectiveness of sensor placement methods in structural health monitoring

As discussed in Section 4.1, the five existing criteria for sensor placement methods are not consistent with each other very well. Even worse is that one criterion may contradict with another. What causes such discrepancies? A specific objective depends on its applications. Fairly to say, each criterion has its objective and application background as well. A criterion stresses one perspective whereas another pays more attention to another aspect. Compromises have to be made if one or several of the criteria is to be used.

Furthermore, the sensor placement methods discussed in Chapter 2 are directly determined by the criteria selected. For instance, the chosen of the criterion of FIM results straightforwardly in the using of the EI method. The sensor placement methods and their judging criteria are, therefore, inevitably correlated. Consequently, a consistent evaluation criterion has to be established.

4.2.1 The features of SHM in civil engineering

The term SHM was initially proposed in civil engineering with the aim to monitoring the working status of a structure. As is known, civil engineering structures are designed to withstand many kinds of loadings, for instance of a bridge, the passing vehicles, the passengers, the changing wind, the rain and even slight movement of the soil foundation, earthquakes, etc. Furthermore, environment temperature inevitably plays an importance role in SHM by changing the characteristic parameters of the components of a structure. Due to the manifold impacts of various working loads under changing environment conditions, the responses of a structure are changing with the time as well. Consequently, the dominant frequency components in the response

vary with changing working conditions. In order to identify the mode shapes of a structure within desired accuracy, the responses have to be selected at the positions containing adequate information about the mode shapes of interest. The idea will be further developed in details in the following section.

Another feature of civil engineering structures is that the measured responses from field experiments are corrupted with comparatively large noise. The reasons lie in the obvious fact that environmental noise is inevitably very large for an operational structure. Both features have to be included in the consideration of sensor placement criteria for SHM.

4.2.2 A new evaluation criterion of almost global unbiasedness

In this section, we analyze first the mathematical background and the implicit assumptions made in the EI method. Then, a representative least squares estimator is proposed. The aim of the estimator is to achieve the best identification of modal frequencies and mode shapes. The proposed criterion depends on both the characteristics and the actual loading situations of a structure. It selects sensor positions with the best subspace approximation of the vibration responses from the linear space spanned by the mode shapes.

Foremost, a deeper understanding of the physical meaning of the EI method is beneficial to our further investigations. The EI indices, if viewed from statistics, are the leverages of each predicted value on their actual measurements, namely,

$$\hat{\mathbf{y}} = \mathbf{P}\mathbf{y} = \boldsymbol{\Phi}(\boldsymbol{\Phi}^{\mathrm{T}}\boldsymbol{\Phi})^{-1}\boldsymbol{\Phi}^{\mathrm{T}}\mathbf{y} \tag{4.3}$$

where $\hat{\mathbf{y}}$ is the fitted values corresponding to $\mathbf{y}$ and $\mathbf{P}$ is the projection matrix as defined in Eq.(2-8). Considering the i^{th} term of $\hat{\mathbf{y}}$,

$$\hat{y}_i = \sum_{j=1}^{m} p_{ij} y_j = p_{ii} y_i + \sum_{j=1, j\neq i}^{m} p_{ij} y_j \tag{4.4}$$

where p_{ij} is the ij^{th} component of the projection matrix $\mathbf{P}$.

Eq.(4-4) implies that,

$$\frac{\partial \hat{y}_i}{\partial y_i} = p_{ii} \text{ and } \frac{\partial \hat{y}_i}{\partial y_j} = p_{ij} \tag{4.5}$$

Therefore, the term p_{ii} (the EI indices) can be interpreted as the amount of leverage each value y_i has in determining $\hat{y}_i$ regardless of the realized value y_i [*CHATTERJEE* 1988; *RAO and TOUTENBURG* 1995]. The second term of Eq.(4-5) may be interpreted, analogously, as the influence of y_j in determining $\hat{y}_i$. Leverage values p_{ii} provide a measure of separateness of data points and its importance in fitting the regression line and indicate the distance of a data point from the bulk of the whole data [*COOK and WEISBERG* 1982]. Large leverage points are located near the edge of a data set in the sense of the x-coordinate (indices of data sequences) and pull the regression line near it for the full data set.

In this subsection, the EI will be viewed from another perspective. The rationale behind the EI is that the estimator with the smallest variance gives the best solution among all the unbiased estimators, as stated by Kammer using the well-known Cramer-Rao lower bound variance theorem in Eq.(2.5). An underlying implicit premise for this approach is that all the to-be-compared least squares estimators for different sensor configurations are equally unbiased. The premise is, however, not valid for sensor placement issues under discussion. The problem will be much clear if we examine the measurement equation Eq.(1.1) in further details. We assume here that there are in total 10 response measurements available, $\mathbf{y} = [y_1, y_2, ..., y_{10}]^T$, which maybe obtained by a pretest and that six among of the ten will be finally selected to deploy sensors for online measurements in the future. According to the criteria in Section 4.1 and the sensor placement methods presented in Section 2.1, two different groups of sensor positions maybe selected, for instance, group G1 and group G2. Group G1 may include, for instance, six candidate sensor positions, $\mathbf{y}_{G1} = [y_1, y_3, y_5, y_6, y_8, y_{10}]^T$ and the group G2 includes, $\mathbf{y}_{G2} = [y_2, y_3, y_4, y_6, y_8, y_{10}]^T$. With these two groups of measurements, the modal coordinates can be estimated using ordinary least squares method (OLS) for both groups as,

$$\mathbf{q}_{G1} = \mathbf{\Phi}_{G1}^{+} \mathbf{y}_{G1} \tag{4.6}$$

$$\mathbf{q}_{G2} = \mathbf{\Phi}_{G2}^{+} \mathbf{y}_{G2} \tag{4.7}$$

where $\mathbf{\Phi}_{G1}$ and $\mathbf{\Phi}_{G2}$ are the reduced mode shapes consisting of the rows of the full mode shapes specified by $\mathbf{y}_{G1}$ and $\mathbf{y}_{G2}$.

In addition, the estimate of the modal coordinates with the initial total ten measurements is,

$$\mathbf{q}_0 = \mathbf{\Phi}^{+}\mathbf{y} \tag{4.8}$$

It is apparent that the three estimates of the modal coordinates $\mathbf{q}_{G1}$, $\mathbf{q}_{G2}$ and $\mathbf{q}_0$ are unbiased themselves in terms of the group data points by which they are computed. However, the three estimates $\mathbf{q}_{G1}$, $\mathbf{q}_{G2}$ and $\mathbf{q}_0$ are not necessarily guaranteed to equal each other. Consequently, it is questionable to compare the variances of different least squares estimators without prior consideration of the prerequisite equal unbiasdness. Nevertheless, the EI compares the variances of the $\mathbf{q}_{G1}$ and $\mathbf{q}_{G2}$ and will select the one with a smaller variance. When the estimator $\mathbf{q}_{G1}$ does not equal to $\mathbf{q}_{G2}$ which occurs in most instances, such comparison of variances of the $\mathbf{q}_{G1}$ and $\mathbf{q}_{G2}$ turns out to be meaningless.

When the parameters to be estimated are deterministic, a reasonable approach is to bound the MSE(Mean Squared Error) achievable within the class of unbiased estimators. Although it is well-known that lower MSE can be obtained by allowing for a bias, in applications it is typically unclear how to choose an appropriate bias.

The following question arises naturally: why has the EI method gained so much influence in the technical literature, been recommended in the classical monographs by Ewins [*EWINS* 2000] and Friswell etc.[*FRISWELL and MOTTERSHEAD* 1995], and even embedded in commercial software MSC/NASTRAN [*PECK and TORRES* 2004] ? One reason accounting for the popularity of the EI is that the EI gives the solution of an iterated version of the straightforward MKE, which is a traditionally heuristic method used by dynamic experimenter and has the advantage of improving the signal to noise ratio. Another reason resides in that the EI does provide approximately orthogonal mode shapes for the reduced system, which is preferred in modal analysis. In fact, the reduced mode shapes corresponding to the retained sensors need not absolutely necessary to be orthogonal, as is a feature of the full mode shapes of a structure with respect to the mass matrix. The third reason preferring the EI is that it may

give acceptable results for some testing cases because sensor positions with large EI values (high leverage points) have, in general, large influences on the estimation of the parameters in the global sense. The last key reason defending for the EI is that when the measurement noises for all sensor positions are of similar magnitudes, the assumption of unbiasedness is not severely violated.

Although the EI has gained much attention in the technical community and has its benefits, it cannot guarantee the quality of its selection since the implicit assumptions are not always valid during its iterations. We continue our analysis further.

Since both $\mathbf{q}_{G1}$ and $\mathbf{q}_{G2}$ are biased estimators of $\mathbf{q}_0$, the closeness of the variances of $\mathbf{q}_{G1}$ and $\mathbf{q}_{G2}$ to the Cramer-Rao lower bound is not an adequate means to evaluate their performance anymore. In fact, unbiased estimators are always sought as a priority in linear regression over biased ones. The estimate accuracy of $\mathbf{q}_0$ determines the linear fitting quality of the equation (1.1) and thus the accuracy of the mode shapes to be identified. However, an unbiased estimate of $\mathbf{q}_0$ is unreachable in many cases, if not totally impossible, to find in sensor placement issues. Among all biased estimators of $\mathbf{q}_0$, the one which is much closer to the unbiased one is consequently more desirable. Therefore, the objective should be to minimize the Euclidean distance between the ideal unbiased estimator $\mathbf{q}_0$ and an almost unbiased one. For this purpose, a new criterion other than the FIM, namely almost global unbiasedness, is proposed in the dissertation. Under the term ‘almost global unbiasedness’, we mean that unbiasedness is of greater priority than variance (dispersion) when sensor placement is considered and that the objective is to choose a given number of sensor positions which obtain an almost unbiased coefficient estimator nearest to the unbiased estimator achieved by all candidate sensor positions as follows,

$$\mathbf{J}_{\mathrm{gu}} = (\hat{\mathbf{q}}_{\mathrm{s}} - \hat{\mathbf{q}}_{\mathrm{OLS}})^{\mathrm{T}} (\hat{\mathbf{q}}_{\mathrm{s}} - \hat{\mathbf{q}}_{\mathrm{OLS}}) \tag{4.9}$$

where $\mathbf{J}_{\mathbf{gu}}$ is the objective function of the almost global unbiasedness, and $\hat{\mathbf{q}}_{\mathbf{s}}$ is the ordinary least squares estimator with a subset of *s* components (required *s* sensor positions),

$$\hat{\mathbf{q}}_{\mathbf{S}} = (\mathbf{\Phi}_{\mathbf{s}}^{\mathbf{T}} \mathbf{\Phi}_{\mathbf{s}})^{-1} \mathbf{\Phi}_{\mathbf{s}}^{\mathbf{T}} \mathbf{y}_{\mathbf{s}} \tag{4.10}$$

where the subscript $_S$ denotes a set of *s* components including possible combinations of selecting *s* out of *n* rows, and $\hat{\mathbf{q}}_{\mathrm{OLS}}$ is an OLS estimator with all *n* components,

$$\hat{\mathbf{q}}_{\mathrm{OLS}} = (\boldsymbol{\Phi}^{\mathrm{T}}\boldsymbol{\Phi})^{-1}\boldsymbol{\Phi}^{\mathrm{T}}\mathbf{y} \tag{4.11}$$

The physical significance of the almost global unbiasedness is clear at this stage with the objective function $\mathbf{J}_{\mathrm{gu}}$ measuring the distance between an OLS estimator $\hat{\mathbf{q}}_{\mathrm{OLS}}$ with all *n* components and a biased estimator $\hat{\mathbf{q}}_{\mathrm{s}}$ with only partially *s* components. We call this method Representative Least squares (RLS) method [*Li et al.* 2009b].

The proposed RLS method approximates the original least squares estimator with the whole data set. An RLS estimator $\hat{\mathbf{q}}_{\mathrm{s}}$ is the best estimator which achieves the smallest $\mathbf{J}_{\mathrm{gu}}$ among all possible combinations including *s* components drawn from total *n* components. The selected data subset is, therefore, required to be representative and sufficiently approaching to portrait the scenario defined by the original full data set. In essence, the criterion of almost global unbiasedness shares many common aspects as that of the mean-squared error in statistics. The details of the criterion of almost global unbiasedness and its application in sensor placement are discussed and solved in the next chapter with the solution of the RLS method.

5 Load Dependent Sensor Placement Method Based on the Representative Least Squares Method

According to the discussions in Section 4.2.2, an unbiased estimator for sensor placement when all candidate sensor positions are considered is harder or even impossible to obtain. Therefore, our objective is alternatively to seek for an almost unbiased estimator which has the shortest distance to the ideal unbiased estimator among all biased ones. In this chapter, a novel load dependent sensor placement method is proposed to achieve this objective. Furthermore, a representative least squares method is correspondingly developed to deal with related mathematical computations.

5.1 Proposal of load dependent sensor placement method

Under the term ‘load dependent’, we mean that the proposed sensor placement method is dependent on actual loading conditions of a structure, and consequently, on the responses and inherent characteristics of a structure. In other words, the fitting of the multivariate regression in Eq.(4.6) is determined by both the mode shape matrix and the responses, but not only by the mode shape matrix as conventional methods conceived. As commented in Section 2.2, existing sensor placement methods share a common feature, which is that sensor positions are solely determined provided that the mode shape of a structure is known. No matter what responses the structure will undergo, the final selected sensor positions are the same and don’t take actual structural responses into consideration.

Contrast to existing sensor placement methods, the load dependent sensor placement method under discussion allows consideration of the degree to which individual mode shapes participate in actual structural responses. Its objective function is almost global unbiasedness criterion as proposed in Eq.(4.9) in Section 4.2.2. Under the almost global unbiasedness criterion, we strive to choose a given number of sensor positions that map the mode shapes of interest to the actual structural responses as closely as possible. In other words, structural responses will fall into the space spanned by the mode shapes as much as possible. Only in this way, can we fit the structural responses with the mode shapes, of course a truncated one, as accurately as possible. This is also the requirement for better modal parameter identification.

The essential feature of current widely used modal parameter estimation methods, for instance, the least squares complex exponential, the polyreference time domain, Ibrahim time domain, eigensystem realization algorithm[*JUANG* 1994], rational fraction polynomial, polyreference frequency domain and the complex mode indication function methods, is to fit the measured structural responses with the to-be-identified mode shapes as good as possible [*ALLEMANG and RESERVED* 1999; *EWINS* 2000]. If measured structural responses can be regressed by the to-be-identified mode shapes at certain sensor positions better than other alternatives, these sensor position are the best choice since all the modal parameter estimation methods are implicitly or explicitly based on the principle of the least squares method in regression no matter it is in the frequency or the time domain [*ALLEMANG and BROWN* 1998]. Therefore, the objective of the proposed load dependent sensor placement method agrees naturally to the aim of modal parameter estimation methods.

Obviously, the objective of the proposed load dependent sensor placement method cannot be fully achieved when the theoretical mode shapes, which are used to determine sensor positions a priori, deviate much from that of estimated mode shapes from actual structural responses. This is a basic assumption for all sensor placement methods assumed throughout the dissertation. Another implicit assumption is that the mode shapes participate actively in measured structural responses. In other words, much of the measured energy of structural responses is contained in the interested mode shapes. Otherwise, identified mode shapes can not sufficiently reflect structural dynamic features and loss of information will be resulted.

Hence, sensor placement can be cast into a function of both structural characteristics and of where and how the structure is excited. This is our initial concept to propose the load dependent sensor placement method. To achieve this goal, the criterion of almost global unbiasedness is developed and will be solved under the general framework of the representative least squares method to be developed in the sequel.

5.2 Theory of the representative least squares method

The traditional ordinary least squares method is described first for symbol explanation and to facilitate our development of the representative least squares method. The mathematical symbols to be used here are different from those in Section 4.2.2

to accommodate the conventional notations in mathematics, whereas the symbols in Section 4.2.2 are widely utilized in the field of structural dynamics.

5.2.1 The ordinary least squares method

The mathematical concept of the OLS method dates back to Laplace, Gauss and Legendre [*NIEVERGELT* 2000]. The purpose of a least squares model, which is the cornerstone of the classical linear theory, is to fit equations with independent coefficients to dependent responses. The classical least squares model can be expressed in matrix notation as,

$$\mathbf{y} = \mathbf{X}\beta + \mathbf{e}, \tag{5.1}$$

where $\mathbf{y}$ is an *n* x 1 vector of observations, $\mathbf{X}$ is an *n* x *p* design matrix, β is a *p* x 1 vector of unknown coefficients, and $\mathbf{e}$ is an *n* x 1 vector of unknown observation errors. The observation errors $\mathbf{e}$ are assumed to be independent and identically distributed with zero mean and variance σ^2 [*BECK and ARNOLD* 1977].

The objective of the classical OLS method is to minimize the summation of the squared residuals $\mathbf{r}_i$, which is the difference between the i^{th} response $\mathbf{y}_i$ and its estimate $\hat{\mathbf{y}}_i$,

$$\mathbf{J}_{OLS}(\beta) = \sum_{i=1}^{n} \mathbf{r}_i^2 = \sum_{i=1}^{n} (\mathbf{y}_i - \hat{\mathbf{y}}_i)^2 = \sum_{i=1}^{n} (\mathbf{y}_i - \mathbf{X}_i\hat{\beta})^2 \tag{5.2}$$

The OLS estimate of the unknown coefficients β can then be obtained by differentiating the objective function $\mathbf{J}_{OLS}(\beta)$ with respect to β and letting it equal to zero as follows,

$$\hat{\boldsymbol{\beta}}_{OLS} = (\mathbf{X}^T\mathbf{X})^{-1}\mathbf{X}^T\mathbf{y}, \tag{5.3}$$

where the superscript ^{T} indicates matrix transposition. We assume that the design matrix $\mathbf{X}$ is of full column rank, *i.e.* $rank(\mathbf{X}) = p$, and that $\hat{\boldsymbol{\beta}}_{OLS}$ can be solely determined. For rank deficient design matrix, variable selection and principle component least squares methods may be applied [*JÜRGEN* 2003].

The OLS estimate $\hat{\beta}_{OLS}$ is unbiased and can be regarded as the projection of the response vector $\mathbf{y}$ onto the space spanned by the columns of the design matrix $\mathbf{X}$. It is implicitly assumed in OLS that there is only measurement error in the responses $\mathbf{y}$, and that no error exists in the design matrix $\mathbf{X}$. For cases with errors in both responses $\mathbf{y}$ and the design matrix $\mathbf{X}$, total least squares method or the instrumental variables method can be employed [*NIEVERGELT* 2000].

5.2.2 Representative least squares Method

The OLS method is well known to be extremely sensitive to outliers such that even only one outlier can corrupt the whole estimation [*ROUSSEEUW and LEROY* 1987]. Robust estimation provides an alternative approach to the classical OLS method. The motivation of robust estimation is to produce estimators that are not unduly affected by outliers. Many robust estimators have been proposed, among which the least trimmed sum of squares and the least median of squares estimators are the most influential. To take the least trimmed sum of squares for example, it attempts to minimize a subset of the residuals and regards other cases with larger residues as outliers. The discarded cases are treated as unfaithful measurements or realizations, as will be vividly demonstrated in Section 5.2.3.

However, in our issue of sensor placement we are aware a priori that all the data points, which all contribute valuable information to our model, are faithful. The question is how to select *s* cases for a most informative future experiment. This is equally to say, how to find *s* cases to obtain the best estimator in regression. Here, by best we mean ‘an almost unbiased estimator’ which is the nearest to the OLS estimator with all the cases among all estimators from *s* cases since a guaranteed unbiased estimator is unachievable in a global sense. This is the fundamental idea of the proposed Representative Least Squares (RLS) method.

As discussed in Section 4.2.2, the Cramer-Rao lower bound is not an adequate means to compare and to evaluate the performance of biased estimators. Instead, mean squared error (MSE) can be employed to measure the differences between two (unbiased or biased) estimators as the MSE contains all relevant information about the quality of an arbitrary estimator [*RICE* 1995],

$$MSE(\hat{\boldsymbol{\beta}}) = E(\hat{\boldsymbol{\beta}} - \boldsymbol{\beta})^2 = Var(\hat{\boldsymbol{\beta}}) + (E(\hat{\boldsymbol{\beta}}) - \boldsymbol{\beta})^2 \tag{5.4}$$

Since the closeness of the coefficient estimate to its true value has profound influences on the selection of the data points to be used, unbiasedness tendency is emphasized in the RLS. From this perspective, the RLS is similar to minimize the second term in the MSE in Eq.(5.4) and has its foundation in statistics. The proposed RLS method means to select among the collections of all subsets of size *s* from all the *n* cases to approximate the OLS estimator with all the n cases. It equals to minimize the objective function of a scaled distance between partial and full estimates,

$$\mathbf{J}_{RLS}(\hat{\beta}_S) = (\hat{\beta}_S - \hat{\beta}_{OLS})^T \mathbf{W} (\hat{\beta}_S - \hat{\beta}_{OLS}) \tag{5.5}$$

where $\hat{\boldsymbol{\beta}}_S$ is an OLS estimator with a subset of *s* cases, $\hat{\boldsymbol{\beta}}_S = (\mathbf{X}_S{}^T \mathbf{X}_S)^{-1} \mathbf{X}_S{}^T \mathbf{y}_S$, the subscript $_S$ denotes a set of *s* cases including possible combinations of selecting *s* out of *n* rows, and $\hat{\beta}_{OLS} = (\mathbf{X}^T\mathbf{X})^{-1}\mathbf{X}^T\mathbf{y}$ is the OLS estimator with all *n* cases. $\mathbf{W}$ is a weight matrix. If $\mathbf{W}$ is an identity matrix $\mathbf{I}_p$, the objective function in Eq.(5.5) is simply a Euclidean distance, whereas if $\mathbf{W}$ is the inverse of the covariance matrix of $\hat{\boldsymbol{\beta}}_{OLS}$ ($\text{var}(\hat{\boldsymbol{\beta}}_{OLS}) = \boldsymbol{\sigma}^2(\mathbf{X}^T\mathbf{X})^{-1}$), the objective function in Eq.(5.5) is a squared Mahalanobis distance.

The criterion defined in Eq.(5.5), which is not known in literature, is quite different from that in Eq.(5.2) and is tentatively termed representative least squares (RLS) method in the dissertation, which is mentioned in Eq.(4.9) in Section 4.2.2. The definition of the RLS estimator is due to its representative feature of the whole data set as an analog to representatives of a population sample.

Obviously, a RLS estimator turns out to be an OLS estimator when the size of the subset is expanded to the whole data set. As the name ‘representative least squares’ indicates, a subset of cases is supposed to approximately characterize the entire data set. The selected cases in RLS are not necessarily successive, but they are required to be representative and sufficiently approaching to portrait the scenarios of the original whole data set.

5.2.2.1. Squared Mahalanobis distance in RLS.

As mentioned in the last section, the objective function in Eq.(5.5) is a squared Mahalanobis distance when $\mathbf{W}$ is the inverse of the covariance matrix of $\hat{\boldsymbol{\beta}}_{OLS}$ ($\mathrm{var}(\hat{\boldsymbol{\beta}}_{OLS}) = \boldsymbol{\sigma}^2(\mathbf{X}^T\mathbf{X})^{-1}$). Under this circumstance, the objective function can be rewritten in another form as follows,

$$\begin{aligned}\mathbf{J}_{RLS}(\hat{\boldsymbol{\beta}}_S) &= (\hat{\boldsymbol{\beta}}_S - \hat{\boldsymbol{\beta}}_{OLS})^T\mathbf{X}^T\mathbf{X}(\hat{\boldsymbol{\beta}}_S - \hat{\boldsymbol{\beta}}_{OLS}) = (\mathbf{X}\hat{\boldsymbol{\beta}}_S - \mathbf{X}\hat{\boldsymbol{\beta}}_{OLS})^T(\mathbf{X}\hat{\boldsymbol{\beta}}_S - \mathbf{X}\hat{\boldsymbol{\beta}}_{OLS}) \\ &= \sum_{i=1}^{n}(\hat{\mathbf{y}}_{S,i} - \hat{\mathbf{y}}_{OLS,i})^2 = \sum_{i=1}^{n}\hat{\mathbf{r}}_i^{\,2}\end{aligned} \tag{5.6}$$

where the $\hat{\mathbf{r}}_i^{\,2}$ is the i^{th} residual between the i^{th} response prediction using a partial estimator $\hat{\boldsymbol{\beta}}_S$ and that using the OLS estimate $\hat{\boldsymbol{\beta}}_{OLS}$, $\hat{\mathbf{r}}_i = \hat{\mathbf{y}}_{S,i} - \hat{\mathbf{y}}_{OLS,i}$. The predication residue $\hat{\mathbf{r}}_i^{\,2}$ has a similar form as a normal OLS residual in Eq.(5.2) and measures response forecast difference between the entire data set and a subset with *s* cases. In Eq.(5.6), it is worth to note that a constant σ is not included in the inverse of the covariance matrix, $\mathbf{W}$, for simplicity since it does not affect consequent analysis.

The objective function of the RLS in Eq.(5.6) takes a comparative or similar form as that of the OLS in Eq.(5.2) and has, therefore, the merit of its own despite its application in sensor placement. It is a feature of a squared Mahalanobis distance that it takes into account the correlations of the cases and is scale-invariant, *i.e*. not dependent on the scale of measurements. Furthermore, it is observed here that the objective function in Eq.(5.6) with the inverse of the covariance matrix as the weight minimizes the fitted residuals only at the selected *s* cases, which can be compared with the Euclidean distance.

5.2.2.2. Euclidean distance in RLS.

When $\mathbf{W}$ is an identity matrix $\mathbf{I}_p$, the objective function in Eq.(5.5) reduces simply to a Euclidean distance. In this case, the objective function can be reformulated as follows,

$$\mathbf{J}_{RLS}(\hat{\boldsymbol{\beta}}_S) = (\hat{\boldsymbol{\beta}}_S - \hat{\boldsymbol{\beta}}_{OLS})^T(\hat{\boldsymbol{\beta}}_S - \hat{\boldsymbol{\beta}}_{OLS}) = \left\|\hat{\boldsymbol{\beta}}_S - \hat{\boldsymbol{\beta}}_{OLS}\right\|_2^2 \tag{5.7}$$

Consequently, the difference between measured responses and their fitted values is,

$$\mathbf{y} - \hat{\mathbf{y}} = \mathbf{X}(\hat{\boldsymbol{\beta}}_S - \hat{\boldsymbol{\beta}}_{OLS}) \tag{5.8}$$

It can be observed that when the objective function in Eq.(5.7) is minimized, the difference in Eq.(5.8) is minimized as well since the design matrix, $\mathbf{X}$, is a known constant matrix. Moreover, the minimized difference between measured responses and their fitted values is applied to all measured responses, but not limited to the selected *s* cases, as determined in the squared Mahalanobis distance in Section 5.2.2.1.

The implications of such observations are profound. Even only the selected *s* cases are chosen in the RLS, all the residuals of the responses are minimized. It seems as if the other unselected *n*-*s* cases are also considered implicitly. Such an advantage is not foreseen. Therefore, an identity weight matrix in Eq.(5.5) is preferred and will be used throughout the remainder of the paper if not indicated otherwise.

Table 5-1. Two sets of data for the regressions fitted in Fig.5-1 and Fig.5-2

No. of data point		1	2	3	4	5	6	7	8	9	10	11
Case 1 &2	X	10	8	13	9	11	14	6	4	12	7	5
Case 1	Y	8.04	6.95	7.58	8.81	8.33	9.96	7.24	4.26	10.84	4.82	5.68
Case 2	Y	7.46	6.77	12.74	7.11	7.81	8.84	6.08	5.39	8.15	6.42	5.73
Leverage values		0.10	0.10	0.24	0.09	0.13	0.32	0.17	0.32	0.17	0.13	0.24

5.2.2.3. Discussion of the solutions to the RLS.

An RLS estimator $\hat{\beta}_{RLS}$ can be obtained when the objective function in Eq.(5.5) is minimized. Consequently, the *s* cases are thus determined. The RLS estimator is designed to have least prediction residuals among other alternatives. In cases, it is possible to have several equivalent optimum solutions of $\hat{\beta}_{RLS}$. Under such circumstances, the one with the maximal determinant $\det(\mathbf{X}^T\mathbf{X})$ will be chosen because of its small variance than others as argued for the Effective Independence method in Section 2.1.4.

Furthermore, the number of cases *s* retained in the RLS is required to be more than or at least equals to that of the parameters. Otherwise, no unique solution exists. At the same time, the number of cases *s* is usually much less than the number of all *n* cases, as explained in Section 2.1. In practice, the selection of *s* cases in the RLS must guarantee that $\hat{\beta}_{RLS}$ is an appropriate approximate of $\hat{\beta}_{OLS}$. Trial and error is recommended to find a suitable quantity and to avoid loss of much information.

5.2.3 A demonstration example of the mechanisms of the RLS

To illustrate the basic ideas and fundamentals of the proposed RLS in Section 5.2.2, a simple regression example is employed. Table 5-1 shows the data for drawing Fig.5-1 and Fig.5-2. The data is borrowed from Example 5.1 in [*WEISBERG* 1980]. Fig.5-1 is drawn from the data set of Case 1 in Table 5-1, and Fig.5-2 from the data set of Case 2. The *x* coordinates for both cases are the same and the difference resides only in the responses *y*.

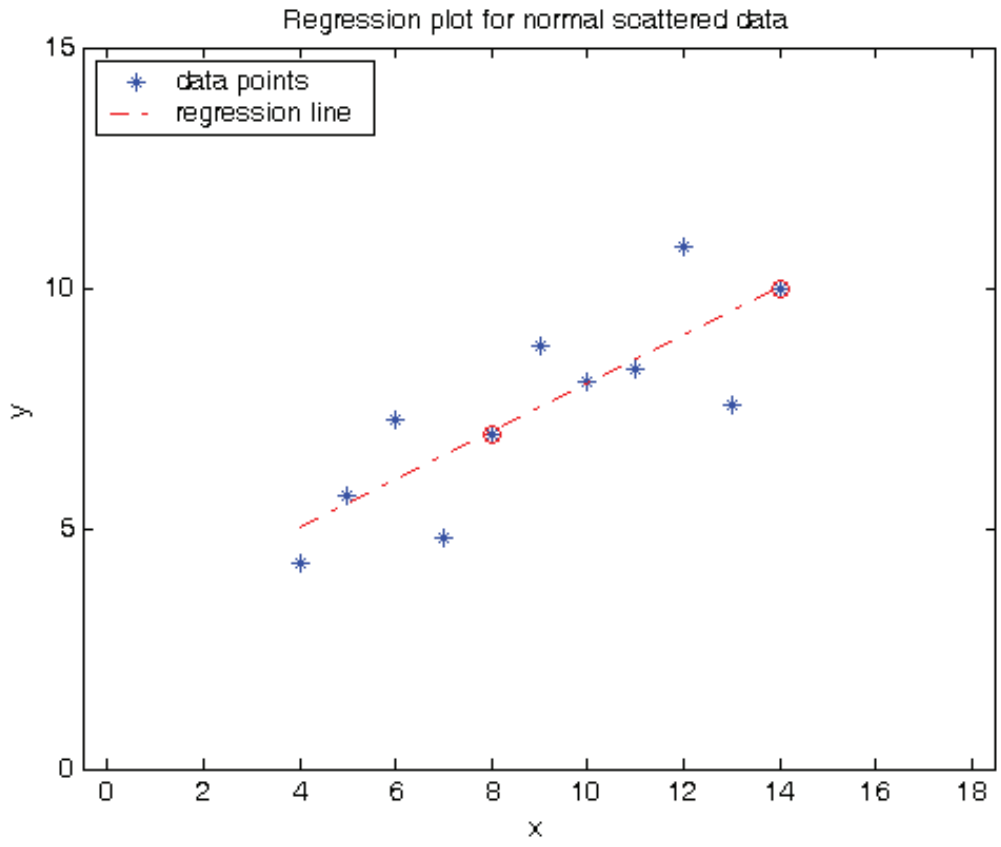

Fig.5-1 Regression line for normal scattered data

Fig.5-1 and Fig.5-2 show two different scenarios. In Fig.5-1, all the data are randomly scattered and can be said to approximate a normal distribution. However, in Fig.5-2, almost all the data except one (data point 13) are located on a robust regression line (the red dotted line with *s* of 13). The regression line of the OLS is the centered line in Fig.5-2. The robust estimator deviates much from that of the OLS because of their difference in the judgment of all cases. The OLS used all cases for regression, whereas the robust estimation used only 13 out of the total 14 points (without data point 13).

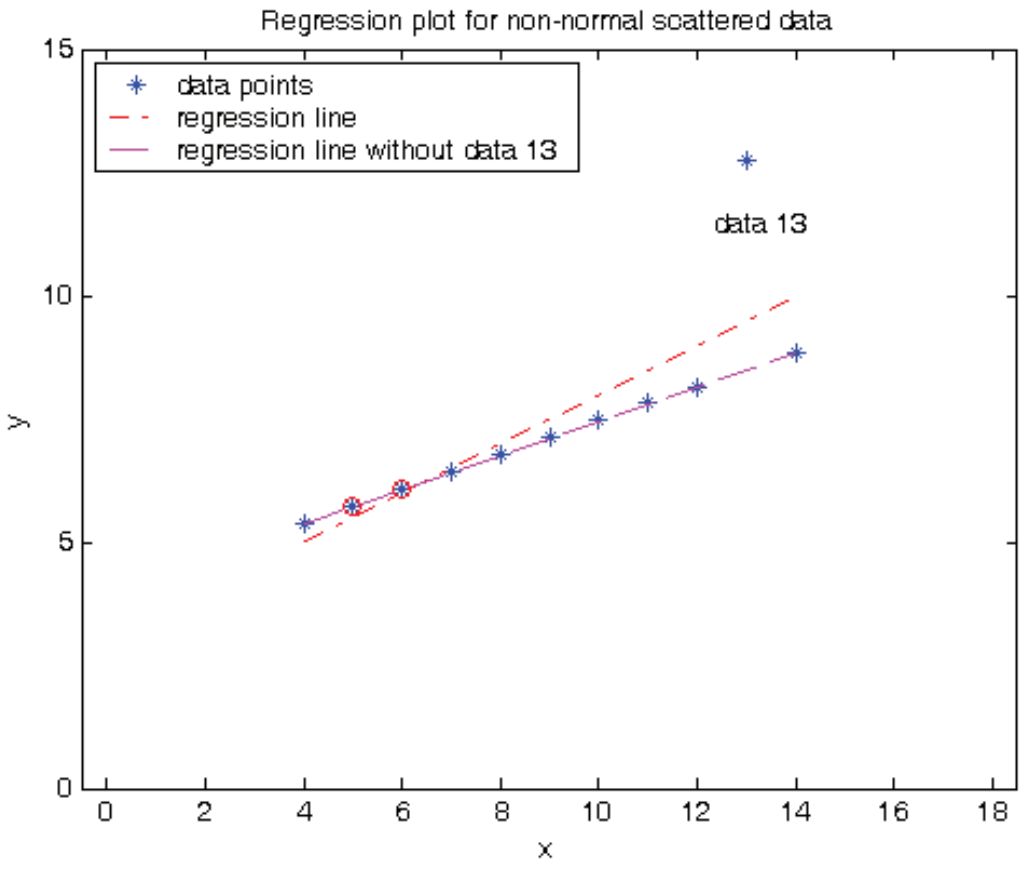

Fig.5-2 Regression line for non-normal scattered data

Of course, the example is an extreme case, in which the regression parameter is pathologically affected by the data point 13. Nevertheless, it demonstrates the fundamental idea behind the proposed RLS, i.e. to approximate the OLS estimator of

the whole data set with an almost unbiased estimator with a limited data set that includes only *s* data points.

We recur to Fig.5-1 and Fig.5-2 for explaining the representative feature of the RLS method. If *m* equals to 2 in the RLS, the selected data points are indicated by circles in both figures. For Case 1, data points No.2 and No.6 are finally selected and the regression line fitted by the RLS approximates that by OLS perfectly. For Case 2, however, data points No.7 and No.11 are selected. This simple regression example demonstrates the basic ideas behind RLS, *i.e.*, to choose the optimal approximation of the coefficients estimation provided that the number of data points is limited.

5.3 Computation of the representative least squares method

It is obvious that the RLS estimator is not monotonically non-decreasing with *s*, and the RLS fit has to be found by examining all subsets of size *s*. As also mentioned in the Introduction, the sensor placement problem is fundamentally a discrete integer optimization problem. The total selection pool includes $C_n^s = \frac{n!}{(n-s)!s!}$ options. When the number of candidate sensors *n* is very large, the global optimal search for combinations of different sensor positions is prohibitive. To obtain some insights in the prohibitiveness of possible combinations, we take a small example in which *n* equals 200 and *s* equals 20. Even in this small example, the total selection alternatives will reach as great as 1.6136e+027. Therefore, heuristic search is incapable of the intensive computation of the proposed RLS.

In this section, three sub-optimal methods will be investigated to solve the hard optimization problem, namely, genetic algorithm, bidirectional search algorithm and subspace approximation method.

5.3.1 Computation of the RLS estimator through genetic algorithm

Genetic algorithms are a particular class of evolutionary algorithms that use techniques inspired by evolutionary biology such as inheritance, mutation, selection, and crossover [COLEY 1999; GOLDBERG 2002]. A tailored genetic algorithm is implemented as a computer simulation in which the genome evolves toward better solutions.

The genome or chromosomes are a population of abstract representations of candidate solutions to an RLS minimization problem. Each solution is called an individual. Solutions are represented in binary strings of 0s and 1s in our implementation. The evolution starts from a population of randomly generated individuals and happens in generations. In each generation, the fitness of each individual in the population is evaluated. A predefined amount of individuals are stochastically selected according to a rose wheel from the current population based on their fitness, and are possibly recombined (crossover) or even mutated to form a new population. The new population is then used in the next iteration of the algorithm.

Genetic algorithms, categorized as global search heuristics method, are expected to find the global optimum solution [*GUO et al.* 2004; *MITCHELL* 1996]. In the following, we describe briefly the coding, crossover and mutation parts of our algorithm, which is a modified version of the fortran program in [*COLEY* 1999]. Other common parts, such as initialization, selection, are similar to a common genetic algorithms approach.

Coding part

A binary coding is embedded, and the coding length is n (the number of rows of the design matrix, or number of candidate sensor positions). If the ith bit of a string is 1, then the ith row of the design matrix is selected. The number of bits of value 1 in a string equals to *s* (the number of rows of the design matrix to be selected). For instance, a string 000010000010 indicates that the fifth and tenth rows are selected, and that *s* equals 2, and *n* equals to 11 respectively.

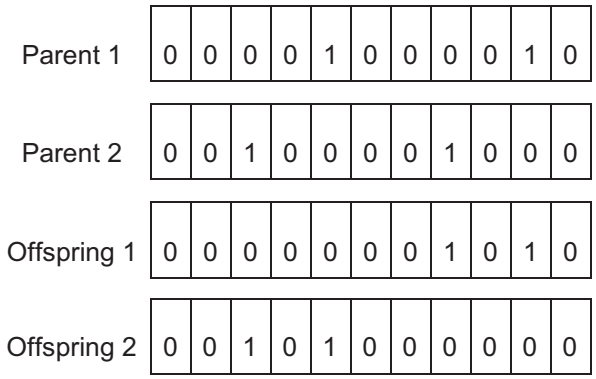

Fig.5-3 Sketch of crossover template

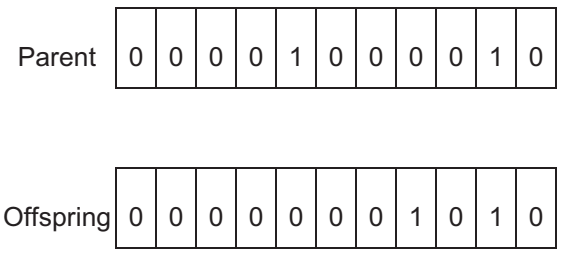

Fig.5-4 Sketch of mutation scheme

Crossover part

A crossover template is tailored for the RLS problem. First, two parent strings are compared and a crossover template is searched, in which both strings have the same number of 1s. Although the length of a crossover template varies with different parent combinations, such a template is always guaranteed to be found. The two parent strings then exchange the selected section of the crossover template, and give birth to two offsprings. Fig.5-3 illustrates this process. The use of crossover template assures the consistency of the number of 1s in an offspring string inherited from parents. In other words, the total number of sensors to be selected would not unexpectedly increase or decrease.

Table 5-2 Cases selected for RLS estimators using genetic algorithm

Number of cases	Data cases selected by genetic algorithm	Values of the objective function
2	2,6	0.02695
3	1,2,6	0.00279
4	1,2,5,6	0.02872
5	2,5,6,7,8	0.02661
6	3,4,5, 6, 8, 9	0.02005
7	3,4,6,7,8,9,10	0.01360
8	3,4,5,7,8,9,10,11	0.00106
9	2,3,4,5,7,8,9,10,11	0.00010
10	2,3,4,5,6,7,8,9,10,11	0.00019

An epoch approach is embedded in the algorithm [*VAN NIMWEGEN et al.* 1999]. The idea is based on the observation of brief bursts of change between epochs in natural evolution, and innovation is then introduced. In this way, epoch behavior aids to enhance genome diversity in a generation and as well to avoid premature. Moreover, the search speed is improved by using elitism, by which the best member in a generation is ensured to propagate into the next generation. In this manner, the possibility

of the algorithm to locate the true global optimum is increased. These genetic algorithm techniques have been coded into a Matlab program.

Table 5-2 shows the computation results using the genetic algorithm described above. The number of cases regressed for RLS estimators range from 2 to 10 for Case 1 of Table 5-1. The data cases selected in a smaller data subset does not necessarily be included in a relative larger dataset. For instance, data 2 are chosen for the number of cases, *s* of 2, 3, 4, and 5 respectively, but not selected for *s* of 6. It is noted that the search result using the genetic algorithm for *s* of 2 agrees exactly with that of a traditional combinational search, which is simple for this small-scale problem. This validates the effectiveness of the techniques used in the coded genetic algorithm program.

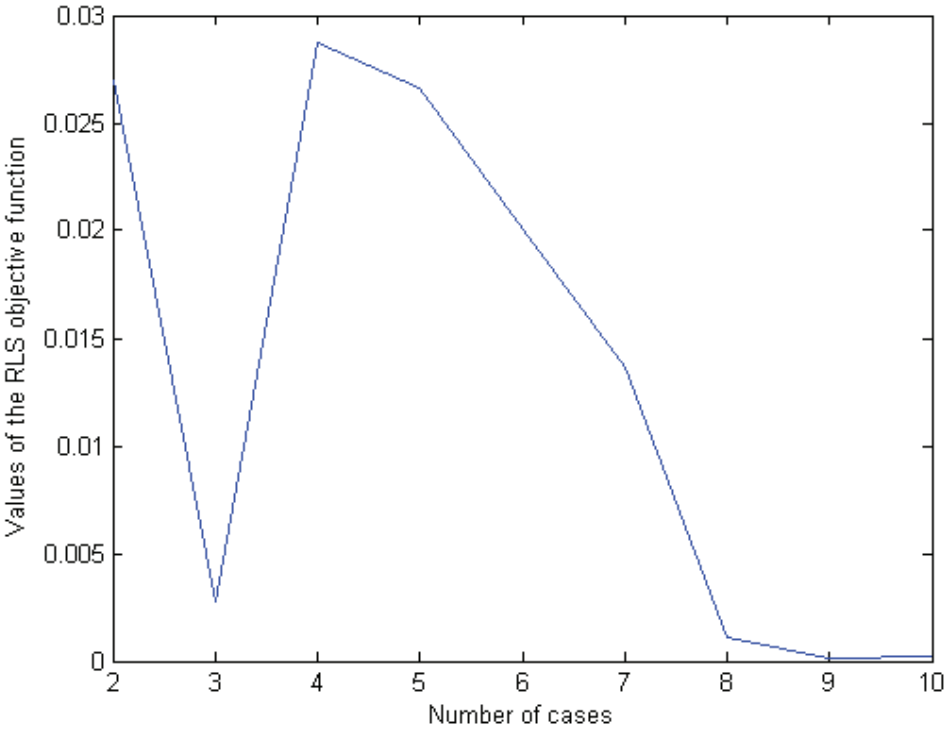

Fig.5-5 Values of the RLS objective function for increasing number of cases

The values of the objective function according to Eq.(5.6) are listed in the 3rd column of Table 5-2, and are also drawn in Fig.5-5. The curve has a decreasing trend with

the increase of the number of cases *s*. This is evident since the RLS estimator with more cases is expected to approximate the OLS estimator with all the cases with more accuracy [*ROUSSEEUW and LEROY* 1987]. However, the curve is not monotonically decreasing as stated in the first paragraph of this section. For instance, the RLS estimator with 3 cases is better than that with neighboring cases. The fluctuation of objective function may indicate certain potential applications in choosing an optimum number of cases for RLS (or optimum number of sensors in sensor placement problem), which deserves further research.

5.3.2 Computation of the RLS estimator through subspace approximation

A suboptimal deterministic solution through subspace approximation in finite steps can be found by taking the weight matrix $\mathbf{W}$ in Eq.(5.5) as an identity matrix. In this case, the objective function then boils down to minimize

$$\mathbf{J}_{RLS}(\hat{\beta}_S) = \left\| \hat{\beta}_S - \hat{\beta}_{OLS} \right\|^2 . \tag{5.9}$$

The selection of *s* out of *n* rows of $\mathbf{X}$ is equivalent to multiplying a permutation matrix $\mathbf{P}$, $\mathbf{P} \in \mathbf{R}^{n \times n}$, so that

$$\mathbf{PX} = \begin{bmatrix} \mathbf{A} \\ \mathbf{B} \end{bmatrix}, \ \mathbf{A} \in \mathbf{R}^{s \times p}, \tag{5.10}$$

where $\mathbf{A}$ is formed by *s* rows of $\mathbf{X}$. We wish to find $\mathbf{A}$ in a deterministic manner to minimize the objective function in Eq.(5.9).

If we assume first the nonsingular matrix $\mathbf{A}$ is known, then $\hat{\beta}_S$ can be written as follows,

$$\hat{\beta}_S = (\mathbf{A}^T \mathbf{A})^{-1} \mathbf{A}^T y_s = \mathbf{A}^+ y_s , \tag{5.11}$$

where y_s is formed by *s* rows of y specified by the permutation matrix $\mathbf{P}$ as $\mathbf{A}$ out of $\mathbf{X}$. Since we have fitted the underlying linear model using all the rows of $\mathbf{X}$, that is,

$$\hat{\mathbf{y}} = \mathbf{X}\hat{\beta}_{OLS} = \mathbf{X}(\mathbf{X}^T\mathbf{X})^{-1}\mathbf{X}^T y \,, \tag{5.12}$$

where $\mathbf{y} = \hat{\mathbf{y}} + \mathbf{r},\ \hat{\mathbf{y}} \in range(\mathbf{X})$, and r_i, $i = 1,2,...,n$ are the fitting errors.

The OLS estimator $\hat{\beta}_{OLS}$ is obtained with all the candidate data points. We manage to compute $\hat{\beta}_{OLS}$ with the submatrix $\mathbf{A}$ in the sequel. Eq.(5.12) can be multiplied at both sides by the permutation matrix $\mathbf{P}$ as follows:

$$\mathbf{P}\hat{\mathbf{y}} = \mathbf{P}\mathbf{X}\hat{\beta}_{OLS} \tag{5.13}$$

Substituting Eq.(5.10) into Eq.(5.13), one obtains,

$$\begin{bmatrix} \hat{\mathbf{y}}_s \\ \hat{\mathbf{y}}_o \end{bmatrix} = \begin{bmatrix} \mathbf{A} \\ \mathbf{B} \end{bmatrix} \hat{\beta}_{OLS} \tag{5.14}$$

where $\hat{y}_s$ is formed by *s* rows of $\hat{y}$ specified by the permutation matrix $\mathbf{P}$, and $\hat{y}_o$ is formed by the other *n-s* rows of $\hat{y}$. Then, we can compute $\hat{\beta}_{OLS}$ only by $\mathbf{A}$ as follows,

$$\hat{\beta}_{OLS} = (\mathbf{A}^T\mathbf{A})^{-1}\mathbf{A}^T\hat{\mathbf{y}}_s = \mathbf{A}^+\hat{\mathbf{y}}_s \tag{5.15}$$

Therefore, the objective function in Eq.(5.9) is equivalent to minimize

$$\mathbf{J}_{RLS}(\hat{\beta}_S) = \left\|\hat{\beta}_S - \hat{\beta}_{OLS}\right\|^2 \le \left\|\mathbf{A}^+\right\|^2 \left\|\hat{\mathbf{y}}_s - \mathbf{y}_s\right\|^2 = \left\|\mathbf{A}^+\right\|^2 \left\|\mathbf{r}_s\right\|^2 \tag{5.16}$$

To simplify our analysis, we assume first that the responses, y, are with identical independent fitting errors. Then, we will analyze the influence of responses with different fitting errors.

When the fitting errors of all the responses, y, equal with each other, the Frobenius norm of the selected *s* rows of $\mathbf{r}$, $\left\|\mathbf{r}_s\right\|^2$, can then be simplified by a constant no matter which combination of rows are selected as long as the number of rows, *s*, is fixed. The objective function in Eq.(5.16) can be further simplified to minimize the pseudo inverse of the selected submatrix, $\left\|\mathbf{A}^+\right\|^2$. Based on the concept of local maximum volume, which is defined as product of the singular values of a matrix, a deletion

scheme is adopted to find the required submatrix $\mathbf{A}$ [*PAN* 2000]. To determine if a submatrix $\mathbf{A}$ has a local maximum volume, one only needs to compare its volume with the volumes of other neighboring submatrices (they differ from $\mathbf{A}$ in exactly one row). An algorithm can then be established to find the suboptimal matrix $\mathbf{A}$, which has a local maximum volume. Specifically, starting from the original full matrix $\mathbf{X}$, we delete one row to minimize the Frobenius norm of the pseudo inverse of the candidate submatrices (the number of the submatrices equals to the rows of the matrix) at each step until the required number of rows is reached. The analytical lower bound of the Frobenius norm of the pseudo inverse of the required submatrix $\mathbf{A}$ is given in [*DE HOOG and MATTHEIJ* 2007]. The search of the submatrix $\mathbf{A}$ equals to find a reduced subspace spanned by the columns of $\mathbf{A}$ approximating to the subspace originally spanned by the columns of $\mathbf{X}$.

Table 5-3 Cases selected for the RLS estimator through subspace approximation

Number of cases	Data cases selected by SA	Data cases selected by EI
2	1,11	1,11
3	1,2,11	1,10,11
4	1,2,3,11	1,2,10,11
5	1,2,3,10,11	1,2,3,10,11
6	1,2,3,4,10,11	1,2,3,9,10,11
7	1,2,3,4,5,10,11	1,2,3,8,9,10,11
8	1,2,3,4,5,9,10,11	1,2,3,4,8,9,10,11
9	1,2,3,4,5,6,9,10,11	1,2,3,4,7,8,9,10,11
10	1,2,3,4,5,6,8,9,10,11	1,2,3,4,5,7,8,9,10,11

The example of Case 1 in Table 5-1 is employed here again for demonstration purposes. Table 5-3 shows the results using the subspace approximation (SA) approach. The number of cases regressed for RLS estimators range from 2 to 10. The 3rd column lists also the selection result by the Effective Independence (EI) method. It can

be found that subspace approximation approach selects similar positions as EI in many cases with only slight differences.

The algorithm in the last paragraph can be extended to the case of responses with different fitting errors, which are more common in engineering practice. Under such circumstances, the required suboptimal matrix $\mathbf{A}$ is not determined only by the Frobenius norm of its pseudo inverse, but by the Frobenius norm of its pseudo inverse multiplied by the norm of the fitting errors of the selected *s* rows.

For multiple columns of observations or measurements as different time instants, the linear model in Eq.(5.5) can be extended with multiple regression coefficients corresponding to the set of observations as,

$$\mathbf{Y} = \mathbf{X}\Theta + \mathrm{E}, \tag{5.17}$$

where $\mathbf{Y}$ is an *n* x *m* matrix of observations, $\mathbf{X}$ is an *n* x *p* design matrix, Θ is a *p* x *m* matrix of unknown coefficients at specified time instants, and **E** is an *n* x *m* matrix of unknown measurement errors. The errors are assumed to be independent and identically distributed with zero mean and variance σ^2 for a single column of observations, and assumed to be stationary for a single row.

The solution of representative least squares boils down to find an approximation of Θ with a submatrix $\mathbf{A}$ with a smaller row dimension,

$$\mathbf{J}_{RLS}(\hat{\Theta}_S) = \left\| \hat{\Theta}_S - \hat{\Theta}_{OLS} \right\|^2 = \left\| \mathbf{Y}^{+}\mathbf{X} - \mathbf{A}^{+}\mathbf{X}_{S(A)} \right\|^2 \tag{5.18}$$

We can use the concept of the Gauss-Jordan idea to invert a matrix and get its approximation. Then, we can arrive at some norm approximation of the column estimates of the coefficients. For multiple responses, y, the fitting errors norm of the selected *s* rows can be perhaps approximated by the standard deviation of each row of the multiple responses, y, which deserves yet further investigations.

5.3.3 Computation of the RLS estimator through backward and forward combinational approach

Alternatively, the RLS estimator can be solved through a backward and forward combinational approach. The hybrid approach, which combines the advantages of both forward addition and backward deletion approaches, is inspired by the idea in our solution of the Extended MinMAC algorithm proposed in Chapter 3. It is of interest to note that the RLS estimator is not monotonically increasing or decreasing with the addition or deletion of an additional point, which is quite similar to the feature of the MinMAC algorithm. Therefore, we can search from both forward and backward directions to approximate the global minimization of the objective function defined in Eq.(5.5) and select the one with a smaller distance. This is the fundamental concept of the approach.

Similar to that of the extended MinMAC algorithm, the backward approach can be directly applied to the solution of the RLS to delete one point in a step. The objective function can then be drawn with respect to the decrease of the number of points used. Consequently, an optimal point can be located.

However, the forward approach has to be modified to adapt to the characteristics of the RLS since it is not straightforward and easy enough to find an intuition point set that can satisfy the objective function in Eq.(5.5). Nevertheless, an initial set with certain number of points has to be selected for the forward approach. It is known that the least number of points in the initial set has to be no less than the number of the columns of the design matrix $\mathbf{X}$ since otherwise no unique solution exists for the RLS estimator. A convenient choice of the least number of an initial point set is to equal it to the column dimension of the design matrix. The distribution of the chosen points in the initial point set can be found using the genetic algorithm approach as outlined in Section 5.3.1. Once the initial point set is chosen, we can then consider an additional point one by one, and select one that minimizes the objective function at each step until a required number of points are selected. This is the backward sequential approach. A curve describing the minimized objective function in each addition step is obtained with respect to the increasing of the number of points used.

The third step of the hybrid approach is select one curve that has a smaller objective function value at the desired number of points. Consequently, the RLS is obtained and the fitted points are determined as the same time.

5.3.4 Discussions on the computations of the RLS estimator

Although three approaches have been investigated to find the solution to the RLS estimate, there is no perfect algorithm to find the global optimum up to date. The last two methods are suboptimal in the sense that they are approximate and only optimal in the step the computation is performed. The first genetic computation approach outperforms the other two. However, it has the disadvantage of complexity and suffers from huge computation burden.

5.4 Discussions on the representative least squares estimator

According to the theory of matrix perturbation analysis, the RLS estimator can be regarded as a perturbed OLS estimator after certain rows of the observation vector and the design matrix are zeroed out. The subsection will concentrate on this aspect and discuss the contributing factors that influence the RLS estimator. Furthermore, a simplified approximate to the RLS estimator utilizing the special structure of the RLS problem is obtained.

5.4.1 Analysis of the RLS estimator with normal equations

For the convenience of subsequent analysis, we employ the normal equation of Eq.(5.1) for analyzing its sensitivity to perturbations in $\mathbf{X}$ and $\mathbf{y}$ as follows,

$$\mathbf{A}\boldsymbol{\beta} = \mathbf{b} \tag{5.19}$$

where $\mathbf{A} = \mathbf{X}^{\mathrm{T}}\mathbf{X} \in \mathbf{R}^{p\times p}$ and $\mathbf{b} = \mathbf{X}^{\mathrm{T}}\mathbf{y} \in \mathbf{R}^{p}$. $\mathbf{A}$ is nonsingular since $\mathbf{X}$ is of full column rank. A measure of the linear system sensitivity of Eq.(5.19) can be obtained by considering the parameterized system,

$$(\mathbf{A} + \varepsilon\mathbf{F})\boldsymbol{\beta}(\varepsilon) = \mathbf{b} + \varepsilon\mathbf{f}, \boldsymbol{\beta}(0) = \boldsymbol{\beta} \tag{5.20}$$

where $\mathbf{F} \in \mathbf{R}^{p\times p}$ and $\mathbf{f} \in \mathbf{R}^{p}$. Since $\boldsymbol{\beta}(\varepsilon)$ is differentiable in a neighborhood of zero considering that $\mathbf{A}$ is nonsingular, the Taylor series expansion for $\boldsymbol{\beta}(\varepsilon)$ has the form

$$\boldsymbol{\beta}(\varepsilon) = \boldsymbol{\beta} + \varepsilon\dot{\boldsymbol{\beta}}(0) + O(\varepsilon^2) \tag{5.21}$$

where $\dot{\boldsymbol{\beta}}(0) = \mathbf{A}^{-1}(\mathbf{f} - \mathbf{F}\boldsymbol{\beta})$ [*GOLUB and VAN LOAN* 1996]. Using the 2-norm, the following relationship can be established,

$$\frac{\|\boldsymbol{\beta}(\varepsilon) - \boldsymbol{\beta}\|_2}{\|\boldsymbol{\beta}\|_2} \le |\varepsilon| \|\mathbf{A}^{-1}\|_2 \left\{ \frac{\|\mathbf{f}\|_2}{\|\boldsymbol{\beta}\|_2} + \|\mathbf{F}\|_2 \right\} + O(\varepsilon^2) \tag{5.22}$$

Substituting the inequality $\|\mathbf{b}\|_2 \le \|\mathbf{A}\|_2 \|\boldsymbol{\beta}\|_2$ into Eq.(5.22), we obtain,

$$\frac{\|\boldsymbol{\beta}(\varepsilon) - \boldsymbol{\beta}\|_2}{\|\boldsymbol{\beta}\|_2} \le \|\mathbf{A}^{-1}\|_2 \|\mathbf{A}\|_2 \left\{ |\varepsilon| \frac{\|\mathbf{f}\|_2}{\|\mathbf{b}\|_2} + |\varepsilon| \frac{\|\mathbf{F}\|_2}{\|\mathbf{A}\|_2} \right\} + O(\varepsilon^2) \tag{5.23}$$

The terms in the r.h.s. of Eq.(5.23), $|\varepsilon| \frac{\|\mathbf{f}\|_2}{\|\mathbf{b}\|_2}$ and $|\varepsilon| \frac{\|\mathbf{F}\|_2}{\|\mathbf{A}\|_2}$, represent the relative errors in $\mathbf{A}$ and $\mathbf{b}$, respectively. The condition number, $\kappa(\mathbf{A})$, is defined by

$$\kappa(\mathbf{A}) = \|\mathbf{A}^{-1}\|_2 \|\mathbf{A}\|_2 \tag{5.24}$$

From Eq.(5.23), it is clear that the relative error in $\boldsymbol{\beta}(\varepsilon)$ can be $\kappa(\mathbf{A})$ times the relative error in $\mathbf{A}$ and $\mathbf{b}$. In this sense, the condition number quantifies the sensitivity of the linear equation in Eq.(5.19). It is worth noting that condition number can be defined by other consistent norms, and the condition number of a singular matrix is infinity for convention, i.e. $\kappa(\mathbf{A}) = \infty$ for a singular $\mathbf{A}$.

Since the 2-norm of $\mathbf{A}$ is its largest singular value, the condition number of $\mathbf{A}$ can be further rewritten as,

$$\kappa(\mathbf{A}) = \|\mathbf{A}^{-1}\|_2 \|\mathbf{A}\|_2 = \frac{\sigma_1(\mathbf{A})}{\sigma_p(\mathbf{A})} \tag{5.25}$$

where $\sigma_1(\mathbf{A})$ and $\sigma_p(\mathbf{A})$ are the largest and smallest singular value of $\mathbf{A}$, respectively. When $\kappa(\mathbf{A})$ is large, then $\mathbf{A}$ is said to be an ill-conditioned matrix. On the contrary, matrices with small condition numbers are said to be well-conditioned. The condition number of $\mathbf{A}$ is a squared $\kappa(\mathbf{X})$ since $\mathbf{A} = \mathbf{X}^{\mathrm{T}}\mathbf{X} \in \mathbf{R}^{p \times p}$.

Recall that the change of $\boldsymbol{\beta}(\varepsilon)$ in Eq.(5.23) comes from two contributions, one is the change in the design matrix $\mathbf{A}$ and the other in the responses $\mathbf{b}$. An interesting but

very difficult mathematical problem concerns the evaluation of both contributions. When all the components of the responses, y, lay on the fitting line perfectly, i.e., the rows other than the first *m* rows in the design matrix can be expressed as linear combinations of the first *m* rows., then the only remaining factor to determine the regression coefficient is $\boldsymbol{\kappa}(\mathbf{A})$. In general, the variation in the design matrix can be said to have much more impact on $\boldsymbol{\beta}(\boldsymbol{\varepsilon})$ since the condition number of the design matrix has an amplification effect on the total changes.

Nevertheless, it should be noted that the above derivation is based on the assumptions that the change in $\mathbf{A}$ and $\mathbf{b}$ are relatively small. In fact, certain rows in $\mathbf{A}$ and $\mathbf{b}$ are changed to zeros for sensor placement methods or in RLS method and consequently such small perturbation assumption can't always hold. Which one contributes much dominantly to the total relative error than the other is depending on the applications. Therefore, the result in Eq.(5.23) can only provide us with a rough idea in what respect we should pay attention to, but not confine us to its quantitative bounds.

5.4.2 Analysis of the RLS estimator through matrix perturbation

Due to the special structure and the feature of the RLS, a very simple RLS estimate can be obtained through matrix perturbation. In RLS, certain rows of the observations and the design matrix are to be removed (zeroed). For the convenience of derivation, we operate directly on Eq.(5.1) and it is assumed that the to be removed *r* rows is exchanged to the last *r* rows in $\mathbf{y}$ and $\mathbf{X}$. The perturbations can be written as,

$$\widetilde{\mathbf{y}} = \mathbf{y} + \boldsymbol{\delta}\mathbf{y}\,,\ \widetilde{\mathbf{X}} = \mathbf{X} + \boldsymbol{\delta}\mathbf{X} \tag{5.26}$$

The perturbed parts can be viewed as a linear row combination of the original matrices,

$$\boldsymbol{\delta}\mathbf{y} = \mathbf{S}\mathbf{y}\,,\ \boldsymbol{\delta}\mathbf{X} = \mathbf{S}\mathbf{X} \tag{5.27}$$

Where the selection matrix $\mathbf{S}$ is zeros everywhere except the last *r* rows with -1 as their diagonals as follows,

$$\mathbf{S} = \begin{bmatrix} 0 & & & & & & 0 \\ & \ddots & & & & & \\ & & 0 & & & & \\ & & & -1 & & & \\ & & & & \ddots & & \\ 0 & & & & & & -1 \end{bmatrix} \tag{5.28}$$

One basic premise is that the perturbed matrices are small and the matrices after perturbation are of full column rank and not degenerated. Thus, the perturbed RLS solution to the original OLS one is,

$$\widetilde{\boldsymbol{\beta}} = \boldsymbol{\beta} + \delta\boldsymbol{\beta} = \boldsymbol{\beta}_{RLS} \tag{5.29}$$

We start deriving the expression for the perturbation in the RLS solution, $\delta\boldsymbol{\beta}$. The perturbed solution, $\boldsymbol{\beta} + \delta\boldsymbol{\beta}$, satisfies the normal equations

$$(\mathbf{X} + \delta\mathbf{X})^T((\mathbf{X} + \delta\mathbf{X})(\boldsymbol{\beta} + \delta\boldsymbol{\beta}) - (\mathbf{y} + \delta\mathbf{y})) = 0 \tag{5.30}$$

Subtracting, $\mathbf{X}^T(\mathbf{X}\boldsymbol{\beta} - \mathbf{y}) = 0$, and neglecting second-order terms, we get

$$\delta\boldsymbol{\beta} = \mathbf{X}^+(\delta\mathbf{y} - \delta\mathbf{X}\boldsymbol{\beta}) + (\mathbf{X}^T\mathbf{X})^{-1}\delta\mathbf{X}^T\mathbf{r} \tag{5.31}$$

where, $\mathbf{X}^+ = (\mathbf{X}^T\mathbf{X})^{-1}\mathbf{X}^T$ and $\mathbf{r} = \mathbf{y} - \mathbf{X}\boldsymbol{\beta}$. Eq.(5.31) is a general perturbation solution to the original one, $\boldsymbol{\beta}$. For the RLS at hand, by substituting Eq.(5.27) into Eq.(5.31) the perturbed solution becomes,

$$\delta\boldsymbol{\beta} = \mathbf{X}^+(\mathbf{S}\mathbf{y} - \mathbf{S}\mathbf{X}\boldsymbol{\beta}) + (\mathbf{X}^T\mathbf{X})^{-1}\mathbf{X}^T\mathbf{S}^T\mathbf{r} = 2\mathbf{X}^+\mathbf{S}\mathbf{r} = 2\mathbf{X}^+\delta\mathbf{r} \tag{5.32}$$

Where the symmetry feature of the selection matrix, $\mathbf{S} = \mathbf{S}^T$, is exploited, and, $\delta\mathbf{r} = \mathbf{S}\mathbf{r}$, is the last *r* rows of the residuals of the original OLS equation.

Eq.(5.32) looks very nice and of great beauty in addition to its simplicity since the perturbation solution depends only on the inverse of $\mathbf{X}$ and perturbed residuals . However, it is worth noting that the assumptions made during the derivation is that the perturbed matrices, $\delta\mathbf{y}$, $\delta\mathbf{X}$ are relatively small in norm sense compared to their unperturbed counterparts. Since the whole rows are to be removed in RLS, such as-

sumptions could not always be valid and only in special cases can Eq.(5.32) be directly applied.

Nevertheless, a common conclusion can be drawn from the last two subsections. That is, the condition number of the design matrix has significant or decisive influences on the RLS estimator. From the definition of the RLS estimator in Eq.(5.5) and its step-by-step approximation in Eq.(5.32), it is easily observed that the inverse of the observation matrix has critical influence on the solution. The bounds for the perturbed solution depends critically on the condition number of the design matrix. When the responses are nearly linear to the design matrix, i.e. the responses fall almost in the subspace spanned by the column of the design matrix, then the fitting residuals are approximate to equal to each other. Under these circumstances, the RLS estimator is almost completely controlled by the condition number of the observation matrix, $cond(\mathbf{X})$. Consequently, it is reasonable to use $cond(\mathbf{X})$ as a criterion as a good approximate of the RLS estimate. In the situations that the responses behave nonlinearly or the fitting residuals varies significantly, the RLS estimator cannot be simply substituted by $cond(\mathbf{X})$.

5.4.3 Connection between the criterion of the Effective Independence and that of the RLS

As analyzed in last two sections, the condition number of the design matrix plays a critical role in the RLS. In many cases, the RLS estimator could even be simply substituted by $cond(\mathbf{X})$. In this section, the connection between the criterion used in the Effective Independence and that of the condition number is discussed in details.

The design matrix can be decomposed by the QR decomposition in Section 2.2.1.3 as,

$$\mathbf{A} = \begin{pmatrix} z^T \\ \mathbf{A}_1 \end{pmatrix} = \mathbf{QR} = \begin{pmatrix} p^T \\ \mathbf{Q}_1 \end{pmatrix} \mathbf{R} \tag{5.33}$$

Since the condition number of a matrix is invariant under orthogonal transformation [*HORN and JOHNSON* 1991], we have,

$$cond(\mathbf{A}) = cond(\mathbf{R}) \tag{5.34}$$

On the other hand, Eq.(5.33) can be alternatively rewritten as,

$$\mathbf{A} = \begin{pmatrix} z^T \\ \mathbf{A}_1 \end{pmatrix} = \mathbf{Q}\begin{pmatrix} \mathbf{R} \\ \mathbf{0} \end{pmatrix} \tag{5.35}$$

Likewise, the reduced design matrix after a row is deleted can be written as,

$$\mathbf{A}_1 = \begin{pmatrix} z_2{}^T \\ \mathbf{A}_2 \end{pmatrix} = \mathbf{Q}_1\begin{pmatrix} \mathbf{R}_1 \\ \mathbf{0} \end{pmatrix} \tag{5.36}$$

Consequently, the connection between the condition number of $\mathbf{A}_1$ and that of $\mathbf{A}$ can be obtained when the relationship between $\mathbf{R}_1$ and $\mathbf{R}$ are derived. Multiplying Eq.(5.35) by its transpose on both sides, it follows that,

$$\mathbf{A}_1{}^T\mathbf{A}_1 = \mathbf{A}^T\mathbf{A} - z * z^T \tag{5.37}$$

Substituting the QR decomposition of $\mathbf{A}$ in Eq.(5.35) and that of $\mathbf{A}_1$ in Eq.(5.36), the relationship between $\mathbf{R}_1$ and $\mathbf{R}$ can be established as,

$$\mathbf{R}_1{}^T\mathbf{R}_1 = \mathbf{R}^T\mathbf{R} - z * z^T \tag{5.38}$$

Therefore, $\mathbf{R}_1$ can be regarded as a rank-one modification to $\mathbf{R}$. Since the eigenvalues of an upper triangular matrix are its diagonal terms, the condition number of $\mathbf{R}$ is completely controlled by its diagonal components. Moreover, the change of the diagonal terms of the upper triangular matrix after a row is removed from the design matrix can be further simplified as,

$$\mathbf{R}_{1kk}{}^2 = \mathbf{R}_{kk}{}^2 - z_k^2 \tag{5.39}$$

By the principle of the EI in Section 2.2.1.3, the row with the minimum norm of the mode shape matrix will be removed in each iteration, i.e., the row to-be-removed has the minimum norm among all other candidate rows, $\|z\|_2$ is minimized in each step. Consequently, $\mathbf{R}_1$ is the minimum perturbation of $\mathbf{R}$ among other alternatives, which

results in that the change of the condition number of $\mathbf{R}_1$ from that of $\mathbf{R}$ is minimally changed in each iteration of the EI.

When the solution of the RLS is implemented in a sub-optimal sense, i.e. to seek for the minimum change of the condition number of the design matrix, the criterion of the RLS agrees exactly with the Effective Independence method. Furthermore, The RLS searches the minimum change of its original condition number of the design matrix with combinational rows in a global sense, whereas the EI tracks the minimum change of the condition number in each of its iterations. Therefore, the RLS can be regarded as an extension of the EI in this sense, which further justifies the proposal of the RLS as a general criterion for sensor placement in structural health monitoring.

5.5 Load dependent sensor placement method based on the RLS

Based on the insights gathered in the proposed new evaluation criterion in Section 4.2 and the RLS theory developed in Section 5.2, a novel load dependent sensor placement method is advanced in this section.

5.5.1 Basic concept of the proposed load dependent sensor placement method

Under the term ‘load dependent’, we mean that the proposed sensor placement method is dependent on the responses of a structure, and consequently, on the actual loading situations besides the inherent characteristics of a structure: that is, the fitting of the multivariate regression equation is determined by both the mode shape matrix and the responses. As commented in Section 2.2, the existing sensor placement methods share a comment feature, which is that sensor positions are determined once the mode shape of a structure is given. No matter what responses will the structure undergo, the finally selected sensor positions are the same and don’t take actual structural responses into consideration.

Contrast to the existing sensor placement methods, the load dependent sensor placement method under discussion allows the consideration of the degree to which the mode shapes participate in actual structural responses. Its objective function is

the criterion proposed in Eq.(4.9) in Section 4.2.2. Under the almost global unbiasedness criterion, we strive to choose a given number of sensor positions that map the mode shapes of interest to the actual structural responses as closely as possible. In other words, structural responses will fall into the space spanned by the mode shapes as much as possible. Only in this way, can we fit the structural responses with the mode shapes, of course a truncated one, as accurately as possible. This is also the requirement for better modal parameter identification.

The essential feature of the widely used modal parameter estimation methods, for instance, the least squares complex exponential, the polyreference time domain, Ibrahim time domain, eigensystem realization algorithm[*JUANG* 1994], rational fraction polynomial, polyreference frequency domain and the complex mode indication function methods, is to fit the measured structural responses with the to-be-identified mode shapes as good as possible [*ALLEMANG and RESERVED* 1999; *EWINS* 2000]. If the measured structural responses can be regressed by the to-be-identified mode shapes at certain sensor positions better than other alternatives, these sensor position are the best choice since all the modal parameter estimation methods are implicitly or explicitly based on the principle of the least squares method in regression no matter it is in the frequency or the time domain [*ALLEMANG and BROWN* 1998]. Therefore, the objective of the proposed load dependent sensor placement method agrees naturally to the aim of modal parameter estimation methods.

Obviously, the objective of the proposed load dependent sensor placement method can not be fully achieved when the theoretical mode shapes, which are to determine sensor positions a priori, deviate much from that of estimated mode shapes from actual structural responses. This is a basic assumption for all sensor placement methods assumed throughout the dissertation. Another implicit assumption is that the mode shapes participate actively in the measured structural responses. In other words, much of the measured energy of the structural responses is contained in the interested mode shapes. Otherwise, the identified mode shapes can not sufficiently reflect structural dynamic features and result in loss of information.

Hence, sensor placement can be cast into a function of both structural characteristics and of where and how the structure is excited. This is the initial concept to propose the load dependent sensor placement method to achieve better identification of structural dynamic characteristics.

5.5.2 Computational considerations of the load dependent sensor placement method

The solution of the proposed load dependent sensor placement method can be achieved through the three methods as explained in Section 5.3.

Usually, multiple responses at different time instants are measured and will be fitted such as that in the RLS. Therefore, the RLS objective will be used in the norm sense of a matrix with each column corresponding to a time instant. The minimum thus achieved will be regarded as the best sensor positions to identify interested mode shapes as illustrated in Section 5.3.2.

Another consideration is related to unavailable responses. Structural responses used in Eq.(5.1) can be gathered by a pretest for an existing structure for health monitoring. It is, of course, not necessary to measure the responses at all candidate sensor locations. However, it is recommended to locate the pretest measurements in a spatially separated manner so that the measured responses can represent more rationally the behavior of the structure. For a structure to be built, the required measured responses can be approximated through analytical computation by assuming several loading cases as is normal in the design phase of a structure. If there are empirical measurements about the loadings in site where the structure will be constructed, for example for a bridge, the speed and spectrum of the wind, and the estimated traffic loadings, then the predicted responses will be more reliable.

Load dependent doesn’t necessarily mean that we have to totally change the sensor positions every time for structural dynamic testings or long-term health monitoring, which it not only inconvenient but unpractical. What we want to emphasize is that the sensors should be deployed with the consideration of typical structural loading cases in order to realize better modal identification. For a structure, it bears, in normal cases, several loading conditions. The combinations of these loading conditions can be used to find typical structural responses, and thus to locate better sensor positions with the idea of the proposed load dependent sensor placement method.

5.5.3 Application of load dependent sensor placement method to the I-40 bridge

We use again the I-40 Bridge to illustrate the idea and computation of the loading dependent sensor placement method. The details of the I-40 Bridge were already introduced in Section 3.3 where the responses were assumed to have same amplitudes for all candidate sensor positions.

The actual responses, except the frequency response functions, have not been recorded during the bridge tests. We simulated the responses with the six modes of interest and a mode participation factor. Five percent of Gaussian random noise multiplied by amplitude of the maximum of the simulated response was added.

Under these circumstances, the sensor positions computed by subspace approximation of the load dependent sensor placement idea were S7,S8,S11,S12,N2,N12 (refer to Fig.3-1), which differ apparently much from that given by the EI (S3,S7,S11,N3,N7,N11). The sensor set chosen by this case with a relative small subset approximate to the original least squares estimator with the whole data set. These sensors are considered representative and sufficiently approaching to portrait the scenario defined by the original full data set under such loading conditions.

6 Experimental Validation

In this Chapter, the load dependent sensor placement method based on the Representative Least Squares method proposed in Chapter 5 is to be applied to a truss structure. The identified mode shapes are employed to verify the effectiveness of the load dependent sensor placement method through comparing it with other commonly used sensor placement methods as discussed in Section 2.1 in terms of modal identification accuracy.

6.1 Model structure

The experimental structure is a space frame truss with 6 bays as shown in Fig.6-1. The dimension of each bay is 500mm in x direction, 300mm in y direction, and 500mm in z direction. The y and z dimensions are such arranged to allow the y dimension relatively weak and to decrease the participation of torsional modes as little as possible. The total height of the truss is 3 meters and the 6 bays are equally divided. The truss is pinned firmly at one end on the floor with x direction upward pointed through a steel base. The bays of the truss are numbered 1 to 6 from the bottom upwards. The steel bars used to construct the truss are formed rectangular hollow bars, I 20mm x 20 mm x 2mm according to the standards of DIN59410.

Table 6-1. First 14 calculated natural frequencies and modes.

Mode Number	1	2	3	4	5	6	7
Frequencies (Hz)	5.482	17.049	17.770	25.939	30.640	42.537	44.982
Mode property	1st Bending in Y	2nd Bending in Y	1st Torsional	1st Bending in Z	3nd Bending in Y	2nd Torsional	4th Bending in Y
Mode Number	8	9	10	11	12	13	14
Frequencies (Hz)	53.129	59.283	62.855	70.101	72.287	79.438	82.901
Mode property	3nd Torsional	4th Bending in Y	5th Bending in Y Mixed with little Torsion	Mixed Bending and Torsional	Mixed Bending and Torsional	Mixed Bending and Torsional	Mixed Bending and Torsional

In order to decrease the natural frequencies of the truss within the measurement range of our experiment facilities, lumped masses of 2kg are attached at each node, respectively. In total, 24 masses are used. At a result, fourteen modes fall below 100

Hetz, among which five are bending modes in the weak y direction as shown in Table 6-1.

Fig.6-1 Truss structure in experiment

The frequencies listed in Table 6-1 are computed from the FE model as shown in Fig.6-2. The Young's modulus of the bars is 210,000 MPa, the Poisson's ratio is 0.33 and the density of steel is 7850 kg/m^3. There are in total 28 nodes, among which four nodes are fixed to the floor base as shown in the photograph in Fig.6-1. In Fig.6-2, the numbers in bracket indicate node numbers. The bars are modeled of space frame elements to compute the theoretical eigenfrequencies and mode shapes. A space frame element is a straight bar of uniform cross section which is capable of resisting axial forces, bending moments about the two principle axes in the plane of its cross section and twisting moment about its centroidal axis, and a consistent mass matrix is used [*RAO* 2005], i.e. the same displacement model is used for the derivation of both stiffness matrix and mass matrix. Each node has six DOFs and there are in total 168 DOFs, among them 84 are rotational dofs that are not measured in the following experiments due to its difficulty [*KATTAN* 2003].

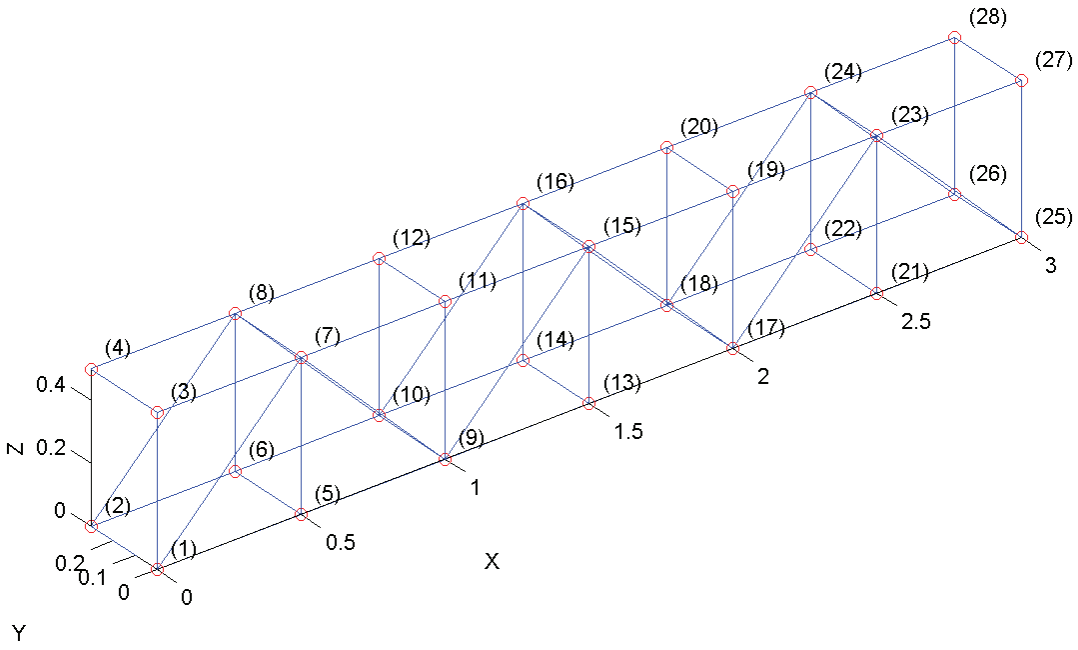

Fig.6-2 Finite element model of the truss

Fig.6-3 and Fig.6-4 show the first two bending modes in the weak y direction, respectively. It can be easily observed that all bays translate when the truss vibrates in a certain bending mode. Under such circumstances, the torsional responses are min-

imized and can, therefore, be neglected. Consequently, one node in a bay can sufficiently indicates the dynamic behaviour of the whole bay. In the subsequent sections, the truss is then represented by only six nodes, each of which represents a bay where it locates when presenting mode shapes as shown in Fig.6-5.

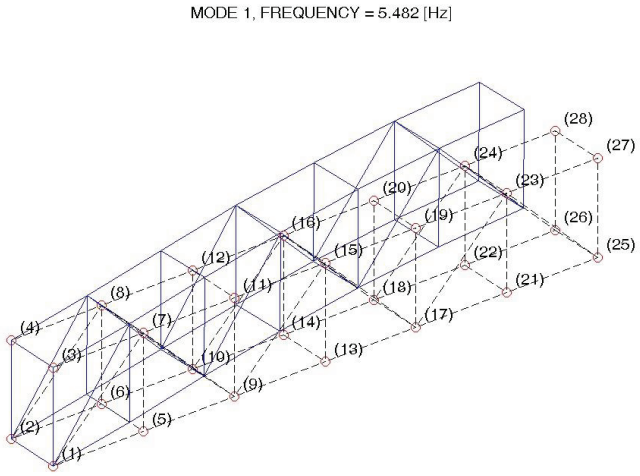

Fig.6-3 the 1st mode of the truss. (1st bending mode in the y direction)

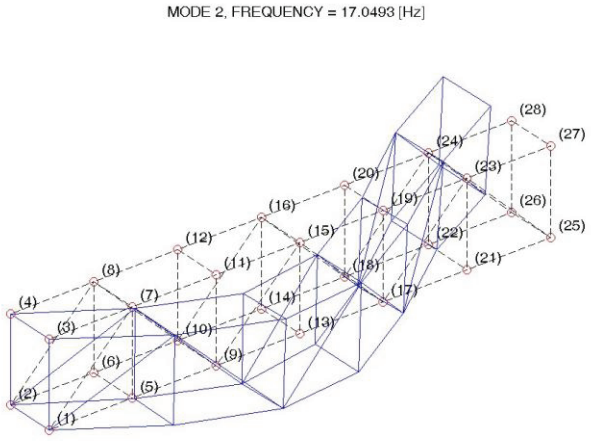

Fig.6-4 the 2nd mode of the truss. (2nd bending mode in the y direction)

6.2 Experiment setup

In our laboratory, 12 accelerometers are available. They are 8 PCB ICP accelerometers (Frequency range: 1 ~ 1000 Hz), and 4 HBM B12/200 accelerometers (Frequency range: 0 ~ 100 Hz). Therefore, the effective measurement range of our accelerometers is below 100 Hz, which sufficiently covers the first 14 mode shapes as observed in Table 6-1.

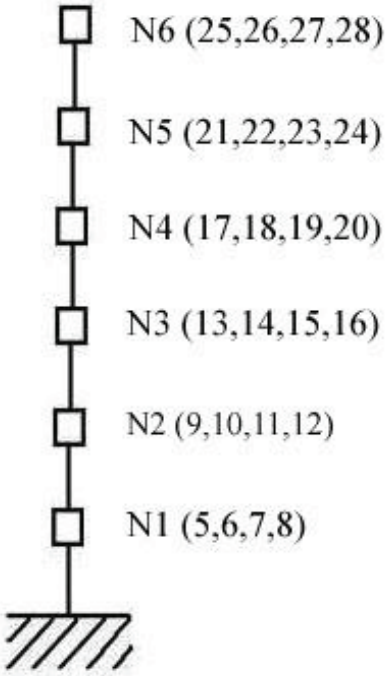

Fig.6-5 Simplified truss representation with each node indicating one bay (numbers in brackets are corresponding node numbers in Fig.6-2)

The data acquisition system is DIAdem with Spider 8 by HBM. The 12 acceleration signals as well as two force signals from the shakers are sampled at a rate of 1200 Hz and stored in the computer in .asc format for later processing. All A/D converters operate synchronized and supply up to 9,600 measurements/s from each channel with a resolution of 16 bit. Two electromagnetic shakers are fixed horizontally on the wall of our laboratory in parallel to excite the truss synchronously. To minimize the torsional responses of the truss, the excitation signals input to the shakers share the same signal generator. The type of the signal generator is Agilent 3312A, which can produce signals up to 15MHz with arbitrary waveforms. The generated signals are then amplified by an amplifier and coupler Kistler Type 5134 and redirected to the two shakers to excite the truss.

Moreover, a small crane, which was used to move the two shakers with steel ropes, was fixed just under the room ceiling as indicated on the top of Fig.6-1. The two shakers can, therefore, be conveniently lifted up or lowered down by the crane to any of the six bays in order to excite the truss at different horizontal levels. This experimental arrangement is deliberately designed to test the influence of different excitation positions on the placement of sensors, which is the central concept of Chapter 5, i.e. sensors placement depends not only on the structure itself, but also on its actual loading conditions in order to achieve better modal identification accuracy.

Six setups with different shaker positions are tested. In each setup, both shakers are bolted to two horizontal nodes of a bay in both sides of the truss to excite it translationally. To take the Setup 2 for example, both shakers are connected to the Bay 2 at side nodes as shown in Fig.6-1. Similarly, Setup 1 to Setup 6 are tested when the shakers are located at the Bay 1 to Bay 6 to excite the truss sequentially. In all of the six setups, the identification accuracy of the frequencies and mode shapes can then be obtained and is compared among different setups to evaluate which of the combination of sensor positions are better than others.

6.3 Sensor placement for the truss with traditional methods

As discussed in Section 2.2, the existing sensor placement methods share a common feature, which is that the sensor positions are solely determined by the structure. Once a structure model is given, the sensor positions are thus determined as well. To take the truss structure under experiment for example, the optimal positions to deploy sensor are consequently determined once a certain sensor placement method is chosen no matter what responses the structure undergoes.

In this section, the seven influential sensor placement methods detailed in Section 2.1 will be computed to choose sensor positions for the truss. Table 6-2 lists the seven methods and their ranking of the six candidate sensor positions on the truss. In the table, the bays of the truss are numbered 1 to 6 from the bottom to the top as shown in Fig.6-4.

Table 6-2 shows that almost all the seven methods rank the candidate sensor positions 6, 5 and 1 the most important and the sensor positions 2, 4, and 3 the least important. For the truss, our final goal is to select five out of the six sensor positions to deploy sensors. According to the EI, MKE, MSSP, DPR and QR, the unselected candidate sensor positions should be 3, whereas 2 and 4 according to the ECP and MinMAC, respectively.

Table 6-2. Ranking of six candidate sensor positions with the seven methods.

MKE	6	1	5	2	4	3
MKE Index	1.103	0.92557	0.86855	0.7667	0.70649	0.62966
EI	6	1	5	2	4	3
EI Index	0.98512	0.92069	0.87701	0.77901	0.74128	0.69688
ECP	6	1	5	4	3	2
ECP Index	0.016056	0.004868	0.004503	0.002851	0.00166	0.000916
MSSP	6	1	5	4	2	3
MSSPIndex	2.2759	1.9825	1.9201	1.7322	1.7194	1.6156
DPR	6	1	5	2	4	3
DPR Index	1.103	0.92557	0.86855	0.7667	0.70649	0.62966
QR	6	1	5	2	4	3
MinMAC	5	6	2	1	3	4

6.4 Comparison of the mode shapes identified with all six candidate sensor positions with theoretical mode shapes

In this section, the first five mode shapes of the truss are identified with all six sensor positions with measured acceleration responses. Moreover, the identified mode shapes are compared with theoretical ones to confirm that the modeling of the truss is adequate to characterize the actual dynamics of the truss.

The mode shapes in our investigations are identified with the commercial software ME'scopeVES Version 4.0 accompanied with B&K 3560C. Frequency Response Functions (FRFs) for each response point were transferred to ME'scope via the Universal File Format (UFF). The structure was modeled in ME'scope as a wireframe,

and each transfer FRF of impact point was associated with the appropriate DOF at each response location. The composite FRF data set for the whole structure was assembled from individual field data sets to highlight all possible global modal frequencies. Five identified mode shapes with all six candidate sensor positions are listed in Table.6-3.

Table.6-3, Identified mode shapes with all six candidate sensor positions

Mode No.	Frequency	Units	Damping (%)
1	5.13	Hz	0.028
2	17.9	Hz	1.51
3	32	Hz	0.156
4	47.7	Hz	0.271
5	63.2	Hz	0.153

Node No.	Meas.Type	DOFs	Units	Mode 1	Mode 2	Mode 3	Mode 4	Mode 5
1	Residue mode shape	1Y:2Y	(m/s^2)/ N-sec	0.1348	0.3513	0.5244	-0.5288	0.4791
2	Residue mode shape	2Y:2Y	(m/s^2)/ N-sec	0.2627	0.55	0.3892	0.1159	-0.5001
3	Residue mode shape	3Y:2Y	(m/s^2)/ N-sec	0.3448	0.4766	-0.2101	0.5176	0.1366
4	Residue mode shape	4Y:2Y	(m/s^2)/ N-sec	0.4705	0.1608	-0.5295	-0.2557	0.3414
5	Residue mode shape	5Y:2Y	(m/s^2)/ N-sec	0.5096	-0.2317	-0.1396	-0.4509	-0.554
6	Residue mode shape	6Y:2Y	(m/s^2)/ N-sec	0.5593	-0.517	0.4791	0.4126	0.2797

The theoretical mode shapes computed by the FEM are numerically listed in Table.6-4 for comparison purpose. Fig.6-6 illustrates experimentally identified mode shapes as red dashed lines with all six candidate sensor positions. The theoretical mode shapes computed by the FEM are shown as blue solid lines. The lower-right plot in Fig.6-6 illustrates relative identification errors of the identified mode shapes compared with theoretical ones. The identification error is summed for all six positions that define the mode shapes of the truss according to $\varepsilon(\%) = \left\| \mathbf{\Phi}_A - \mathbf{\Phi}_E \right\|_1 \Big/ \left\| \mathbf{\Phi}_A \right\|_1$, where

$\|\Phi_A\|_1$ is the absolute summation of each mode shape components. The comparison is conducted in relative difference in amplitude of the mode shapes when both mode shapes are normalized to unit length. It is obviously observed that the identification error for the 4th mode shape is the largest and the 3rd mode is the most accurately identified mode shape with the smallest identification error.

Table 6-4. Five theoretical mode shapes of the truss

Node No.	Mode 1	Mode 2	Mode 3	Mode 4	Mode 5
1	0.1115	-0.3285	0.5057	-0.5960	0.4408
2	0.2362	-0.5289	0.3973	0.0354	-0.5216
3	0.3532	-0.4561	-0.2254	0.4872	0.0939
4	0.4513	-0.1347	-0.5365	-0.2307	0.3789
5	0.5260	0.2702	-0.1308	-0.4312	-0.5620
6	0.5715	0.5597	0.4803	0.4088	0.2557

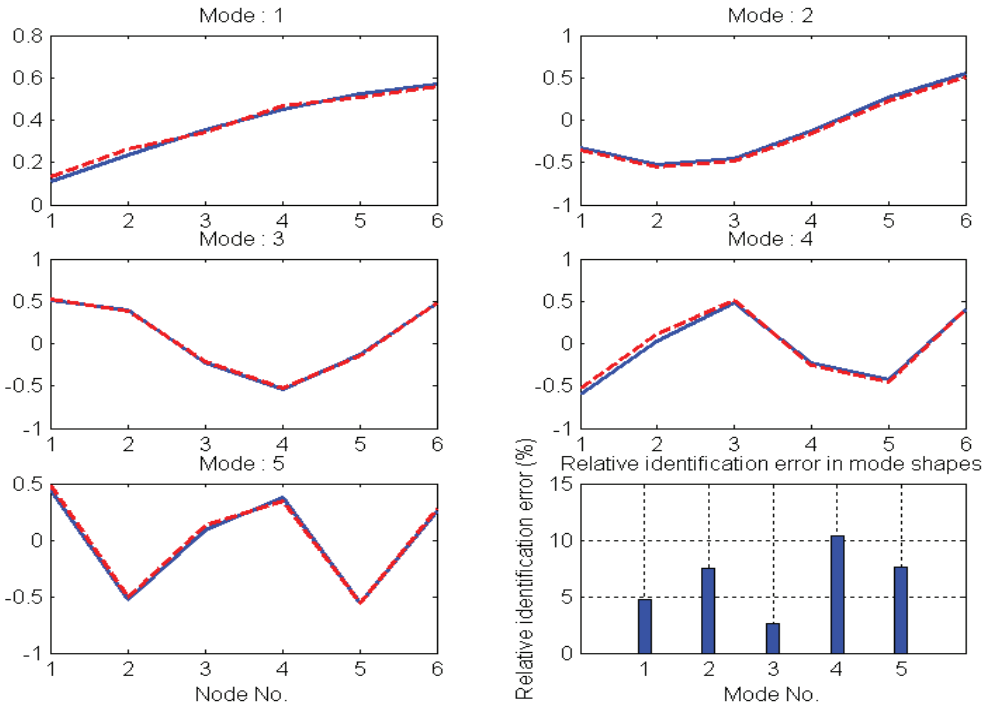

Fig.6-6 Mode shape comparison, blue solid line – theoretical; red dashed line – identified.

Moreover, the MAC matrix is computed as the same time as another alternative evaluation means. Fig.6-7 shows the MAC values between the identified mode shapes with all six candidate sensor positions and the theoretical ones in Fig.6-7b and the plot in Fig.6-7a. The MAC values shows also that the 3rd mode shape is most accurately identified whereas the 4th is comparatively not, which confirms the conclusion drawn from Fig.6-6 once again.

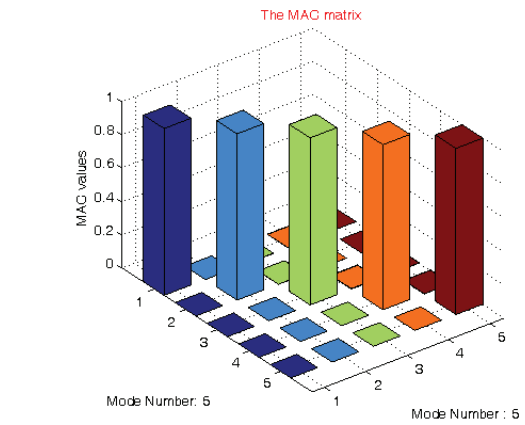

Fig.6-7a. MAC plot.

0.9979	0.0001	0.0014	0.0012	0.0000
	0.9946	0.0004	0.0004	0.0000
		0.9992	0.0032	0.0013
			0.9871	0.0014
Sym.				0.9942

Fig.6-7b. MAC values.

Furthermore, all the values of the diagonals of the MAC matrix in Fig.6-7b are exceeding 0.98. Therefore, the identified mode shapes agree, in general, with the theoretical ones perfectly well. It is worth noting that the identified mode shapes in this section are obtained from measured responses at all the six candidate sensor positions, which is not the case for the subsequent comparisons anymore and noted here for distinction.

6.5 Experimental verification of the load dependent sensor placement method

In this section, the difference between the mode shapes identified with all the six candidate sensor positions and the mode shapes identified with only certain five candidate sensor positions is compared, which is used to verify the theory of the load dependent sensor placement method proposed in Chapter 5.

In the truss model, we can identify the mode shapes of the truss with six different setups. Therefore, it is more convenient and vivid to directly compare the accuracy of

the identified mode shapes instead of the response fitting since mode shapes are the ultimate goal for evaluating sensor placement in the theory of the load dependent sensor placement method. In fact, the comparison of mode shapes is equivalent to comparison of goodness-of-fit of responses in the RLS in the computed cases as discussed in Section 5.5. In the following, the measured responses in Setup 2 and Setup 5 are employed to identify the first five mode shapes and the identification accuracy is then compared.

6.5.1 Comparison of the identified mode shapes with five candidate sensor positions in Setup 2 with theoretical ones

In this subsection, the measured responses of Setup 2 will be used to identify the mode shapes of the truss. In Setup 2, both shakers excite directly the truss through the two connection nodes at the Bay 2 and six acceleration responses are recorded. Furthermore, we will sequentially exclude one measurement at a certain sensor position and identify the five mode shapes with the responses at the five remaining sensor positions. The identified mode shapes with five components are then compared with the theoretical ones that are reduced accordingly. First, Sensor 1 at Bay 1 will be excluded and then Sensor 2 at Bay 2 until Sensor 6 at Bay 6. These cases are dubbed as Case 1 to Case 6 and listed in Table 6-5. All the cases are conducted under Setup 2.

Table 6-5. Mode shape identification error in Setup 2

Case No.	Mode 1	Mode 2	Mode 3	Mode 4	Mode 5	Absolute Error	Relative Error
1	0.0652	0.1631	0.0369	0.1377	0.1351	0.5380	0.2637
2	0.0611	0.1875	0.0594	0.1520	0.1759	0.6358	0.3067
3	0.1029	0.1767	0.0488	0.2406	0.1269	0.6959	0.3422
4	0.1093	0.1515	0.0642	0.2125	0.1475	0.6849	0.3338
5	0.1076	0.4094	0.0507	0.2371	0.1977	1.0025	0.4912
6	0.1452	0.1067	0.0676	0.2438	0.1476	0.7110	0.3519

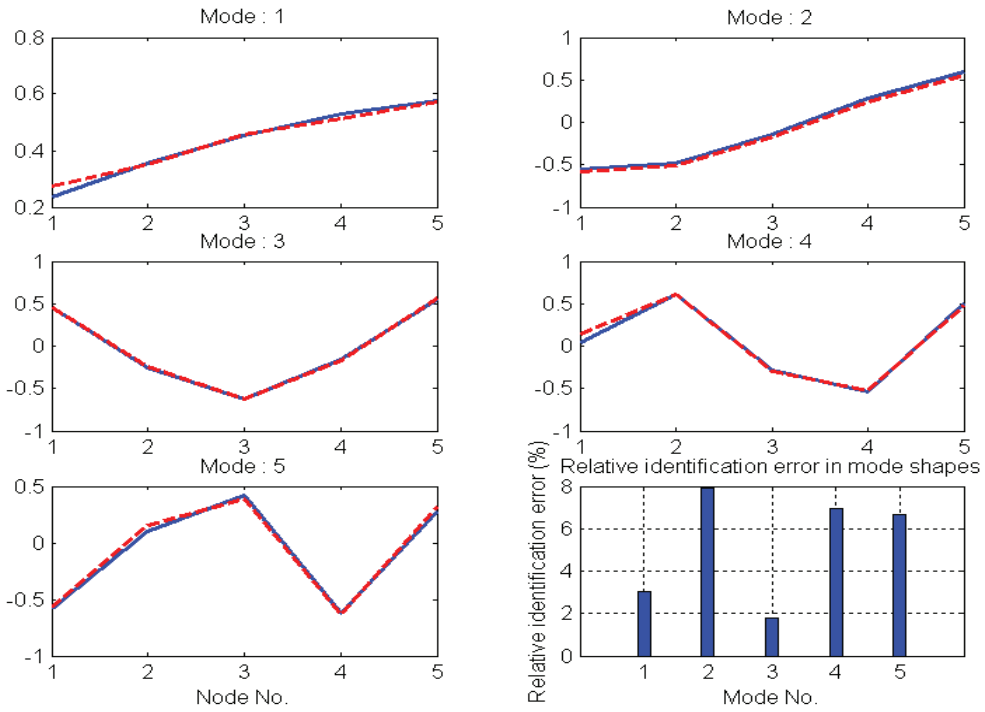

Fig.6-8(a) Mode shape comparison for Case 1, blue solid line – theoretical; red dashed line – identified.

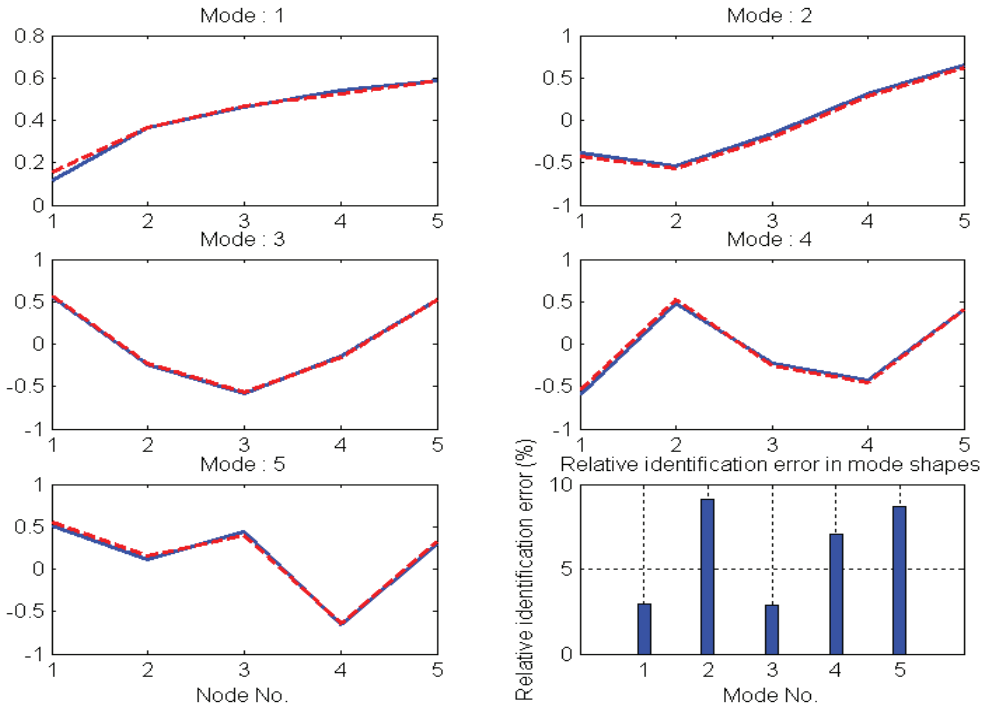

Fig.6-8(b) Mode shape comparison for Case 2, blue solid line – theoretical; red dashed line – identified.

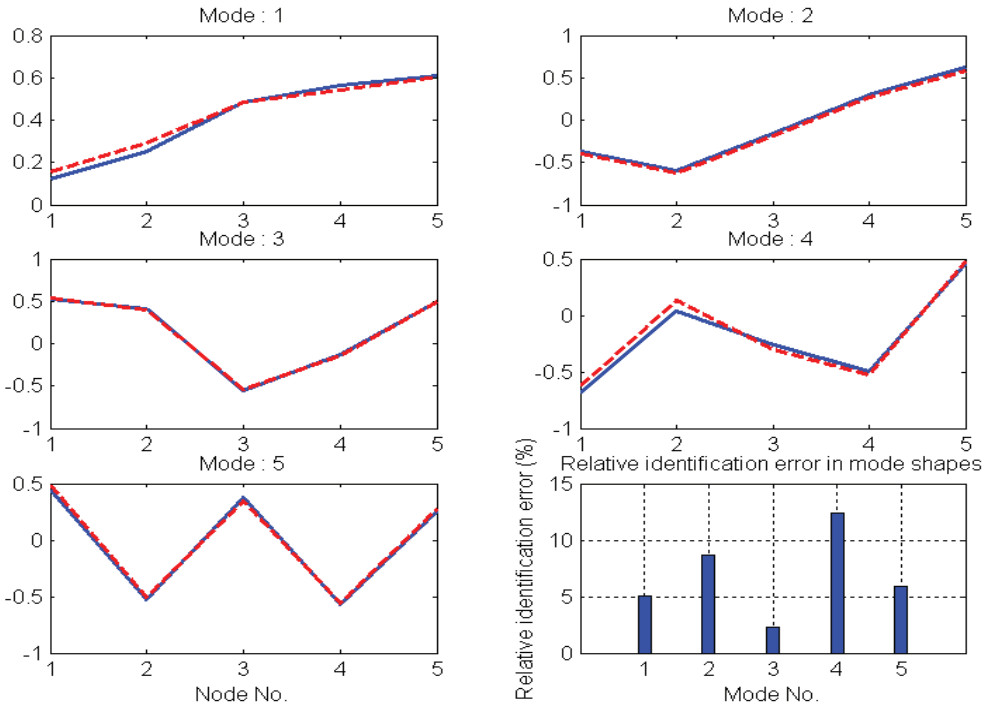

Fig.6-8(c) Mode shape comparison for Case 3, blue solid line – theoretical; red dashed line – identified.

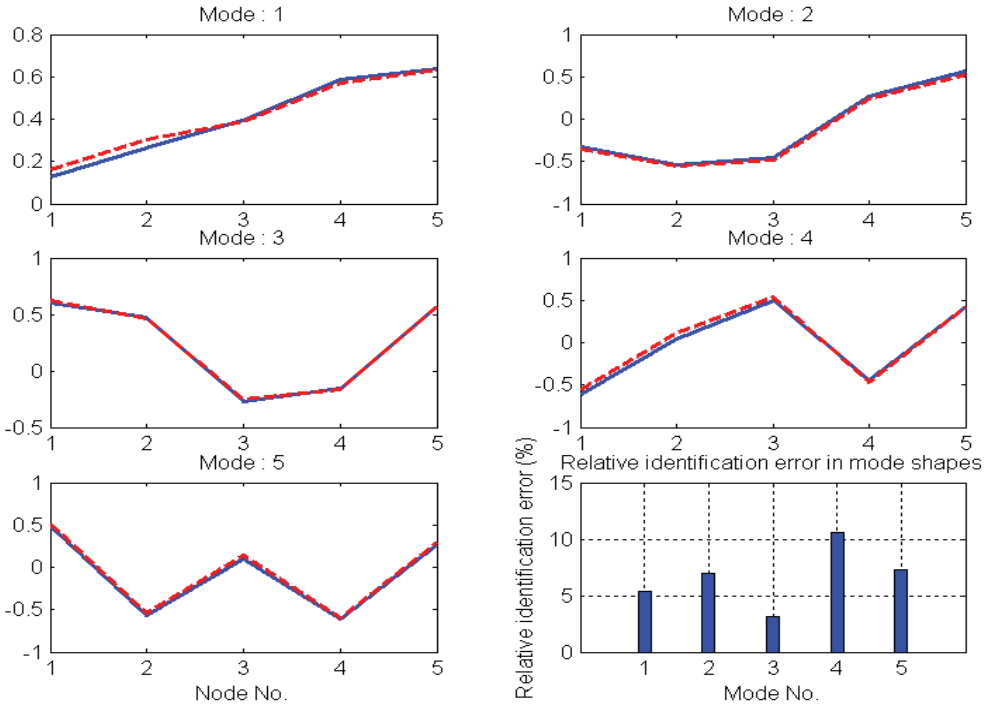

Fig.6-8(d) Mode shape comparison for Case 4, blue solid line – theoretical; red dashed line – identified.

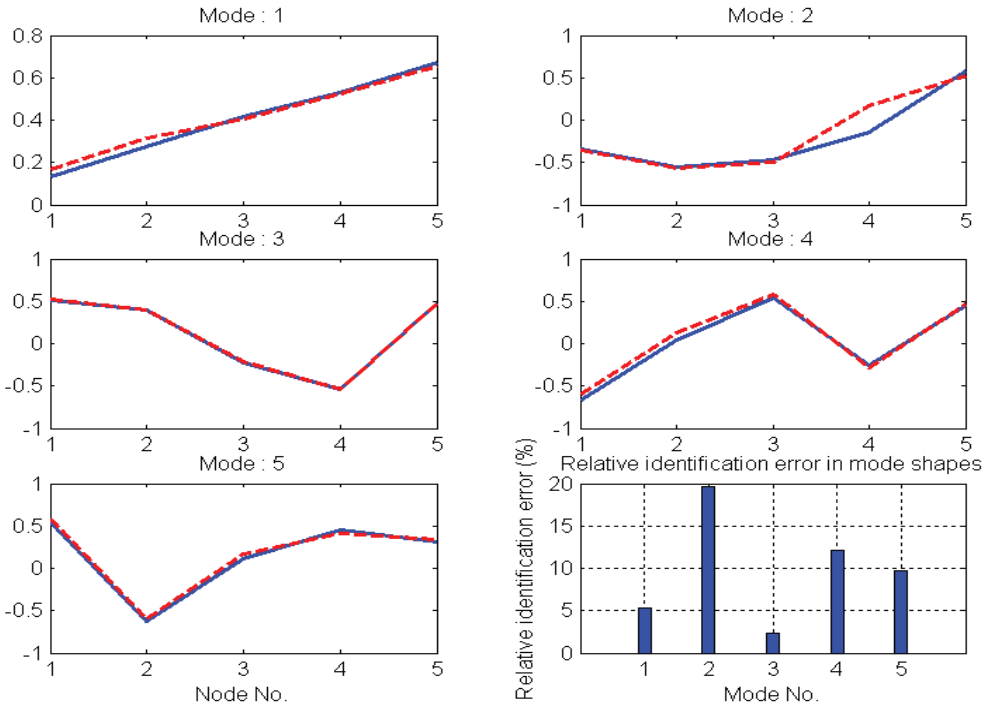

Fig.6-8(e) Mode shape comparison for Case 5, blue solid line – theoretical; red dashed line – identified.

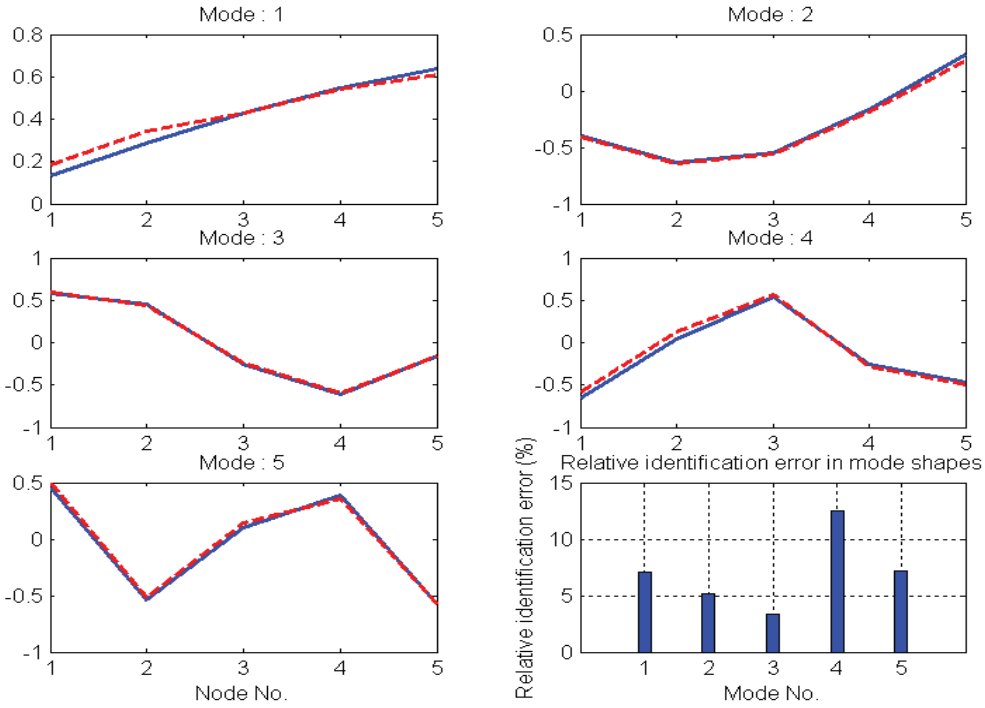

Fig.6-8(f) Mode shape comparison for Case 6, blue solid line – theoretical; red dashed line – identified.

Fig 6-8 illustrates the comparison for all 6 cases. The first five plots in Fig.6-8 illustrate the theoretical mode shapes in blue solid lines, whereas the experimentally identified mode shapes in red dashed lines. From Fig.6-8 (f), it is easily observed that Mode 4 has a large identification error than the other 4 mode shapes in Case 6. If the measurement responses at Bay 5 are not used in the identification, Mode 2 deviates much from its theoretical one in Case 5 as interpreted from Fig.6-8 (e).

The lower-right plot in Fig.6-8 shows relative identification errors (%) of the identified mode shapes compared with theoretical ones. The absolute identification error for each mode and each case are numerically listed in Table 6-5. The summations of absolute and relative identification errors for all 6 cases are listed in last two columns of Table 6-5, respectively. If one sensor position is absent, for instance, Node 1 absent in Case1 and the identification error is large, then that sensor position would be more important. Consequently, the relative importance of all the six candidate sensor positions is ranked decreasingly as: 5, 6, 3, 4, 2, and 1 according to Table 6-5.

Therefore, the best sensor sequence is 5, 6, 3, 4, 2, and 1 for the loading case of Setup 2. This sensor sequence differs much from those ranking sequences by the traditional methods as in Section 6.3, where most of the methods indicate that Node 1 is very important. However, Node 1 ranks the least importance in Setup 2. This result infers that sensor placement should be dynamic and sensors ought to be deployed according its actual responses.

6.5.2 Comparison of the identified mode shapes with five candidate sensor positions in Setup 5 with theoretical ones

Similar to Section 6.5.1, we will sequentially exclude one measurement at a certain sensor position and identify the five mode shapes with the remaining five sensor positions and compare it with the reduced theoretical mode shape in Setup 5, i.e. the two shakers are now located at the Bay 5 to excite the truss. First, Sensor 1 at Bay 1 will be excluded and then Sensor 2 at Bay 2 until Sensor 6 at Bay 6, and these cases are dubbed as Case 1 to Case 6 and listed in Table 6-6. All the cases are conducted under Setup 5.

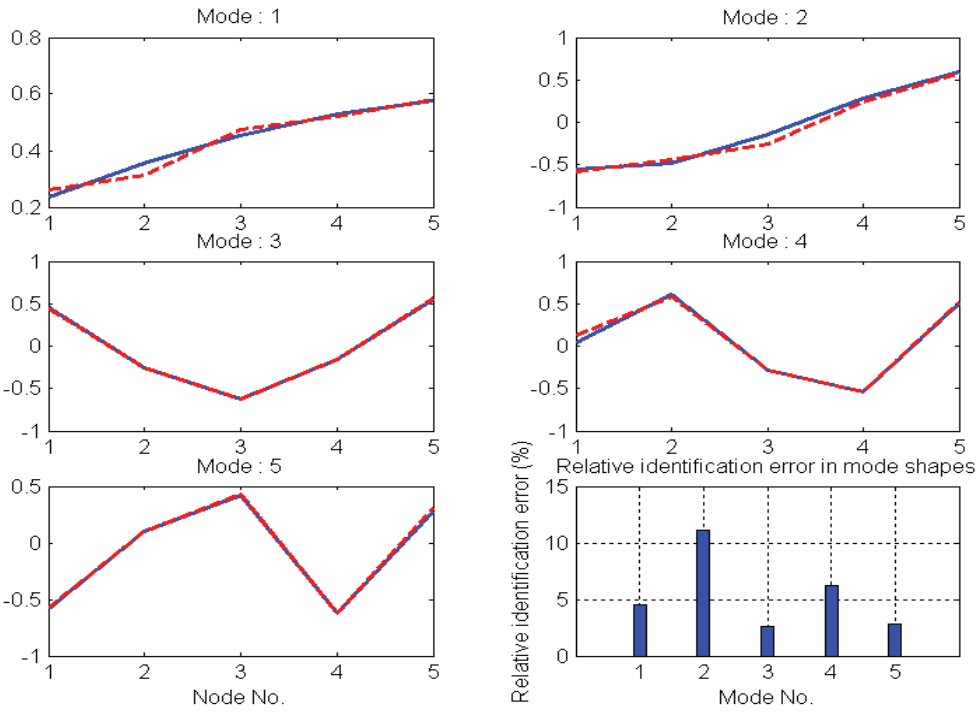

Fig.6-9 (a) Mode shape comparison for Case 1. Blue solid line – theoretical; red dashed line - identified.

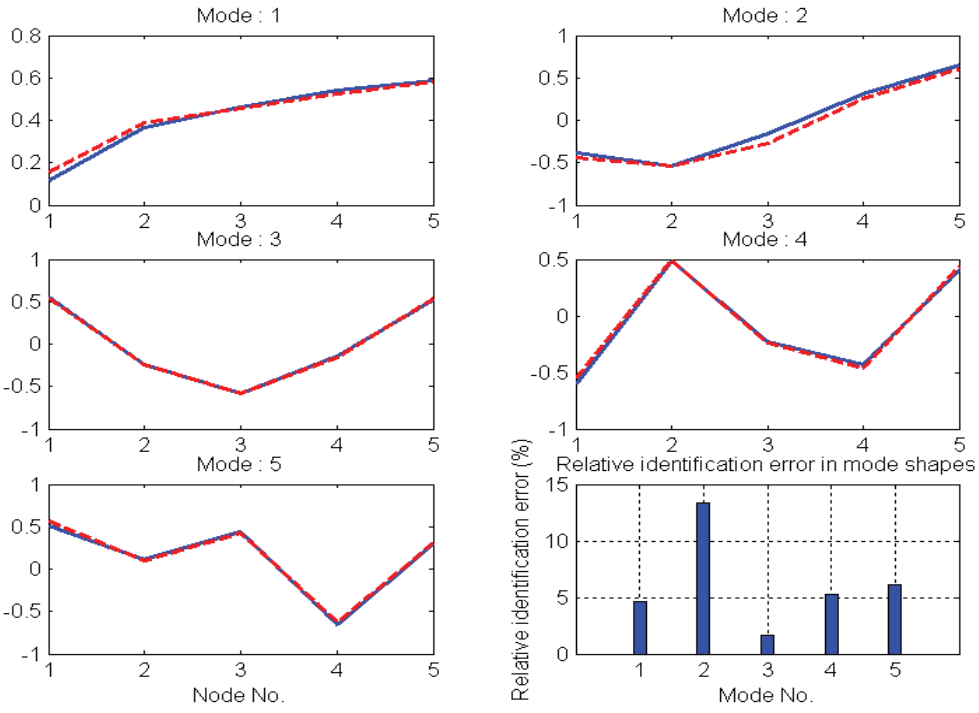

Fig.6-9 (b) Mode shape comparison for Case 2. Blue solid line – theoretical; red dashed line - identified.

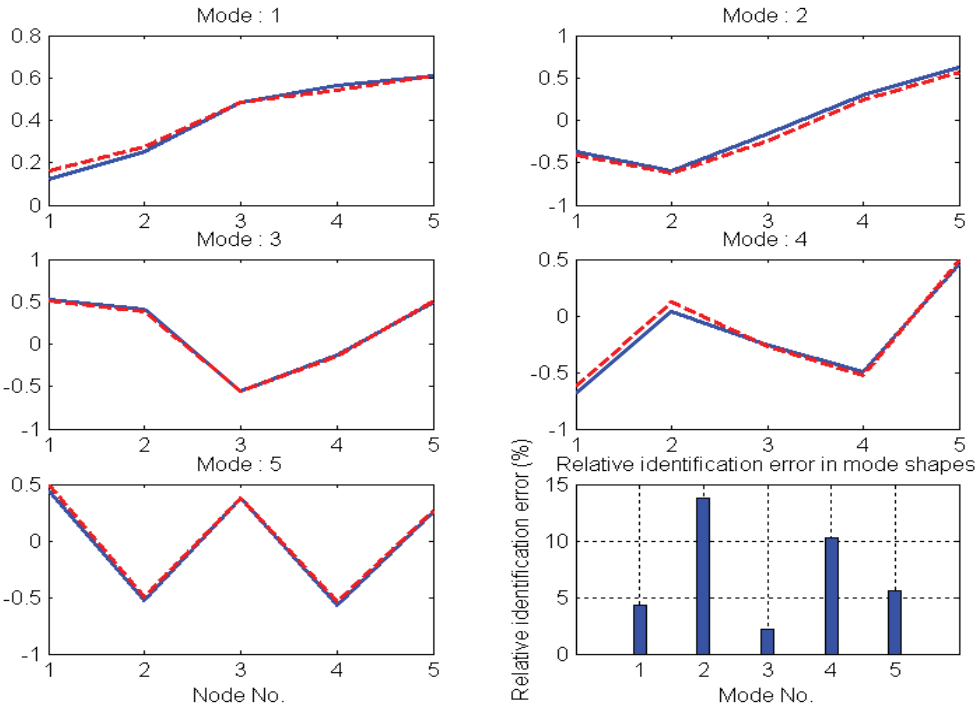

Fig.6-9 (c) Mode shape comparison for Case 3. Blue solid line – theoretical; red dashed line - identified.

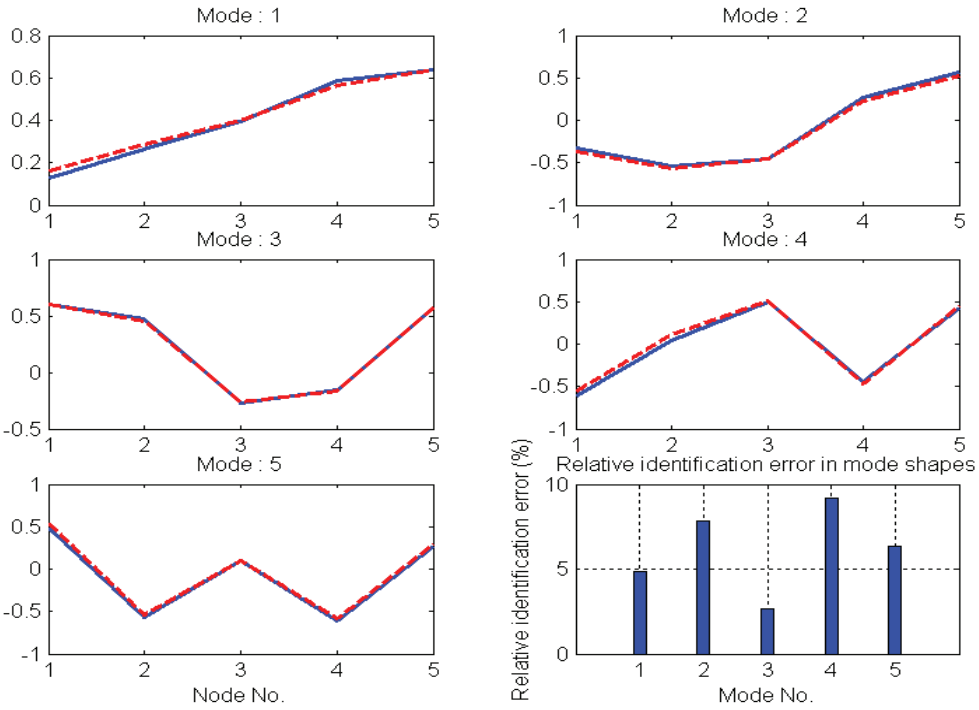

Fig.6-9 (d) Mode shape comparison for Case 4. Blue solid line – theoretical; red dashed line - identified.

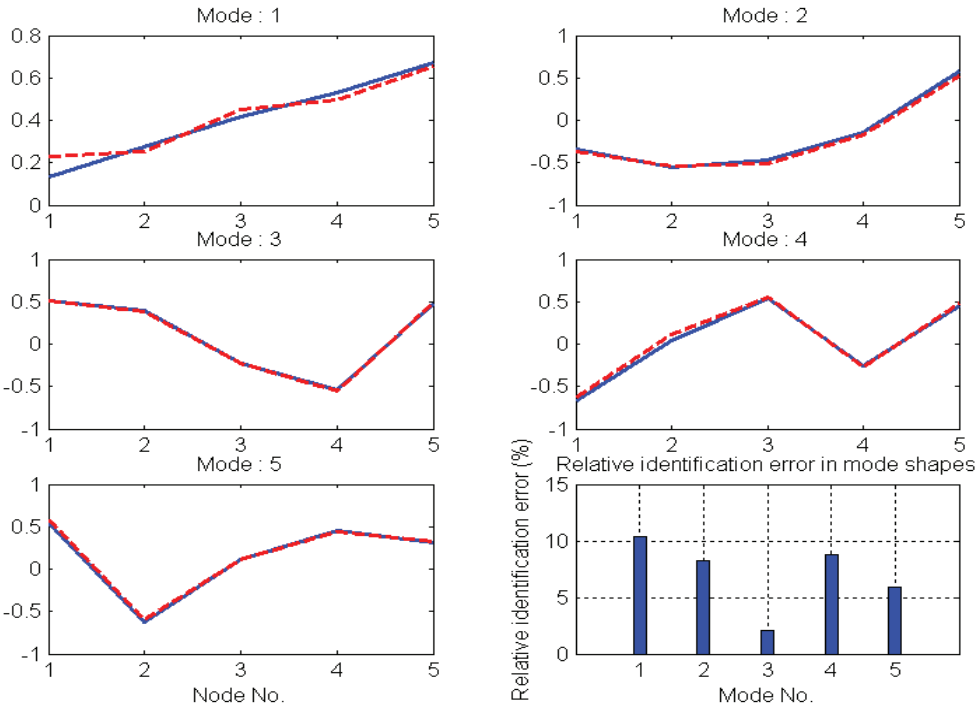

Fig.6-9 (e) Mode shape comparison for Case 5. Blue solid line – theoretical; red dashed line - identified.

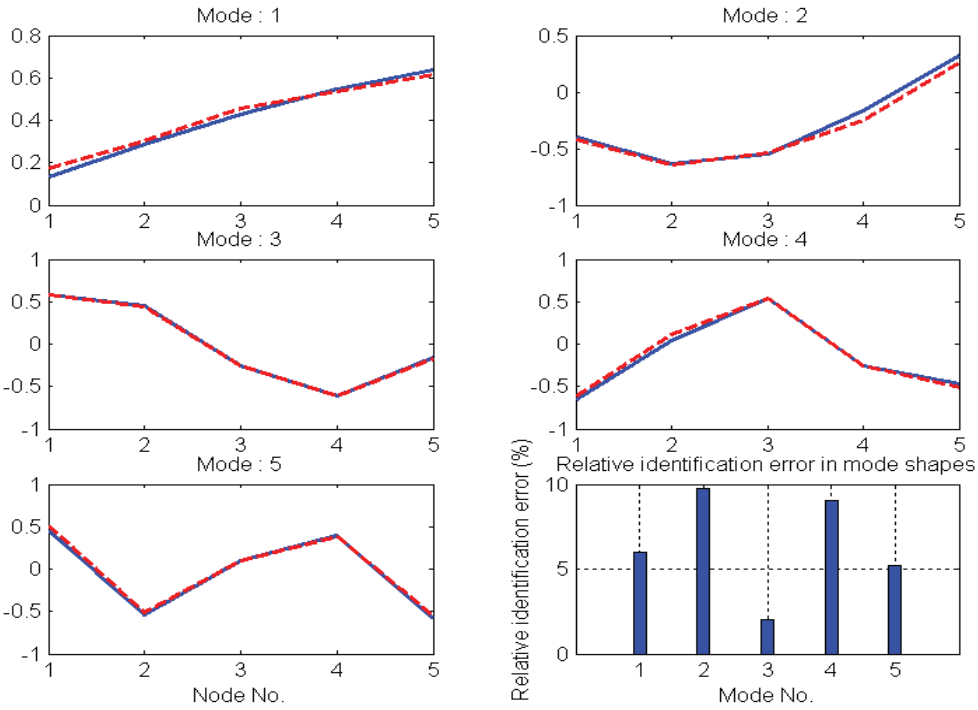

Fig.6-9 (f) Mode shape comparison for Case 6. Blue solid line – theoretical; red dashed line - identified.

Fig 6-9 illustrates the comparison for all 6 cases. The first five plots in Fig.6-9 illustrate the theoretical mode shapes in blue solid lines, whereas the experimentally identified mode shapes in red dashed lines. Fig.6-9 (c) shows that Mode 2 and Mode 4 will have relatively large identification errors if the measurement responses at Bay 3 are excluded in the identification process. By comparison, the mode shapes identified in Case 6 deviate much from its theoretical ones than those identified in Case 5 as interpreted from Fig.6-9(e) and Fig.6-9(f).

The lower-right plot in Fig.6-9 shows relative identification errors (%) of the identified mode shapes compared with theoretical ones. The absolute identification error for each mode and each case are numerically listed in Table 6-6. The summations of absolute and relative identification errors for all 6 cases are listed in last two columns of Table 6-8, respectively. The relative importance of all the six candidate sensor positions in terms of the identification accuracy for the mode shapes is ranked decreasingly as: 3, 5, 6, 2, 4 and 1 according to Table 6-6.

Table 6-6. Mode shape identification error in Setup 5

Node No.	Mode 1	Mode 2	Mode 3	Mode 4	Mode 5	Absolute Error	Relative Error
1	0.0973	0.2293	0.0529	0.1238	0.0570	0.5604	0.2728
2	0.0954	0.2749	0.0336	0.1146	0.1234	0.6417	0.3098
3	0.0881	0.2827	0.0468	0.2011	0.1203	0.7390	0.3624
4	0.0976	0.1693	0.0545	0.1850	0.1282	0.6346	0.3084
5	0.2093	0.1719	0.0442	0.1709	0.1203	0.7166	0.3527
6	0.1231	0.2017	0.0412	0.1757	0.1079	0.6496	0.3199

The candidate sensor sequence, 3, 5, 6, 2, 4 and 1 in Setup 5, is much different from that determined in Setup 2, in which the sequence is: 5, 6, 3, 4, 2, and 1. Especially, the identification error in Setup 2 as in the last section is in reverse order for Case 3 and Case 5 compared to the error in Setup 5. Therefore, we can easily observe that the relative importance of the six candidate sensor positions are changing with the loading conditions of the truss structure. The experiments have, therefore, powerfully verified that loading conditions under various working environment have to be accounted for when the issue of sensor placement is arisen.

6.5.3 Discussion of experimental results

Since the load dependent sensor placement method deploys sensors taking actual loading conditions of a structure into consideration, the sensor positions are not solely determined by the structure itself. For the truss under discussion, it means that the sensors have to be deployed at various positions for different loading cases.

In our experiments, Setup 2 and Setup 5 are selected as two typical loading conditions of the truss. The load dependent sensor placement method indicates two different sensor topologies for the same structure with two loading conditions. On the other hand, the traditional methods give only one sensor positions' ranking sequence no matter what the actual loading conditions of the structure change.

In the comparison of theoretical and experimentally identified mode shapes in Section 6.5.1 and Section 6.5.2, only a reduction of 6 to 5 sensors is compared due to available experiment facilities. The validation experiment is, thus, rather limited. If more candidate sensor positions are involved, the comparison will be much apparent.

On the other hand, only one load a time is designed in our validation experiments. In fact, many kinds of loads can act on a structure simultaneously, for instance, a combination of loads may excite the truss at several points. Moreover, their frequency range and effects deserve further investigations in the frequency domain.

Furthermore, the comparison of mode shapes is measured by their relative difference, which is an indirect means of the objective function defined in Chapter 5. As is known, the identification of mode shapes from recorded accelerations is a complicated process. Overdetermination and redundancy are common is many mode shape identification methods to improve identification accuracy. The direct linear relationship in the response equations could not be easily observed in the overdetermined mode shape identification equations as expected.

Nevertheless, what is most important in the investigations is that the essential idea of 'load dependence' in the field of sensor placement is established. Sensor positions should be changed when a structure is subjected to various loading conditions.

7 Summary and Future Research

The objective of the current work is to deepen the understanding of existing influential sensor placement methods and their interrelationship and to develop an effective method to deploy accelerometers suitable for structural health monitoring. Furthermore, we aim to find a sufficient evaluation criterion to judge which topology configuration of sensors outperforms than others.

Three major contributions are made in the dissertation. The connection of the influential Modal Kinetic Energy method and the Effective Independence method is derived and a fast algorithm for computing the Effective Independence method is developed. Furthermore, existing influential sensor placement methods are critically reviewed and discussed. An extended MinMAC algorithm is also proposed.

Secondly, five influential evaluation criteria for sensor placement are treated from a mathematical point of view to reveal their connections and interrelationship. Based on this, an almost unbiasedness criterion is proposed, which is found to be a more general criterion and can be regarded as step-by-step approximate to the Fisher information criterion used by the Effective Independence method.

Finally, a loading dependent sensor placement method is specially developed to incorporate the influences of the structural characteristics and that of actual loading conditions with the aid of the proposed representative least squares method. Three computational approaches to find the solution for the representative least squares method and also for the loading dependent sensor placement method are examined. A truss model structure is used to validate the idea and the proposed methods in the dissertation.

There are two important issues still to be solved in the future. Firstly, the role of the renormalization and reorthogonalization of the mode shapes deserves further investigations combined with the concept of reduced-order system. Although the fundamental assumption of the mode shape identification methods is the linearity of the systems and a linear model is assumed, the detailed relationship of the goodness-of-fit of the linear measurement equation with the accuracy of modal identification is rather complex. The hidden relationship needs further examination.

8 References

ALLEMANG, R. J., and BROWN, D. L., 1982: A Correlation Coefficient for Modal Vector Analysis. *Proceedings of the International Modal Analysis Conference*, 110-116.

ALLEMANG, R. J., and BROWN, D. L., 1998: A Unified Matrix Polynomial Approach to Modal Identification. *Journal of Sound and Vibration*,**211**, 301-322.

ALLEMANG, R. J., and RESERVED, A. R., 1999: Vibrations: Analytical and Experimental Modal Analysis. University of Cincinnati, OH.

BALAGEAS, D., FRITZEN, C. P. and GÜEMES, A., 2006: Structural Health Monitoring. ISTE, London, UK.

BALMES, E., 2005: Orthogonal Maximum Sequence Sensor Placements Algorithms for Modal Tests, Expansion and Visibility. *Proceedings of the 24th International Modal Analysis Conference (IMAC–XXIII), Orlando, FL.*

BASSEVILLE, M., BENVENISTE, A., MOUSTAKIDES, G. V. and ROUGEE, A., 1987: Optimal Sensor-Location for Detecting Changes in Dynamic Behavior. *Ieee Transactions on Automatic Control*,**32**, 1067-1075.

BECK, J. V., and ARNOLD, K. J., 1977: Parameter Estimation in Engineering and Science. John Wiley & Sons.

BICCHI, A., and CANEPA, G., 1994: Optimal Design of Multivariate Sensors. *Measurement Science and Technology*,**5**, 319-332.

BJÖRCK, Å., 1996: Numerical Methods for Least Squares Problems. SIAM, Philadelphia.

BOHLE, K., 2005: Sensitivitätsbasierte Methoden Zur Modellgestützten Schadendiagnose Mit Modaldaten, University of Siegen.

BOS., A. V. D., 2007: Parameter Estimation for Scientists and Engineers. Wiley-Interscience, Hoboken, N.J.

CARNE, T. G., and DOHRMANN, C. R., 1995: A Modal Test Design Strategy for Model Correlation. *International Modal Analysis Conference, 13 th, Nashville, TN, Proceedings.*,**1**, 927-933.

CHATTERJEE, S., 1988: Sensitivity Analysis in Linear Regression. John Wiley & Sons, Inc. New York, NY, USA.

CHERNG, A. P., 2003: Optimal Sensor Placement for Modal Parameter Identification Using Signal Subspace Correlation Techniques. *Mechanical Systems and Signal Processing*,**17**, 361-378.

CHUNG, Y. T., and MOORE, D., 1993: On-Orbit Sensor Placement and System Identification of Space Station with Limited Instrumentations. *Proceedings of the 11th International Modal Analysis Conference*, 41-46.

CLOUGH, R. W., and PENZIEN, J., 1993: Dynamics of Structures. McGraw-Hill, New York.

COLEY, D. A., 1999: An Introduction to Genetic Algorithms for Scientists and Engineers. World Scientific, Singapore; River Edge, NJ.

COOK, R. D., and WEISBERG, S., 1982: Residuals and Influence in Regression. Chapman and Hall, N.Y.

COOTE, J. E., LIEVEN, N. A. J. and SKINGLE, G. W., 2005: Sensor Placement Optimisation for Modal Testing of a Helicopter Fuselage. *Proceedings of the 24th International Modal Analysis Conference (IMAC–XXIII), Orlando, Fl., January*, Paper No. s50p07.

DANIEL, J. W., GRAGG, W. B., KAUFMAN, L. and STEWART, G. W., 1976: Reorthogonalization and Stable Algorithms for Updating the Gram-Schmidt Qr Factorization. *Mathematics of Computation*,**30**, 772-795.

DE CLERCK, J. P., and AVITABLE, P., 1998: Development of Several New Tools for Pre-Test Evaluation. *Proceedings of the 16th International Modal Analysis Conference*, 1272-1277.

DE HOOG, F. R., and MATTHEIJ, R. M. M., 2007: Subset Selection for Matrices. *Linear Algebra and Its Applications*,**422**, 349-359.

DOEBLING, S. W., FARRAR, C. R., PRIME, M. B. and SHEVITZ, D. W., 1996: Damage Identification and Health Monitoring of Structural and Mechanical Systems from Changes in Their Vibration Characteristics: A Literature Review, pp. LA--13070-MS, Los Alamos National Lab., NM.

EMERY, A. F., and NENAROKOMOV, A. V., 1998: Optimal Experiment Design. *Measurement Science & Technology*,**9**, 864-876.

EWINS, D. J., 2000: Modal Testing: Theory, Practice, and Application. Research Studies Press, Baldock, Hertfordshire, England; Philadelphia, PA.

FARRAR, C. R., BAKER, W. E., BELL, T. M., CONE, K. M., DARLING, T. W. *et al.*, 1994: Dynamic Characterization and Damage Detection in the I-40 Bridge over the Rio Grande, pp. LA-

12767-MS, Los Alamos National Lab., NM (United States).

FARRAR, C. R., and LIEVEN, N. A. J., 2007: Damage Prognosis: The Future of Structural Health Monitoring. *Philosophical Transactions of the Royal Society a-Mathematical Physical and Engineering Sciences*,**365**, 623-632.

FLANIGAN, C. C., and BOTOS, C. D., 1992: Automated Selection of Accelerometer Locations for Modal Survey Tests. *International Modal Analysis Conference, 10th, San Diego, CA, Feb. 3-7, 1992*.

FRISWELL, M. I., and MOTTERSHEAD, J. E., 1995: Finite Element Model Updating in Structural Dynamics. Kluwer Academic Publishers.

GAWRONSKI, W. K., 2004: Dynamics Identification and Control of Structures. Springer-Verlag, New York.

GOLDBERG, D. E., 2002: The Design of Innovation: Lessons from and for Competent Genetic Algorithms. Kluwer Academic Publishers, Boston.

GOLUB, G. H., and VAN LOAN, C. F., 1996: Matrix Computations. Johns Hopkins University Press, Baltimore.

GUO, H. Y., ZHANG, L., ZHANG, L. L. and ZHOU, J. X., 2004: Optimal Placement of Sensors for Structural Health Monitoring Using Improved Genetic Algorithms. *Smart Materials & Structures*,**13**, 528-534.

HEO, G., WANG, M. L. and SATPATHI, D., 1997: Optimal Transducer Placement for Health Monitoring of Long Span Bridge. *Soil Dynamics and Earthquake Engineering*,**16**, 495-502.

HEREDIA-ZAVONI, E., and ESTEVA, L., 1998: Optimal Instrumentation of Uncertain Structural Systems Subject to Earthquake Ground Motions. *Earthquake Engineering & Structural Dynamics*,**27**, 343-362.

HEYLEN, W., LAMMENS, S. and SAS, P., 1998: Modal Analysis Theory and Testing. Katholieke Universiteit Leuven, Faculty of Engineering, Dept. of Mechanical Engineering, Division of Production Engineering, Machine Design and Automation, Belgium.

HIGHAM, D. J., and HIGHAM, N. J., 2005: Matlab Guide. Society for Industrial Mathematics.

HORN, R. A., and JOHNSON, C. R., 1985: Matrix Analysis. Cambridge University Press.

HORN, R. A., and JOHNSON, C. R., 1991: Topics in Matrix Analysis. Cambridge University Press.

HOUSNER, G. W., BERGMAN, L. A., CAUGHEY, T. K., CHASSIAKOS, A. G., CLAUS, R. O. *et al.*, 1997: Structural Control: Past, Present, and Future. *Journal of Engineering Mechanics-Asce*,**123**, 897-971.

INMAN, D. J., 2006: Vibration with Control. Wiley.

JUANG, J. N., 1994: Applied System Identification. Prentice-Hall, Inc. Upper Saddle River, NJ, USA.

JÜRGEN, G., 2003: Linear Regression. Springer, Berlin; New York.

KAMMER, D. C., 1991: Sensor Placement for on-Orbit Modal Identification and Correlation of Large Space Structures. *Journal of Guidance Control and Dynamics*,**14**, 251-259.

KAMMER, D. C., and TINKER, M. L., 2004: Optimal Placement of Triaxial Accelerometers for Modal Vibration Tests. *Mechanical Systems and Signal Processing*,**18**, 29-41.

KAMMER, D. C., and YAO, L., 1994: Enhancement of on-Orbit Modal Identification of Large Space Structures through Sensor Placement. *Journal of Sound and Vibration*,**171**, 119-139.

KATTAN, P. I., 2003: Matlab Guide to Finite Elements: An Interactive Approach. Springer-Verlag Berlin and Heidelberg GmbH & Co.

KIENTZY, D., RICHARDSON, M. and BLAKELY, K., 1989: Using Finite Element Data to Set up Modal Tests. *Sound and Vibration*, 16-23.

KO, J. M., NI, Y. Q., SUN, Z. G. and CHAN, H. T., 2003: Remote Visualized Health Monitoring of Cable-Supported Bridges. *Proceedings of SPIE: Smart Structures and Materials and Nondestructive Evaluation for Health Monitoring and Diagnostics*,**4337**, 368-378.

KORTE, B. H., and VYGEN, J., 2000: Combinatorial Optimization: Theory and Algorithms. Springer, Berlin; New York.

KUBRUSLY, C. S., and MALEBRANCHE, H., 1985: Sensors and Controllers Location in Distributed Systems - a Survey. *Automatica*,**21**, 117-128.

LARSON, C. B., ZIMMERMAN, D. C. and MAREK, E. L., 1994: A Comparison of Modal Test Planning Techniques: Excitation and Sensor Placement Using the Nasa 8 Bay Truss. *Proceedings of the 12th International Modal Analysis Conference*, 205-211.

LI, D. S., FRITZEN, C. P. and LI, H. N., 2008: Extended Minmac Algorithm and Comparison of Sensor Placement Methods, pp. Paper No. 78. in *Proceedings of the 26th International Modal Analysis Conference (IMAC–XXVI)*, Orlando, Fl., U.S.A.

LI, D. S., LI, H. N. and FRITZEN, C. P., 2006: On the Physical Significance of the Norm Based Sensor Placement Method, pp. 1542–1550 in *Proceedings of the Third European Workshop on Structural Health Monitoring.*, edited by A. GUEMES, Granada, Spain.

LI, D. S., LI, H. N. and FRITZEN, C. P., 2007: The Connection between Effective Independence and Modal Kinetic Energy Methods for Sensor Placement. *Journal of Sound and Vibration*, 945-955.

LI, D. S., LI, H. N. and FRITZEN, C. P., 2009a: A Note on Fast Computation of Effective Independence through Qr Downdating for Sensor Placement. *Mechanical Systems and Signal Processing*,**23**, 1160-1168.

LI, D. S., LI, H. N. and FRITZEN, C. P., 2009b: On Optimal Sensor Placement Criterion for Structural Health Monitoring with Representative Least Squares Method. *Key Engineering Materials*,**413**, 383-391.

LI, H. N., LI, D. S. and SONG, G. B., 2004: Recent Applications of Fiber Optic Sensors to Health Monitoring in Civil Engineering. *Engineering Structures*,**26**, 1647-1657.

LIMONGELLI, M. P., 2003: Optimal Location of Sensors for Reconstruction of Seismic Responses through Spline Function Interpolation. *Earthquake Engineering & Structural Dynamics*,**32**, 1055-1074.

LIU, X., CAI, J. and LIU, H., 2002: Bridge Damage Diagnosis(in Chinese). China Communications Press, Beijing, China.

MATLAB, Www.Mathworks.Com.

MEO, M., and ZUMPANO, G., 2005: On the Optimal Sensor Placement Techniques for a Bridge Structure. *Engineering Structures*,**27**, 1488-1497.

MITCHELL, M., 1996: An Introduction to Genetic Algorithms. MIT Press, Cambridge, Mass.

MOORE, M., and WISS, J., 2001: Reliability of Visual Inspection for Highway Bridges. US Dept. of Transportation,Federal Highway Administration Report, No. FHWA-RD-01-020 & FHWA-RD-01-021.

NIEVERGELT, Y., 2000: A Tutorial History of Least Squares with Applications to Astronomy and Geodesy. *Journal of Computational and Applied Mathematics*,**121**, 37-72.

O'CALLAHAN, J., AVITABILE, P., RIEMER, R. and LOWELL, M., 1989: System Equivalent Reduction Expansion Process (Serep). *Proceedings of the 7th InternationalModal Analysis Conference (Las Vegas, NV), Union College, Schenectady,NY*, 29-37.

PAN, C. T., 2000: On the Existence and Computation of Rank-Revealing Lu Factorizations. *Linear Algebra and Its Applications*,**316**, 199-222.

PAPADIMITRIOU, C., 2004: Optimal Sensor Placement Methodology for Parametric Identification of Structural Systems. *Journal of Sound and Vibration*,**278**, 923-947.

PAPADOPOULOS, M., and GARCIA, E., 1996: Improvement in Model Reduction Schemes Using the System Equivalent Reduction Expansion Process. *AIAA Journal*,**34**, 2217-2219.

PAPADOPOULOS, M., and GARCIA, E., 1998: Sensor Placement Methodologies for Dynamic Testing. *AIAA Journal*,**36**, 256-263.

PAPE, D. A., 1994: Measurement Locations for Experimental Modal Analysis. *IMAC-XXI*, 34-41.

PARK, Y. S., and KIM, H. B., 1996: Sensor Placement Guide for Model Comparison and Improvement. *International Modal Analysis Conference(IMAC), 14 th, Dearborn, MI, Proceedings.*,**1**, 404-409.

PECK, J., and TORRES, I., 2004: A Dmap Program for the Selection of Accelerometer Locations in Msc/Nastran. *45 th AIAA/ASME/ASCE/AHS/ASC Structures, Structural Dynamics and Materials Conference*.

PENNY, J. E. T., FRISWELL, M. I. and GARVEY, S. D., 1994: Automatic Choice of Measurement Locations for Dynamic Testing. *Aiaa Journal*,**32**, 407-414.

PICKREL, C. R., 1999: A Practical Approach to Modal Pretest Design. *Mechanical Systems and Signal Processing*,**13**, 271-295.

PREUMONT, A., 2002: Vibration Control of Active Structures. Kluwer Academic Publishers Boston.

RAO, C. R., and TOUTENBURG, H., 1995: Linear Models: Least Squares and Alternatives. Springer, New York.

RAO, S. S., 2005: The Finite Element Method in Engineering. Elsevier/Butterworth Heinemann, Amsterdam; Boston, MA.

REYNIER, M., and ABOU-KANDIL, H., 1999: Sensors Location for Updating Problems. *Mechanical Systems and Signal Processing*,**13**, 297-314.

RICE, J. A., 1995: Mathematical Statistics and Data Analysis. Duxbury Press Belmont, CA.

ROBERT-NICOUD, Y., RAPHAEL, B. and SMITH, I. F. C., 2005: Configuration of Measurement

Systems Using Shannon's Entropy Function. *Computers and Structures*,**83**, 599-612.

ROUSSEEUW, P. J., and LEROY, A. M., 1987: Robust Regression and Outlier Detection. Wiley, New York.

SCHEDLINSKI, C., and LINK, M., 1996: An Approach to Optimal Pick-up and Exciter Placement, pp. 376-382 in *Proceedings of the 14th International Modal Analysis Conference*.

SCHULTE, R. T., 2006: Optimal Sensor Placement for Damage Identification-an Efficient Forward-Backward Selection Algorithm, pp. 1151-1159 in *Proceedings of the Third EWSHM*, Granada, Spain.

SHIH, Y. T., LEE, A. C. and CHEN, J. H., 1998: Sensor and Actuator Placement for Modal Identification. *Mechanical Systems and Signal Processing*,**12**, 641-659.

STASZEWSKI, W., TOMLINSON, G. and BOLLER, C., 2004: Health Monitoring of Aerospace Structures: Smart Sensor Technologies and Signal Processing. Wiley.

STUBBS, N., and PARK, S., 1996: Optimal Sensor Placement for Mode Shapes Via Shannon's Sampling Theorem. *Microcomputers in Civil Engineering*,**11**, 411-419.

TRENDAFILOVA, I., HEYLEN, W. and VAN BRUSSEL, H., 2001: Measurement Point Selection in Damage Detection Using the Mutual Information Concept. *SMART MATERIALS AND STRUCTURES*, 528–533.

UDWADIA, F. E., 1994: Methodology for Optimum Sensor Locations for Parameter-Identification in Dynamic-Systems. *Journal of Engineering Mechanics-Asce*,**120**, 368-390.

VAN NIMWEGEN, E., CRUTCHFIELD, J. P. and MITCHELL, M., 1999: Statistical Dynamics of the Royal Road Genetic Algorithm. *Theoretical Computer Science*,**229**, 41-102.

WALD, M. L., and CHANG, K., 2007: Minneapolis Bridge Had Passed Inspections. *The New York Times*, August 3, 2007.

WEISBERG, S., 1980: Applied Linear Regression. Wiley, New York.

YOO, K., and PARK, H., 1996: Accurate Downdating of a Modified Gram-Schmidt Qr Decomposition. *BIT Numerical Mathematics*,**36**, 166-181.